UNIVERSITY OF CALIFORNIA,
IRVINE

New therapeutic approaches to study brain mechanisms: Utilizing stem cells and gene therapy to investigate brain diseases, learning, and memory

DISSERTATION

submitted in partial satisfaction of the requirements
for the degree of

DOCTOR OF PHILOSOPHY

in Pharmacological Sciences

by

Claire Chiyu Chen

Dissertation Committee:
Professor Andrej Lupták, Chair
Professor Richard Chamberlin
Associate Professor Weian Zhao

2020

DEDICATION

To

the memory of my grandfather

And to

my parents and my family

for their unconditional love and endless support

TABLE OF CONTENTS

LIST OF FIGURES

LIST OF TABLES

ABBREVIATIONS

4sU	4-thiouridine
5BrU	5-bromouridine
5EU	5-ethynyl uridine
AAVs	adeno associated virus vectors
AD	Alzheimer's disease
AJs	adherens junctions
ALS	amyotrophic lateral sclerosis
AMD	age-related macular degeneration
AMPA	α-amino-3-hydroxy-5-methyl-4-isoxazole propionate
AMPAR	α-amino-3-hydroxy-5-methyl-4-isoxazole propionate receptor
AP	anterior-posterior
APA	alternative polyadenylation
ApCPEB	*aplysia* CPEB
ASO	antisense oligonucleotide
BBB	blood-brain barrier
BCA	bicinchonic acid assay
BMECs	brain microvascular endothelial cells
BSA	bovine serum albumin
CA1	cornu ammonis1
CaMKII	Ca^{2+}/Calmodulin dependent protein kinase II
cDNA	complementary DNA
CeNAs	cyclohexene nucleic acids
cLTP	chemical LTP
CNS	central nervous system
CPEB	cytoplasmic polyadenylation element binding protein
CRISPR	clustered regularly interspaced short palindromic repeats
CTZ	coelenterazine
CuAAC	copper(I)-catalyzed azide alkyne cycloaddition
DI	discrimination index
DIV	days *in vitro*
DMD	Duchenne's muscular dystrophy
DMSO	Dimethyl sulfoxide
DV	dorsal-ventral
ECL	enhanced chemiluminescence
EDTA	ethylene diaminetetraacetic acid
EGFR	epidermal growth factor receptor
ENA	2′-O,4′-C-ethylene-bridged nucleic acids
EPSP	excitatory post synaptic potential
EVs	extracellular vesicles

FANA	2′-deoxy-2′-fluoro-b-D-arabino nucleic acid
FXS	fragile X syndrome
GAPDH	glyceraldehyde-3-phosphate dehydrogenase
HBSS	Hank's buffered salt solution
HD	Huntington's disease
HDR	homology directed repair
HDV	hepatitis delta virus
HSCs	hematopoietic stem cells
KCl	potassium chloride
KO	knockout
LNA	locked nucleic acid
LTD	long-term depression
LTP	long-term potentiation
mAb	monoclonal antibody
miRNA	microRNA
ML	medial-lateral
mRNA	messenger ribonucleic acid
MS	multiple sclerosis
MSCs	mesenchymal stem cells
MVBs	multivesicular bodies
NaASc	sodium ascorbate
NHEJ	non-homologous end-joining
NMDA	N-methyl-D-aspartate
NMDAR	N-methyl-D-aspartate receptor
NSCs	neural stem cells
NTA	nanoparticle tracking analysis
OLM	object location memory
PAS	polyadenylation site
PBS	phosphate buffered saline
PCR	polymerase chain reaction
PD	Parkinson's disease
PKA	protein kinase A
PKC	protein kinase C
PMO	phosphoroamidate morpholino oligomer
PNA	peptide nucleic acid
PRPs	plasticity-related proteins
PS	phosphorothioate
PSD	post synaptic density
PVDF	polyvinylidine fluoride
RACE	rapid amplification of cDNA ends
RBPs	RNA-binding proteins

RNAi	RNA interference
RNase	ribonuclease
RT	room temperature
SDS	sodium dodecyl sulfate
SDS-PAGE	sodium dodecyl sulfate – polyacrylamide gel electrophoresis
SELEX	systematic evolution of ligands by exponential enrichment
sgRNA	single guide RNA
siRNA	small interfering RNA
SMA	spinal muscular atrophy
SNP	single nucleotide polymorphism
STAT3	signal transducer and activator of transcription
TBST	tris-buffered saline and Tween20
THPTA	(tris(hydroxypropyltriazolyl)methylamine
TJs	tight junctions
TNF-α	tumor necrosis factor-alpha
UPRT	uracil phophoribosyltransferase
UTR	untranslated region
XTT	2,3-bis [2-Methoxy-4-nitro-5-sulfophenyl]-2H –tetrazolium-5-carboxyanilide inner salt

ACKNOWLEDGMENTS

First, I would like to thank my undergraduate mentors, Professor Paul Micevych and Professor John Kuo, who not only taught me how to conduct scientific research, but also inspired me to pursue advanced research in graduate school. They provided me with opportunities to conduct independent research project, present my preliminary results at national conferences, and publish my research findings in a peer review journal.

I would like to express my heartfelt gratitude to my graduate mentors, Professor Weian Zhao and Professor Andrej Lupták, for their guidance, support, and encouragement throughout these years. Their mentorship truly shaped me into a better scientist. I feel blessed to have this opportunity to be exposed to different research environments and these experiences have not only equipped me with a broad spectrum of expertise and laboratory skills, but also have molded me into a critical and creative thinker.

I would like to thank my committee members: Professor Richard Chamberlin and Professor Weian Zhao for their time, guidance, and encouragement. They were always there to help, and they have been very supportive along the way.

I would like to thank my collaborators for their contributions to my research work. I would like to thank: Dr. Jenu Chacko for confocal microscopy analysis; Dr. Timothy Bredy's lab and Dr. Carl Cotman's lab for primary cortical neurons preparations; Dr. Marcelo Wood lab for stereotaixic surgeries and animal behavioral experiments; Dr. Eniko Kramar for electrophysiology slice recordings; and Ionis Pharmaceuticals for kindly providing us antisense oligonucleotides.

I would like to thank past and present lab members from the Zhao lab and Lupták lab. It has been a pleasure working with them. I enjoyed the days and nights we spent together in the lab, especially during the manuscript deadline, where we were working as a team to help each other to achieve our goals. I would like to thank my undergraduate students and colleagues for their help in my experiments. I would also like to thank my current lab members for their friendship and support. It has been fantastic to be part of this family. They helped me build interdisciplinary research capability, and provided me support outside the lab.

I would like to thank Springer Nature for permission to use copyright material in my dissertation.

I would like to thank my funding support, National Science Foundation, Graduate Research Fellowship Program, Society for Neuroscience, Neuroscience Scholar Program (NSP), and Department of Pharmaceutical Sciences at UCI.

I would like to thank the NSP principle investigators: Dr. Gina Poe and Dr. Julio Ramirez, for giving me this opportunity to advance my career in neuroscience. It is a great honor to participate in such an amazing program and be surrounded by many

outstanding neuroscientists. I would like to thank my NSP mentor, Dr. Ryan Lalumiere, for mentoring me and providing me guidance and support.

I would like to thank my parents and my family, for always being here and supporting me. You've molded me into a motivated and goal-driven individual, and thank you for allowing me to grow up into the person I am today. Your unconditional love and endless support kept me continuing my path and I cannot thank you enough.

I would like to thank all my friends for their support and care throughout graduate school. Thank you for encouraging me when I was frustrated. Thank you for believing in me when I doubted myself. Hospital life is dull and gloomy, yet I am blessed to have such wonderful friends that created Google sheets as a sign-up to keep me company.

I would like to thank my doctors who have been fighting to save my life. They went above and beyond not only for providing medical care but also supporting my career development. A huge thanks to all nurses from step-down units for taking good care of me at my bedside. They have been with me throughout my graduate school journey. They are my top audience when I practice my elevator pitch.

I would like to thank all blood donors who donated blood for me to save my life. Thank you for your generous donations so that I can continue my study and make it this far.

CURRICULUM VITA

Claire C. Chen

Education

University of California, Irvine Irvine, CA
Ph.D. Pharmacological Sciences 2020

University of California, Irvine Irvine, CA
M.S. Pharmacological Sciences 2016

University of California, Los Angeles Los Angeles, CA
B.S. Biochemistry 2012

Research Experience

University of California, Irvine, Dept. of Pharmaceutical Sciences Irvine, CA
Graduate Research Fellow Sep. 2016- Mar. 2020
Research Advisor: Dr. Andrej Lupták

- Initiate and lead an academia-industry collaborative project to study the role of cytoplasmic polyadenylation element binding protein 3 (CPEB3) ribozyme in memory formation *in vitro* and *in vivo*.

University of California, Irvine, Dept. of Pharmaceutical Sciences Irvine, CA
Graduate Research Fellow Sep. 2014-Sep. 2016
Research Advisor: Dr. Weian Zhao

- Led and designed research projects on investigating the interactions of exosomes and blood-brain barrier (BBB) *in vitro* and *in vivo*.

University of California, Los Angeles, David Geffen School of Medicine
Dept. of Obstetrics and Gynecology/ Dept. of Neurobiology Los Angeles, CA
Staff Research Associate/Undergraduate Researcher Sep. 2011-Oct. 2013
Research Advisor: Dr. Paul Micevych and Dr. John Kuo

- Conducted independent research projects on studying estradiol signaling regulation and neuroprogesterone synthesis in hypothalamic astrocytes.

University of California, Los Angeles, David Geffen School of Medicine
Dept. of Neurosurgery Los Angeles, CA
Undergraduate Research Fellow Mar. 2010-Jun. 2011
Research Advisor: Dr. Grace Griesbach and Dr. David Hovda

- Conducted an individual research project on studying the effect of stress response on hippocampal neuroplasticity following TBI.

Publications

1. **Chen C**, Tong L, Han J, Chinn C, Nikan M, Bredy T, Cotman C, Swayze E, Wood M, Lupták A. Role of cytoplasmic polyadenylation element binding protein 3 ribozyme in memory formation (Manuscript in preparation).
2. Liu L, Zhang S, Liao W, Farhoodi H, Wong C, **Chen C**, Ségaliny A, Chacko J, Nguyen L, Lu M, Polovin G, Pone E, Downing T, Lawson D, Digman M, Zhao W. Mechano-Responsive Stem Cells to target cancer metastases through biophysical cues. *Science Translation Medicine*. 2017. Jul 26;9(400). Doi: 10.1126/scitranslmed.aan2966. **Featured in *UCI News*. Featured in *The Scientist*: Stem Cells Seek Out Tumors Based on Stiffness. Featured in *Genetic Engineering and Biotechnology News*: Cell-Based Therapies Soften Up Cancer by Targeting Tumor Stiffness.**
3. **Chen C**, Liu L, Ma F, Wong C, Guo X, Chacko J, Farhoodi H, Zhang S, Zimak J, Ségaliny A, Riazifar M, Pham V, Digman M, Pone E, Zhao W. Elucidation of exosome migration across the blood-brain barrier model *in vitro*. *Cellular and Molecular Bioengineering* 2016, 9(4):509-529. Doi:10.1007/s12195-016-0458-3. **Featured on the cover issue**.
4. **Chen C**, Kuo J, Wong A, Micevych P. Estradiol modulates translocator protein (TSPO) and steroid acute regulatory protein (StAR) via protein kinase A (PKA) signaling in hypothalamic astrocytes. *Endocrinology* 2014 Aug;155(8):2976-85.
5. Kao CT, **Chen C**, Cheong UI, Liu SL, Huang TH. Osteogenic gene expression of murine osteoblastic (MC3T3-E1) cells under cyclic tension. *Laser Phys.* 2014. 24. 085605.
6. Huang TH, **Chen C**, Liu SL, Lu YC, Kao CT. A low-level diode laser therapy reduces the lipopolysaccharide (LPS)-induced periodontal ligament cell inflammation. *Laser Phys. Lett*. 11 2014. 075602.
7. Su YF, Liang CY, Huang, CY, Peng, CY, **Chen C**, Lin MC, Lin, RK, Lin WW, Chou MY, Liao PH, Yang JJ. A putative novel protein, DEPDC1B, is over-expressed in oral cancer patients and enhances anchorage-independent growth in oral cancer cells mediated through Rac1 and ERK. *Journal of Biomedical Science* 2014, 21:67.

Conference Presentations

1. **Chen C**, Tong L, Nikan M, Cotman C, Swayze E, Wood M, Lupták A. Self-cleaving CPEB3 ribozyme regulates pre-mRNA processing and modulates polyadenyltion in the mouse hippocampus. Poster presentation at the 49th annual meeting of the Society for Neuroscience, Oct. 19-23, 2019, Chicago, IL.

2. **Chen C**, Tong L, Lau C, Cotman, CW, Wood M, Lupták A. Cytoplasmic polyadenylation element binding protein 3 ribozyme regulates activity-dependent synaptic plasticity in neurons. Poster presentation at the Southern California RNA Meeting, Apr. 26, 2019, Monrovia, CA.
3. **Chen C**, Hemstedt T, Lau C, Wood M, Lupták A. The effect of CPEB3 ribozyme self-scission on mRNA maturation in the mouse hippocampus. Poster presentation at the 48th annual meeting of the Society for Neuroscience, Nov. 3-7, 2018, San Diego, CA.
4. **Chen C**, Li X, Ke K, Lau C, Bredy T, Lupták A. Activity-dependent modulation of cytoplasmic polyadenylation element binding protein 3 ribozyme. Poster presentation at the 4th international symposium of Ewha Woman's University, Jul. 17, 2018, Irvine, CA.
5. **Chen C**, Li X, Ke K, Lau C, Bredy T, Lupták A. Activity-dependent modulation of cytoplasmic polyadenylation element binding protein 3 ribozyme. Poster presentation at the 23th annual meeting of the RNA society, May 29 – Jun. 3, 2018, Berkeley, CA.
6. **Chen C**, Li X, Ke K, Bredy T, Lupták A. Self-Scission of the CPEB3 ribozyme is activity dependent and may regulate expression of the CPEB3 mRNA. Poster presentation at the 4th annual RNA symposium, Apr. 4, 2018, Irvine, CA.
7. **Chen C**, Li X, Ke K, Bredy T, Lupták A. Self-Scission of the CPEB3 ribozyme is activity dependent and may regulate expression of the CPEB3 mRNA. Poster presentation at the 47th annual meeting of the Society for Neuroscience, Nov. 11-15, 2017, Washington D.C.
8. **Chen C**, Li X, Ke K, Bredy T, Lupták A. Self-Scission of the CPEB3 ribozyme is activity dependent and may regulate expression of the CPEB3 mRNA. Poster presentation at the diversity fellows poster session. Nov. 11, 2017, Washington D.C.
9. **Chen C**, Li X, Ke K, Bredy T, Lupták A. Role of the Cytoplasmic polyadenylation element binding protein 3 Ribozyme in cortical neurons. Poster presentation at 2017 Pathways to Cures: Translational Science Day at UC Irvine, Jun. 13, 2017, Irvine, CA.
10. **Chen C**, Li X, Ke K, Lau C, Bredy T, Lupták A. Role of the cytoplasmic polyadenylation element binding protein 3 ribozyme in cortical neurons. Poster presentation at NSF-GRFP "Training for Tomorrow" research symposium. May 26, 2017, Irvine, CA. **Awarded 3rd place in poster competition.**
11. **Chen C**, Wong C, Liu L, Zhao W. *In Vitro* exosome trafficking across the blood-brain barrier. Poster presentation at the 46th annual meeting of the Society for Neuroscience, Nov. 12-16, 2016, San Diego, CA.

12. **Chen C**, Wong C, Liu L, Zhao W. *In Vitro* exosome trafficking across the blood-brain barrier. Poster presentation at the diversity fellows poster session. Nov. 12, 2016, San Diego, CA.
13. **Chen C**, Wong C, Liu L, Zhao W. *In Vitro* evaluation of exosome migration across the blood-brain barrier model. Poster presentation at 2016 Pathways to Cures: Clinical Translational Research Day at UC Irvine, Jun. 3, 2016, Irvine, CA.
14. **Chen C**, Liu L, Ma F, Wong C, Zhao W. Elucidation of exosome migration across the blood-brain barrier. Poster presentation at the 2nd international symposium of Ewha Woman's University, Jan. 25, 2016, Irvine, CA.
15. **Chen C**, Kuo J, Micevych P. Estradiol membrane signaling modulates the translocator protein (TSPO) via protein kinase A (PKA) in hypothalamic astrocytes. Poster presentation at the 43th annual meeting of the Society for Neuroscience, Nov. 9-13, 2013, San Diego, CA.
16. Kuo J, **Chen C**, Micevych P. Estradiol signaling regulates de novo progesterone synthesis in hypothalamic astrocytes. Poster presentation at the UCLA Brain Research Institute 24th annual neuroscience poster session, Dec. 4, 2012, Los Angeles, CA.
17. Kuo J, **Chen C**, Micevych P. Estradiol signaling regulates de novo progesterone synthesis in hypothalamic astrocytes. Poster presentation at the 42th annual meeting of the Society for Neuroscience, Oct. 13-17, 2012, New Orleans, LA.
18. **Chen C**, Kuo J, Micevych P. Estradiol signaling regulates de novo progesterone synthesis in hypothalamic astrocytes. Poster presentation at the 15th annual UCLA Science Poster Day, May 15, 2012, Los Angeles, CA.
19. **Chen C**, Vincelli J, Tio D, Taylor A, Griesbach GS. The effect of stress response on hippocampal neuroplasticity following mild traumatic brain injury (TBI). Poster presentation at the 14th annual UCLA Science Poster Day, May 17, 2011, Los Angeles, CA.

Teaching/Mentoring Experience

University of California, Irvine, Dept. of Pharmaceutical Sciences Irvine, CA
Graduate Mentor Mar. 2015-Mar. 2020

- Mentor undergraduate students and junior specialists in research experiments, data analysis, scientific presentation/writing, and career development.

University of California, Irvine, Dept. of Chemistry Irvine, CA
Teaching Assistant Apr. 2014-Jun. 2014

- Teaching assistant for undergraduate course in *General Chemistry Laboratory.*
- Led weekly experiments, held review sections, office hours, and graded lab reports/exams.

Honors and Awards

UCI Associated Graduate Student Travel Fellowship	2018
RNA Society Fellowship	2018
UCI Public Impact Fellowship Semi-Finalist	2017
NSF-GRFP Research Symposium Poster Competition – 3rd place	2017
Society for Neuroscience (SfN) Neuroscience Scholar Program (NSP) Fellowship	2016-2018
National Science Foundation Graduate Research Fellowships Program (NSF GRFP)	2016-2020
Graduate Fellowship, University of California, Irvine	2014
Dean's Honors List, University of California, Los Angeles	2012
UCLA Undergraduate Research Fellowship Program (URFP)	2010-2011
UCLA Scholarship Recognition Award	2009-2010
Goldman Scholarship Award	2008
Mosaic Scholarship Award	2008

ABSTRACT OF THE DISSERTATION

New therapeutic approaches to study brain mechanisms: Utilizing stem cells and gene therapy to investigate brain diseases, learning, and memory

By

Claire Chiyu Chen

Doctor of Philosophy in Pharmacological Sciences

University of California, Irvine, 2020

Professor Andrej Lupták, Chair

Despite significant advances in drug discovery, the development of therapeutics to treat central nervous system (CNS) disease including brain tumors, neurodegenerative diseases, trauma, stroke, and autoimmune diseases, remains a major challenge. Conventional treatments have been revolutionized by the emergence of next generation therapeutics, including biologics, stem cells, and gene therapies. These therapies are characterized by high specificity and better therapeutic efficacies, which have shown great promise to repair and restore lost functions.

The dissertation work presented herein utilizes next generation therapeutics to elucidate the neural mechanisms associated with pathological and healthy states. First, I investigated whether stem cell-derived extracellular vesicles (EVs) can cross the blood-brain barrier (BBB), a dynamic interface that restricts and controls the passage of

substances between the peripheral vascular circulation and the CNS. Using the *in vitro* BBB model under conditions that mimic the healthy and inflamed BBB *in vivo*, I examined the interaction between EVs and BBB. My results suggest that EVs can cross the BBB under stroke-like conditions *in vitro*, in effect utilizing the transcellular route of crossing. This work provides insight into the development of nanotherapeutics or diagnostic tools.

The second part of my dissertation focuses on elucidating the role of cytoplasmic polyadenylation element binding protein 3 (CPEB3) ribozyme in learning and memory. I used a gene therapy approach, specifically antisense oligonucleotides (ASOs), to scrutinize the behavioral phenotypes and molecular mechanisms underlying memory consolidation. I demonstrated that the CPEB3 ribozyme plays a role in synaptic plasticity, in which it modulates CPEB3 protein expression. Upon neuronal stimulation or training-induced learning, the CPEB3 ribozyme is shown to facilitate plasticity-related proteins (PRPs) polyadenylation and translation, resulting in upregulation of PRPs at synapses. The regulation of CPEB3 protein and PRPs by CPEB3 ribozyme further leads to a change in long-term memory formation.

Chapter 1: Introduction

Advancements in medicine have revolutionized the treatment of diseases and injuries. Yet despite recent substantial advances in brain research, central nervous system (CNS) diseases remain the major leading cause of disability and death in the world (Collaborators, 2019). Many brain diseases such as Alzheimer's disease (AD), Parkinson's disease (PD), Huntington's disease (HD), amyotrophic lateral sclerosis (ALS), epilepsy, trauma, and stroke are chronic and incurable. The deterioration impairment often leads to physical and cognitive loss, and the disabling effects may continue for years or even decades. Oftentimes, the neurological dysfunction is irreversible and progressive, owing to limited regenerative potential in the CNS. The complexity of the CNS and limited understanding of disease progression make it more challenging to develop therapeutic agents and effectively deliver them to the targeted sites. Although extensive research has expanded our knowledge and uncovered pathological mechanisms of neurological diseases, drug development is still particularly difficult for treatment of CNS diseases. In fact, the patient population with CNS diseases is constantly increasing, and the rising prevalence is driven by an aging population and better diagnostics. It is estimated that neurological disorders contribute to 11.6% of global disability-adjusted life-years (DALYs) and 16.5% of deaths (Collaborators, 2019). Yet the failure rate in late stage clinical trials in CNS based therapies is significantly higher compared to other diseases (Pankevich et al., 2014). Therefore, there is a vast unmet medical need for CNS therapies.

Recently, newer approaches such as biologics, gene therapies, and stem-cell therapies have been shown to offer such a great therapeutic potential to treat neurological diseases that they are widely investigated in pre-clinical and clinical studies. The emergence of these new biopharmaceuticals is considered as the next-generation of therapeutic molecules in the drug development pipeline. Extensive efficacy and safety studies have been conducted for the development of biopharmaceutical drugs to treat various diseases. At present, there are 316 biopharmaceutical products approved by the US Food and Drug Administration (FDA) and over 6,000 products are in clinical development (as of December 2018, (Walsh, 2018). The next-generation therapeutics are promising candidates for CNS therapies, in which they possess different unique properties such as modulating pathological states, regulating gene expression, reducing toxic levels of specific proteins, or releasing paracrine factors to mediate repair damaged neurons (Fouad, 2019; Qosa and Volpe, 2018).

Therapeutic antibodies

Monoclonal antibody (mAb) or engineered antibody therapies have been developed to treat various malignancies, organ transplantation, and immunological diseases (Buss et al., 2012). These antibodies have fragment antigen binding domain (Fab) that can bind to unique antigens (Ags) with high specificity, which in turn have a direct effect on receptor signaling. The known mode of action of therapeutic antibodies includes: neutralization, ligand-receptor interaction disruption, antibody-dependent cell-

mediated cytotoxic (ADCC), complement-dependent cytotoxic (CDC), antibody-dependent cellular phagocytosis (ADCP), receptor downregulation by internalization and degradation, and drug delivery carrier (Suzuki et al., 2015). Currently, mAb therapies are used for neuromuscular disorders and demyelinating diseases (Rommer et al., 2012). More recently, bispecific mAbs have been developed to deliver mAb to the brain for the treatment of Alzheimer's disease. This humanized antibody has been engineered to have one arm targeting transferrin receptor (TfR) and the other arm targeting BACE (β-amyloid precursor protein cleavage enzyme), which is an enzyme that cleaves the membrane amyloid precursor protein (APP) to generate soluble Aβ in AD. Using receptor-mediated transcytosis, the anti-TfR/BACE1 bispecific mAb improves BBB-crossing and reduces Aβ production (Neves et al., 2016; Yu et al., 2014). Although there is exciting progress in therapeutic antibodies development in the CNS diseases, safety and efficacy profiles of engineered antibodies remain to be addressed. Currently, a second and third generation of antibody has been engineered to improve immune functions and efficiency, and they are being evaluated in clinical trials (Chames et al., 2009). Together antibody therapeutics development elicits clinical benefits.

Stem cell therapy

Due to limited endogenous regeneration potential in the CNS, loss of neurons and glial cells results in a progressive degeneration in many neurological diseases. Current approved therapies only address symptomatic management rather than restoration of the diseased or injured tissues. Stem-cell therapies have been considered

as a potential therapeutic approach to repair and regenerate lost cell functions. Cellular sources for stem-cell therapies include embryonic stem cells (ESCs), neural stem cells (NSCs), induced pluripotent stem cells (iPSCs), mesenchymal stem cells (MSCs), and hematopoietic stem cells (HSCs), and they are being widely investigated in regenerative medicine (Lindvall and Kokaia, 2006; Martinez-Morales et al., 2013). Stem cells exhibit self-renewal and multi-directional differentiation capacity. For example, studies by Chu and colleagues demonstrate that NSCs can migrate to the ischemic hippocampus, and differentiate into new neurons and astrocytes in rat stroke models of focal ischemia (Chu et al., 2003). Moreover, NSCs can be genetically programmed to produce neruoprotective molecules such as glial cell line-derived neurotrophic factor (GDNF) to treat PD (Behrstock et al., 2006). In addition to cell differentiation and replacement, stem cells can exert immunomodulatory properties and trophic actions. The secretion of trophic factors may regulate neuroinflammation; stimulate endogenous neurogenesis, angiogenesis, and synaptogenesis; and evoke a better cellular response in the tissue microenvironment (Baraniak and McDevitt, 2010; Martinez-Morales et al., 2013). In an ischemic stroke model, transplantation of MSCs have been shown to decrease infarct size, reduce proinflammatory cytokines, enhance neurogenesis and angiogenesis, and improve neurological deficits (Kim and de Vellis, 2009; Marei et al., 2018; Stonesifer et al., 2017). While stem cells and regenerative medicine have great promise, immunogenicity and tumorigenic potential are major concerns for clinical translation (Marei et al., 2018). Other factors, including dosage and administration time window, should be considered and warranted further investigation in future trials.

More recently, stem cell-derived vesicles, also known as extracellular vesicles (EVs), have gained increasing interest as a novel strategy for alternative to stem cell therapies. We and others explored the role of EVs as drug delivery vehicles as well as potential therapeutics in CNS diseases (Braccioli et al., 2014; Chen et al., 2016; Ophelders et al., 2016). This will be further discussed in Chapter 2.

Gene therapy

With better understanding of disease mechanisms, gene therapy is emerging as an alternative strategy to treat neurological diseases. Genetic interventions aim to modify or correct a defective gene and thereby restore gene expression and attenuate disease progression. To deliver genetic materials to the intracellular compartment of target cells, viral vectors and non-viral vectors were developed in preclinical and clinical settings (Nayerossadat et al., 2012). Virus-mediated gene therapies exploit the ability of viruses to infect specific tissues and hijack the host cell machinery to regulate gene expression of the host. Different viruses have been utilized as vectors for gene therapy based on their transduction efficiency, packaging capacity, immune response, and host genome integration (Choong et al., 2016). The adenoassociated virus vectors (AAVs) are the most widely used viral vector owing to inherently broad tropism, high transduction efficiency in both dividing and non-dividing cells, better transgene expression levels, and a higher safety profile with minimal immune response. Nevertheless, one drawback of AAVs is their limited packaging capacity of the particles (up to 4.8 kb) (Deverman et al., 2018; Lundstrom, 2018). Despite limited transgene capacity, AAVs have yielded a substantial number of gene therapy clinical trials in

various neurological conditions including type I spinal muscular atrophy (SMA), PD, Batten disease, mucopolysaccharidosis (MPS), etc. (Deverman et al., 2018).

Non-viral vector gene therapies have been considered as an attractive alternative due to safety concerns with viral vectors. Short synthetic nucleotides, such as antisense oligonucleotides (ASOs), RNA interference (RNAi), small interfering RNA (siRNA), and microRNA (miRNA), that target specific genes of therapeutic interest have been developed for genetic manipulation in the treatment of CNS diseases. Unlike viral vectors, nucleic acid based gene therapies have reduced immunotoxicity, which allows repeat administrations. Although it is recognized that non-viral vectors exhibit high specificity, versatility, and safety, a major challenge lies in poor transfection efficiency and thus low expression of transgene at the target location. Several methods have been established to circumvent this issue associated with delivery efficiency. Non-viral vectors are delivered to the target cells by utilizing chemical methods such as cationic liposomes, nanoparticles, engineered polymers, or physical methods such as electroporation, ultrasound, and pressure-perfusion (Jayant et al., 2016). These approaches improve extracellular stability, facilitate intracellular trafficking, and decrease opsonization from the reticuloendothelial system (RES) (Jayant et al., 2016). In fact, Patisiran, a double-strand siRNA formulated with lipid nanoparticles, is the first RNAi therapeutic approved by the FDA in 2018 for the treatment of the polyneuropathy of hereditary transthyretin (TTR)-mediated amyloidosis (hATTR) (Adams et al., 2018). Furthermore, many efforts have been made through chemical modifications to

enhance drug-like properties of ASOs, some of which are successfully translated to clinics (Sridharan and Gogtay, 2016). More details will be discussed in Chapter 3.

More recently, a bacterial clustered regularly interspaced short palindromic repeats (CRISPR) together with a CRISPR-associated (Cas) protein has been developed as a powerful gene-editing tool for treating neurological diseases including HD, ALS, AD, PD, and fragile X syndrome (FXS) (Cota-Coronado et al., 2019). This technology provides applications for replacing, modifying, correcting, or regulating specific loci in the genome (Doudna and Charpentier, 2014). This system utilizes a single guide RNA (sgRNA) and a Cas9 endonuclease to perform DNA double-stranded breaks (DSBs) at targeted loci, and these DSBs can be repaired by homology directed repair (HDR) and non-homologous end-joining (NHEJ), which allows disease-causing mutations to be removed and replaced with corrected sequences (Doudna and Charpentier, 2014). A recent study by Lee and colleagues demonstrates that administration of CRISPR-Gold nanoparticles loaded with Cas9 and *Prevotella and Francisella* 1 (Cpf1) ribonucleoproteins targeting the metabotropic glutamate receptor 5 (*mGluR5*) gene to fragile X mental retardation 1 (*Fmr1*) knockout mouse hippocampus or striatum reveals a reduction of mGluR5 mRNA and protein expression, and this lessens autistic phenotypes in the FXS model mice (Lee et al., 2018). Nevertheless, one major disadvantage of the CRISPR-Cas9 is off-target effects, which are due to sgRNA sequences that are homologous to other genomic sites (Zhang et al., 2015). Other factors including HDR and NHEJ efficiency, immunogenicity of viral vectors, and delivering methods are being considered when translating genome editing tools to

therapeutic applications (Walters et al., 2016). Although further investigations are required to advance delivery systems, CRISPR/Cas9 systems provide revolutionary potential for CNS drug discovery in the near future.

In summary, developing biologic therapeutics for complex neurological disorders remains challenging, yet with a better understanding of disease mechanisms and improved delivery methods, there is promise and growth in the discovery of a broad spectrum of CNS diseases. In this dissertation work, we mainly focus on stem cell-derived EVs and ASOs as novel approaches to elucidate the cellular mechanism of EVs trafficking across the BBB and neural mechanisms of learning and memory.

References

Adams, D., Gonzalez-Duarte, A., O'Riordan, W.D., Yang, C.C., Ueda, M., Kristen, A.V., Tournev, I., Schmidt, H.H., Coelho, T., Berk, J.L.*, et al.* (2018). Patisiran, an RNAi Therapeutic, for Hereditary Transthyretin Amyloidosis. N Engl J Med *379*, 11-21.

Baraniak, P.R., and McDevitt, T.C. (2010). Stem cell paracrine actions and tissue regeneration. Regen Med *5*, 121-143.

Behrstock, S., Ebert, A., McHugh, J., Vosberg, S., Moore, J., Schneider, B., Capowski, E., Hei, D., Kordower, J., Aebischer, P.*, et al.* (2006). Human neural progenitors deliver glial cell line-derived neurotrophic factor to parkinsonian rodents and aged primates. Gene Ther *13*, 379-388.

Braccioli, L., van Velthoven, C., and Heijnen, C.J. (2014). Exosomes: a new weapon to treat the central nervous system. Mol Neurobiol *49*, 113-119.

Buss, N.A., Henderson, S.J., McFarlane, M., Shenton, J.M., and de Haan, L. (2012). Monoclonal antibody therapeutics: history and future. Curr Opin Pharmacol *12*, 615-622.

Chames, P., Van Regenmortel, M., Weiss, E., and Baty, D. (2009). Therapeutic antibodies: successes, limitations and hopes for the future. Br J Pharmacol *157*, 220-233.

Chen, C.C., Liu, L.N., Ma, F.X., Wong, C.W., Guo, X.N.E., Chacko, J.V., Farhoodi, H.P., Zhang, S.X., Zimak, J., Segaliny, A.*, et al.* (2016). Elucidation of Exosome Migration Across the Blood-Brain Barrier Model In Vitro. Cell Mol Bioeng *9*, 509-529.

Choong, C.J., Baba, K., and Mochizuki, H. (2016). Gene therapy for neurological disorders. Expert Opin Biol Ther *16*, 143-159.

Chu, K., Park, K.I., Park, H.K., Jung, K.H., Jeong, S.W., Kim, M., and Roh, J.K. (2003). The systemic administration of VEGF and human neural stem cells can improve the functional deficits after stroke in rats. Stroke *34*, 250-250.

Collaborators, G.B.D.N. (2019). Global, regional, and national burden of neurological disorders, 1990-2016: a systematic analysis for the Global Burden of Disease Study 2016. Lancet Neurol *18*, 459-480.

Cota-Coronado, A., Diaz-Martinez, N.F., Padilla-Camberos, E., and Diaz-Martinez, N.E. (2019). Editing the Central Nervous System Through CRISPR/Cas9 Systems. Frontiers in Molecular Neuroscience *12*.

Deverman, B.E., Ravina, B.M., Bankiewicz, K.S., Paul, S.M., and Sah, D.W.Y. (2018). Gene therapy for neurological disorders: progress and prospects. Nat Rev Drug Discov *17*, 767.

Doudna, J.A., and Charpentier, E. (2014). Genome editing. The new frontier of genome engineering with CRISPR-Cas9. Science *346*, 1258096.

Fouad, G.I. (2019). Stem cells as a promising therapeutic approach for Alzheimer's disease: a review.

Jayant, R.D., Sosa, D., Kaushik, A., Atluri, V., Vashist, A., Tomitaka, A., and Nair, M. (2016). Current status of non-viral gene therapy for CNS disorders. Expert Opin Drug Deliv *13*, 1433-1445.

Kim, S.U., and de Vellis, J. (2009). Stem cell-based cell therapy in neurological diseases: a review. J Neurosci Res *87*, 2183-2200.

Lee, B., Lee, K., Panda, S., Gonzales-Rojas, R., Chong, A., Bugay, V., Park, H.M., Brenner, R., Murthy, N., and Lee, H.Y. (2018). Nanoparticle delivery of CRISPR into the brain rescues a mouse model of fragile X syndrome from exaggerated repetitive behaviours. Nat Biomed Eng *2*, 497-507.

Lindvall, O., and Kokaia, Z. (2006). Stem cells for the treatment of neurological disorders. Nature *441*, 1094-1096.

Lundstrom, K. (2018). Viral Vectors in Gene Therapy. Diseases *6*.

Marei, H.E., Hasan, A., Rizzi, R., Althani, A., Afifi, N., Cenciarelli, C., Caceci, T., and Shuaib, A. (2018). Potential of Stem Cell-Based Therapy for Ischemic Stroke. Front Neurol *9*, 34.

Martinez-Morales, P.L., Revilla, A., Ocana, I., Gonzalez, C., Sainz, P., McGuire, D., and Liste, I. (2013). Progress in Stem Cell Therapy for Major Human Neurological Disorders. Stem Cell Rev Rep *9*, 685-699.

Nayerossadat, N., Maedeh, T., and Ali, P.A. (2012). Viral and nonviral delivery systems for gene delivery. Adv Biomed Res *1*, 27.

Neves, V., Aires-da-Silva, F., Corte-Real, S., and Castanho, M.A.R.B. (2016). Antibody Approaches To Treat Brain Diseases. Trends Biotechnol *34*, 36-48.

Ophelders, D.R., Wolfs, T.G., Jellema, R.K., Zwanenburg, A., Andriessen, P., Delhaas, T., Ludwig, A.K., Radtke, S., Peters, V., Janssen, L.*, et al.* (2016). Mesenchymal Stromal Cell-Derived Extracellular Vesicles Protect the Fetal Brain After Hypoxia-Ischemia. Stem Cells Transl Med *5*, 754-763.

Pankevich, D.E., Altevogt, B.M., Dunlop, J., Gage, F.H., and Hyman, S.E. (2014). Improving and accelerating drug development for nervous system disorders. Neuron *84*, 546-553.

Qosa, H., and Volpe, D.A. (2018). The development of biological therapies for neurological diseases: moving on from previous failures. Expert Opin Drug Discov *13*, 283-293.

Rommer, P.S., Patejdl, R., and Zettl, U.K. (2012). Monoclonal antibodies in the treatment of neuroimmunological diseases. Curr Pharm Des *18*, 4498-4507.

Sridharan, K., and Gogtay, N.J. (2016). Therapeutic nucleic acids: current clinical status. Br J Clin Pharmacol *82*, 659-672.

Stonesifer, C., Corey, S., Ghanekar, S., Diamandis, Z., Acosta, S.A., and Borlongan, C.V. (2017). Stem cell therapy for abrogating stroke-induced neuroinflammation and relevant secondary cell death mechanisms. Prog Neurobiol *158*, 94-131.

Suzuki, M., Kato, C., and Kato, A. (2015). Therapeutic antibodies: their mechanisms of action and the pathological findings they induce in toxicity studies. J Toxicol Pathol *28*, 133-139.

Walsh, G. (2018). Biopharmaceutical benchmarks 2018. Nat Biotechnol *36*, 1136-1145.

Walters, B.J., Azam, A.B., Gillon, C.J., Josselyn, S.A., and Zovkic, I.B. (2016). Advanced In vivo Use of CRISPR/Cas9 and Anti-sense DNA Inhibition for Gene Manipulation in the Brain. Front Genet *6*.

Yu, Y.J., Atwal, J.K., Zhang, Y., Tong, R.K., Wildsmith, K.R., Tan, C., Bien-Ly, N., Hersom, M., Maloney, J.A., Meilandt, W.J., *et al.* (2014). Therapeutic bispecific

antibodies cross the blood-brain barrier in nonhuman primates. Sci Transl Med *6*, 261ra154.

Zhang, X.H., Tee, L.Y., Wang, X.G., Huang, Q.S., and Yang, S.H. (2015). Off-target Effects in CRISPR/Cas9-mediated Genome Engineering. Mol Ther Nucleic Acids *4*, e264.

Chapter 2: Elucidation of Exosome Migration across the Blood-Brain Barrier Model *In Vitro*

Claire C. Chen[1,2,7], Linan Liu[1,2,7], Fengxia Ma[1-3], Chi W. Wong[1,2], Xuning E. Guo[1,2], Jenu V. Chacko[2], Henry P. Farhoodi[1,2,4], Shirley X. Zhang[1,2], Jan Zimak[1,2], Aude Ségaliny[1,2], Milad Riazifar[1,2], Victor Pham[1,2], Michelle A. Digman[2,5,6], Egest J. Pone[1,2], Weian Zhao[1,2]

Affiliations:

[1] Department of Pharmaceutical Sciences, Sue and Bill Gross Stem Cell Research Center, Chao Family Comprehensive Cancer Center and Edwards Life sciences Center for Advanced Cardiovascular Technology, 845 Health Sciences Road, University of California-Irvine, Irvine, California, 92697, USA.

[2] Department of Biomedical Engineering, University of California-Irvine, Irvine, California, 92697, USA.

[3] State Key Laboratory of Experimental Hematology, Institute of Hematology and Blood Disease Hospital, Chinese Academy of Medical Sciences and Peking Union Medical College, Tianjin 300020, China

[4] Department of Molecular Biology & Biochemistry, University of California-Irvine, Irvine, California, 92697, USA.

[5] Laboratory for Fluorescence Dynamics, University of California-Irvine, California 92697, USA.

[6] Centre for Bioactive Discovery in Health and Ageing, School of Science and Technology, University of New England, Armidale, New South Wales 2351, Australia.

[7] These authors contributed equally to this work.

Address correspondence to Weian Zhao, Department of Pharmaceutical Sciences, 845 Health Sciences Road, University of California-Irvine, Irvine, California, 92697, USA.

Electronic mail: weianz@uci.edu. Contact telephone number: +01 (949) 824-9744.

2.1 Abstract

The delivery of therapeutics to the central nervous system (CNS) remains a major challenge in part due to the presence of the blood-brain barrier (BBB). Recently, cell-derived vesicles, particularly exosomes, have emerged as an attractive vehicle for targeting drugs to the brain, but whether or how they cross the BBB remains unclear. Here, we investigated the interactions between exosomes and brain microvascular endothelial cells (BMECs) *in vitro* under conditions that mimic the healthy and inflamed BBB *in vivo*. Transwell assays revealed that luciferase-carrying exosomes can cross a BMEC monolayer under stroke-like, inflamed conditions (TNF-α activated) but not under normal conditions. Confocal microscopy showed that exosomes are internalized by BMECs through endocytosis, co-localize with endosomes, in effect primarily utilizing the transcellular route of crossing. Together, these results indicate that cell-derived exosomes can cross the BBB model under stroke-like conditions *in vitro*. This study encourages further development of engineered exosomes as drug delivery vehicles or tracking tools for treating or monitoring neurological diseases.

Keywords—Drug delivery, blood-brain barrier (BBB), exosome, humanized *Gaussia* luciferase (hGluc), stroke, inflammation, endocytosis, exocytosis, transcytosis.

2.2 Introduction

Despite significant advances in drug delivery, a major challenge remains in delivering therapeutics effectively to the brain for the treatment of central nervous system (CNS) diseases, including trauma, stroke, autoimmune diseases, neurodegenerative diseases and tumors (Abbott et al., 2006; Banks, 2016; Obermeier et al., 2013; Rubin and Staddon, 1999; Upadhyay, 2014). Drug delivery to the CNS is limited by the presence of the blood-brain barrier (BBB), a dynamic interface that restricts and controls the passage of substances between the peripheral vascular circulation and the CNS, thus serving to protect the CNS from harmful substances or overzealous immune responses (Andreone et al., 2015; Banks, 2016; Obermeier et al., 2013). The BBB is composed of brain microvascular endothelial cells (BMECs), astrocytes, pericytes, the endothelial basement membrane, and adjacent neurons. The brain endothelial cells have a complex arrangement of tight junctions (TJs) and adherens junctions (AJs), which play key roles in regulating paracellular permeability (Wolburg and Lippoldt, 2002). These junctions prevent transport of most molecules except those normally used for homeostasis, including for nutrition or bidirectional hormonal communication and reflecting the changing properties of the BBB depending on conditions (Banks, 2016).

While this complex interface protects the brain from harmful chemicals or toxins that may be present in systemic circulation, it also results in the inability of therapeutics to cross the BBB, with approximately 98% of small molecule pharmaceuticals and almost all of large molecule biologic drugs, including recombinant proteins, monoclonal

antibodies, or gene-based medicines, failing to cross the BBB (Pardridge, 2005, 2012). However, under certain CNS disease states, the BBB is dysregulated or malfunctioned, which could itself be used as a passive mechanism for targeting therapeutics to the brain (Shlosberg et al., 2010). For example, under ischemic stroke and subsequent reperfusion condition caused by arterial embolism or thrombosis, the integrity of TJs of the BBB is compromised, leading to increase in paracellular permeability and allowing entry of both small and large molecules into the brain (Obermeier et al., 2013; Sandoval and Witt, 2008). And in autoimmune CNS diseases such as multiple sclerosis (MS), lymphocytes can enter sclerotic lesions, though the sequence of pathological events and immune infiltration remain to be fully elucidated(Dendrou et al., 2015). Administration of human basic fibroblast growth factor (bFGF), an endogenous neurotrophin that does not cross the BBB(Whalen et al., 1989), exerted a neuroprotective effects in the post ischemic brain (Song, 2002), implying that it could diffuse across the compromised BBB. Moreover, the so-called enhanced permeability and retention (EPR) effect has also been used to transport anticancer drugs using nanocarriers such as nanoparticles and liposomes that can accumulate and passively extravasate into the tumor vasculature (Peer et al., 2007; Torchilin, 2005). But although particulate drug carriers such as dendrimers (Lee et al., 2005), nanoparticles (Petros and DeSimone, 2010) and liposomes (Torchilin, 2014) have been tested for drug delivery across the BBB, they remain not widely used in the clinic considering their immunogenicity, limited half-life *in vivo*, and, importantly, relative lack of specificity and efficacy in crossing the BBB (Gabathuler, 2010; Upadhyay, 2014).

Cell-based medications are a newer class of drug delivery for CNS diseases (Chen et al., 2003; Liu et al., 2013). Stem cells, such as mesenchymal stem (or stromal) cells (MSC), are known to mobilize from the bone marrow or fat deposits and migrate and home to sites of injury (Sordi et al., 2005), including CNS injury(Chen et al., 2003), where they presumably exert protective and recovery effects via numerous paracrine factors (Lee et al., 2009). Administration of human bone marrow MSC can enhance recovery from CNS injuries (Dulamea, 2015; Liu et al., 2013), by their secretion of exosomes, growth factors, cytokines, and other paracrine factors (Chen et al., 2003; Xin et al., 2013). More recently, natural cell-derived vesicles collectively termed extracellular vesicles (EVs) have been investigated as a new class of carriers of drugs, nucleic acids and diagnostic reagents (Lasser, 2015), including for CNS diseases (Xin et al., 2014). In particular, exosomes that originate from intracellular multivesicular bodies (MVBs) and represent a major subtype of EVs have recently been reported to be involved in a variety of activities in the normal and pathological CNS (El-Andaloussi et al., 2013; Fruhbeis et al., 2012; Kalani et al., 2014), thus rendering them potentially attractive vehicles for delivering agents across the BBB.

There are several reasons for the recent resurgence of activity in testing EVs as therapeutics and as vectors for therapeutic delivery, including for CNS diseases. Although small relative to cells, EVs host a complex mixture of surface receptors and intravascular cargo, including proteins and nucleic acids, that may synergize to enhance therapeutic efficacy compared to isolated factors (Thery et al., 2002; Valadi et al., 2007). EVs have been found to mediate, in part, the curative effects of cell-based

therapies, especially for stem cells (Kourembanas, 2015). In particular, exosomes derived from MSCs have been reported to exhibit neuroprotective effects and promote tissue repair in CNS injury models (Xin et al., 2014; Xin et al., 2013). Similar to MSC, hematopoietic stem cells (HSC), are known to increase their activity in bone marrow as well as enter peripheral circulation in response to infection or injury (Trumpp et al., 2010). Uptake of exosomes purified from HSC and injected into the cerebellum by Purkinje neurons was reported in a cre-reporter model, though whether exosomes could cross the BBB was not investigated (Ridder et al., 2014). Other cell types that possibly secrete exosomes capable of bypassing the BBB are immune cells and CNS cells themselves, including BMECs, neuronal types, astrocytes, microglia and their progenitors. BMEC-derived exosomes were reported to deliver the anticancer drug doxorubicin across the BBB in a glioma model (Yang et al., 2015). Exosomes from dendritic cells (DCs) delivered small interfering RNA (siRNA) to treat Alzheimer's disease to the mouse brain, suggesting they may cross the BBB and deliver siRNA cargos into target cells for specific gene knockdown (Alvarez-Erviti et al., 2011). Exosomes derived from a mouse lymphoma cell line could deliver curcumin across the BBB to microglial cells via intranasal administration to attenuated brain inflammation and autoimmune responses in experimental autoimmune encephalomyelitis (EAE)(Zhuang et al., 2011), whereas curcumin-primed exosomes ameliorated oxidative stress and tightened AJs and TJs induced by hyperhomocysteinemia, leading to a reduction of permeability (Kalani et al., 2014).

Thus, considering that exosomes have recently been found to play key roles in CNS homeostasis, pathology and subsequent recovery, their natural favorable characteristics (lack of immunogenicity and prolonged half-life) could be combined with additional bioengineering approaches to enhance their biodistribution, including increased ability to bypass the BBB (Schiera et al., 2015; Xin et al., 2014). Nevertheless, although published data suggested that exosomes could deliver therapeutics to the brain, the mechanisms of interaction between exosomes and the BBB remain elusive. Therefore, as a step towards efficient therapeutic delivery to the brain using exosomes, this study aims to elucidate whether and how exosomes bypass the BBB (**Fig. 2.1**). Using engineered HEK 293T-derived exosomes and *in vitro* BMEC monolayers as a model system; we demonstrated that cell-derived exosomes can cross the BBB model via mostly active BMEC endocytosis primarily utilizing the transcellular route of crossing under stroke-like conditions *in vitro*.

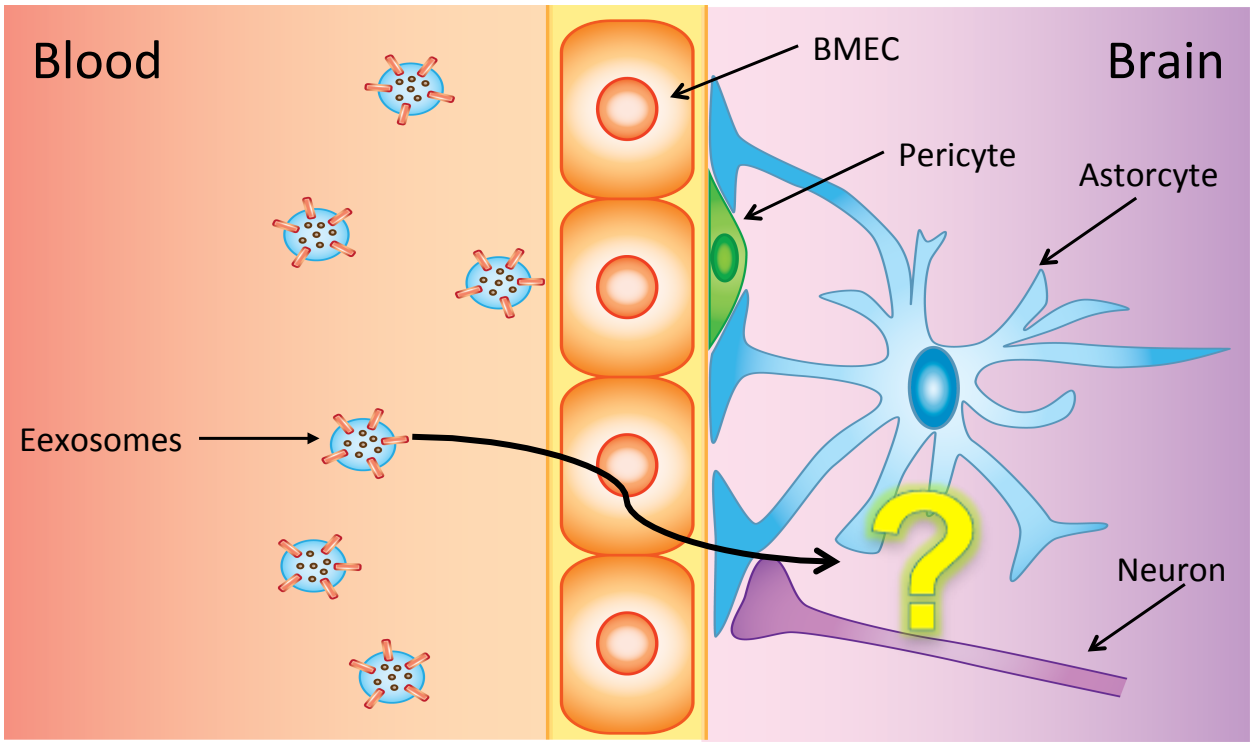

Fig. 2.1. Can exosomes cross the blood-brain barrier?

2.3 Results and Discussion

Exosome preparation, characterization and labeling

In order to monitor their distribution across BMEC monolayers *in vitro,* the exosomes were labeled with hGluc. hGluc was fused with lactadherin, which can be bound to cell membrane phophatidylserines (PS) and is also highly enriched on the outer leaflet of exosomal membrane (Imai et al., 2015; Takahashi et al., 2013). 293T cells were transduced with lentivirus expressing each free hGluc (hGluc 293T), hGluc-Lactadherin without (hGluc-Lact 293T) and with (hGluc-Lact-GFP) a Green Fluorescent Protein (GFP) tag used to monitor transduction efficiency (**Fig. 2.S1a**). A high *Gaussia* luciferase expression was observed from the cell lysates of engineered 293T cells expressing hGluc-Lact (**Fig. 2.S1b**, lane 2) and hGluc-Lact-GFP (**Fig. 2.S1b**, lane 3) fusion proteins but not their counterpart (free hGluc alone, **Fig. 2.S1b**, lane 1). These results indicate that engineered cells correctly expressed the membrane-targeted fused proteins. Moreover, the tagged hGluc proteins (i.e., hGluc-Lact and hGluc-Lact-GFP) were observed to associate with the cell membranes while free hGluc was mostly secreted into the conditioned medium (free hGluc expression in cells = 6.8%-7.8% of tagged hGluc expression in cells, **Fig. 2.S1b** and **2.S1c**).

Exosomes were then collected by ultra-centrifugation from conditioned medium of native and engineered 293T cells (**Fig. 2.2a**) and were characterized by NTA and biochemical analysis. The size distribution of purified exosomes was analyzed using NanoSight NS300 nanoparticle tracking analysis (NTA). NTA showed a similar size

distribution profile for native (96.3 ± 5.4 nm) and hGluc-Lact exosomes (80.3 ± 2.0 nm) (**Fig. 2.2b**). Thus, our exosome preparations have similar size distribution as reported literature(Lai et al., 2014), also suggesting that the modification with the expressed protein tags did not affect the physical properties of exosomes. Next, exosomes were characterized for expression of several typically prominent markers (Thery et al., 2006). Exosomes were captured on beads coated with anti-CD63, a tetraspanin that is highly enriched in late endosomes, lysosomes and exosomes(Pols and Klumperman, 2009), analyzed by flow cytometry after immunostaining with exosomal surface markers anti-CD9, anti-CD63, and anti-CD81 (**Fig. 2.2c**). Consistent with the literature (Mathivanan et al., 2010; Thery et al., 2006; Thery et al., 2002), our prepared exosomes are positive for CD9, CD63 and CD81. Western blotting further confirmed the presence of exosomal proteins CD9, CD81 and CD63 (**Fig. 2.2d**, lane 1). Next we examined whether hGluc-Lact was expressed on exosomes; indeed immunoblotting data showed that hGluc could only be detected on hGluc-Lact-labeled exosomes (hGluc-Lact exosomes) but not on hGluc alone counterparts, indicating that hGluc-Lact bound to exosome membranes with high specificity (**Fig. 2.2d**). Remarkably, the presence of exosomal biomarkers CD9, CD81 and CD63 was confirmed on engineered exosomes, without being affected by lentiviral transduction (**Fig. 2.2d**, lanes 2 and 3).

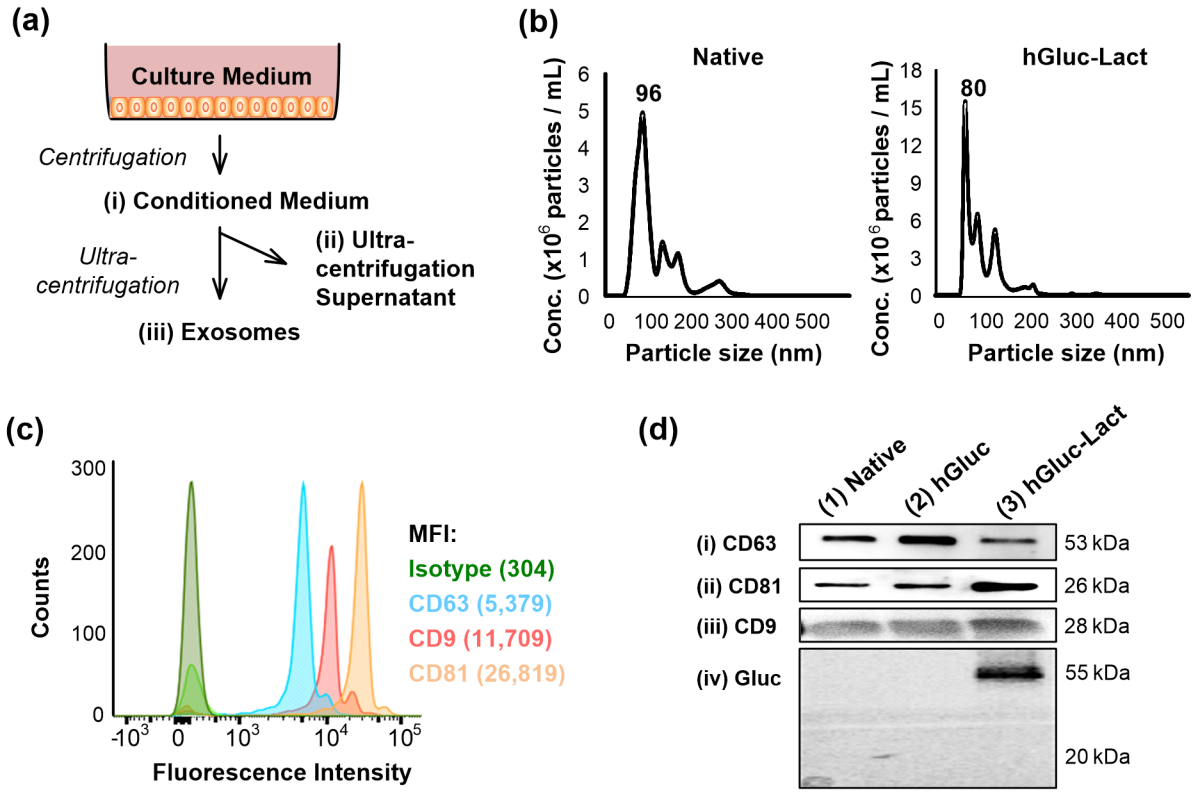

Fig. 2.2. Exosome engineering and characterization. (a) Schematic depiction of the isolation protocol for exosomes. (b) Size distribution of native and hGluc-Lact exosomes measured by nanoparticle tracking analysis (NTA). (c) Flow cytometry detection of exosome characterization. Exosomes were incubated with anti-CD63 Dynabeads and immunostained with exosomal surface markers (CD9, CD63, and CD81). Green histogram is the isotype control. Data were quantified and expressed as MFI (mean fluorescence intensity). (d) Western blot analysis of the marker proteins (i) CD63, (ii) CD81, and (iii) CD9 and (iv) Gluc on exosomes, respectively. Exosomes were purified from conditioned medium and characterized using western blot for the presence of typical exosomal markers CD63, CD81, and CD9. Additionally, Gluc detection by immunoblot of purified exosomes showed that hGluc-Lact fusion protein bound to the exosomal membranes.

A bioluminescence assay was then performed to confirm the presence of active luciferase on exosomes as well as to verify that the reporter is enriched on exosomes (**Fig. 2.3a**). Addition of luciferase substrate CTZ creates a bioluminescent signal whose intensity is proportional to the luciferase activity in the wells(Tannous et al., 2005). First, wells containing conditioned medium and its ultra-centrifugation supernatant from native 293T cells, hGluc 293T and hGluc-Lact 293T were measured for bioluminescent signals (**Fig. 2.3a**). Stronger signals in conditioned medium from hGluc 293T than those from hGluc-Lact 293T conditioned medium indicated that non-fused hGluc was secreted and was free from cells. Supernatant was separated from exosomes by ultra-centrifugation, and the bioluminescent signals in supernatant were of similar intensity to those from conditioned medium, confirming that free active hGluc was secreted as expected. Only isolated exosomes from hGluc-Lact 293T showed bioluminescence, indicating the lactadherin fused to hGluc kept the luciferase bound to the exosomes and could thus serve as a reporter for exosome spatial distribution in our subsequent studies. Moreover, quantitative analysis of bioluminescence from hGluc conditioned medium showed an approximately 10-fold greater signal than that from the hGluc-Lact conditioned medium ($P < 0.0001$, **Fig. 2.3b**). Isolated hGluc-Lact exosomes showed a much higher signal (> 100-fold, $P < 0.0001$, **Fig. 2.3c**) compared to exosomes derived from hGluc 293T, providing further evidence for successful production of exosome-bound luciferase reporter.

The stability of exosomes was analyzed at 37 °C, 25 °C, and 4 °C for 24 hours, using NanoSight analysis to evaluate whether or not temperature altered their size

distribution profiles (**Fig. S2.2a**). No significant difference was observed in exosome size among the three groups. In agreement with NTA, *in vitro* bioluminescence assays also revealed that the luciferase activity of exosomes was not affected by incubation at different temperatures for 24 hours (**Fig. S2.2b**). Similar to previous reports(Ge et al., 2014), the exosomes used in our present studies are highly stable under the conditions of the assays performed throughout these studies.

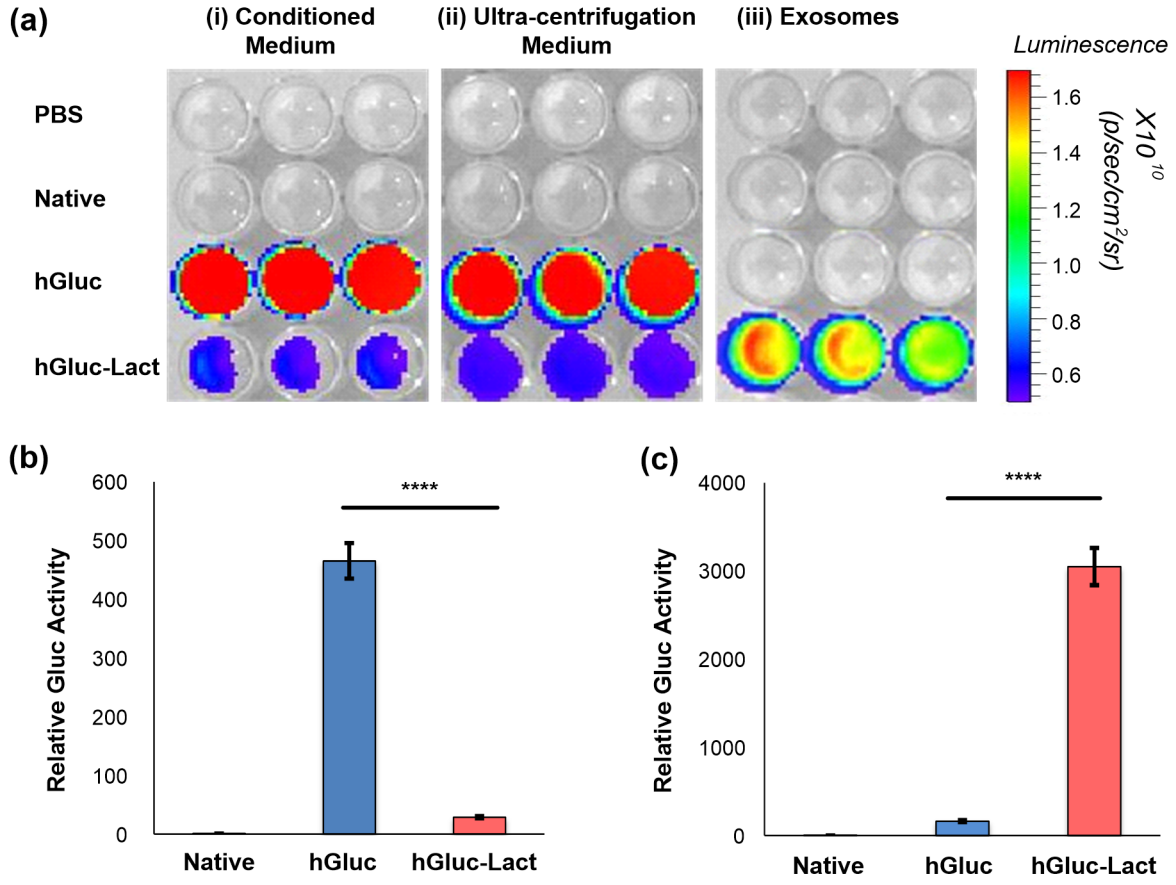

Fig. 2.3. Validation of hGluc-labeled exosomes using *in vitro* bioluminescence assays. (a) *In vitro* bioluminescence assay of conditioned medium, ultra-centrifugation supernatant and exosomes. (i) Conditioned medium collected from 293T cells, (ii) supernatant collected after serial steps of ultra-centrifugation and (iii) exosomes purified from 293T cells through ultra-centrifugation were diluted in PBS. CTZ was then added at a final concentration of 25 μM. *Gaussia* luciferase (hGluc) activity was measured using IVIS Lumina (exposure time 0.5s). (b) hGluc activity was significantly higher in conditioned medium. Error bar: mean ± SEM. ****P < 0.0001. (c) After ultra-centrifugation, hGluc activity was mainly detected in hGluc-Lact exosomes, indicating hGluc was enriched on exosomes. Error bar: mean ± SEM. ****P < 0.0001.

In vitro BBB model

BMEC monolayers were cultured on collagen I-coated transwell insert or coverglass to mimic *in vitro* the BBB, allowing us to investigate the mechanisms involved in exosome interaction with the BBB and its potential bypass. The disruption of the BBB has been described as a crucial step of the neuroinflammatory response in cerebral ischaemia, and the junctional permeability of the BBB is controlled in large part by cytokines and other CNS factors (Obermeier et al., 2013). With this understanding, we investigated the effect of the pro-inflammatory cytokine TNF-α on the tight junction (TJ) integrity and regulation of monolayer permeability in this BBB *in vitro* model (**Fig. 2.4a** and see also Methods). TNF-α is a prominent cytokine involved in neuroinflammatory conditions and influencing BBB properties, and therefore was used here to examine whether it alters the interaction of exosomes with BMECs. As TNF-α is known to induce activation of nuclear factor kappa B (NF-κB) cascade, ultimately leading to apoptosis of some of the cells (Wajant et al., 2003), the potential induction of apoptosis in BMECs by TNF-α was monitored using XTT proliferation assay. XTT assays revealed that intermediate concentrations of TNF-α did not significantly alter cell viability and therefore a concentration of 50 ng/mL was used throughout subsequent studies (**Fig. 2.S3**). The permeability across native BMECs monolayer (measured by FITC-dextran crossing through the transwells) steadily decreased during 48 hours in culture ($P < 0.0001$, **Fig. 2.4b**) as the cells grew next to each other and established their typical junctions in a honeycomb pattern, as expected (**Fig. 2.4c**). In accordance with previous studies on how BMEC monolayer is affected by TNF-α (Deli et al., 1995; Rochfort et al., 2014; Takeshita et al., 2014), the permeability of the BMEC monolayer

that was treated by TNF-α was significantly increased compared to the control BMEC monolayer ($P < 0.01$, **Fig. 2.4b**), suggesting that activation by this cytokine compromised BMEC integrity.

Inflammatory processes have been reported to induce changes in F-actin and vascular endothelial cadherin (VE-cadherin) in endothelial cells concomitant with rearrangement of tight junction components (Deli et al., 1995). As AJs and TJs play a major role in preventing passage through the BBB and maintaining intercellular tight junctions, we next examined if TNF-α alters the function of intercellular tight junctions. The VE-cadherin, zonula 30ccluding-1 (ZO-1) and Claudin-5 expression (**Fig. 2.4c**) were compared in cytokine activated and native conditions of BMECs. Concurrent with the increased paracellular permeability, treatment of confluent BMECs with TNF-α altered the expression of VE-cadherin, ZO-1 and Claudin-5, in which protein expressions were significantly decreased, suggesting a correlation in the levels and localization of these proteins with the integrity of AJs and TJs, as expected. In addition, TJ proteins (e.g., ZO-1) have been reported to shift from the membrane to cytoplasm and nuclei in ischemic hypoxia condition(Fischer et al., 2004). Similar results were also observed in our study in which immunostaining of TJ proteins showed a diffuse pattern at cell membrane, and some of them localized in the cytoplasm and nuclei (**Fig. 2.4c**). Together, these data imply that TNF-α activation leads to a relocalization of AJ and TJ proteins and this disassembly (i.e., protein downregulation and their disengagement of cognate paracellular ligands) is likely responsible for the altered intercellular permeability of BMECs under inflammatory conditions.

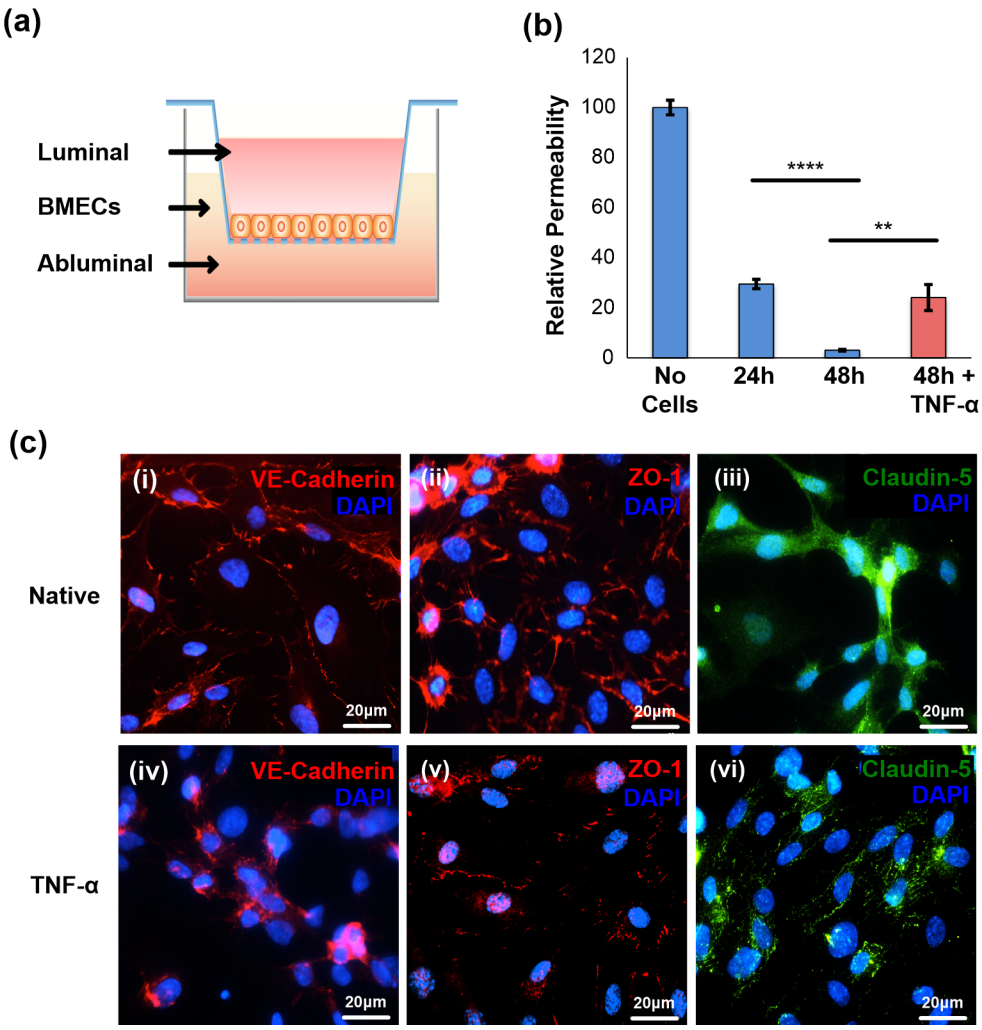

Fig. 2.4. *In vitro* model of the BBB using BMEC monolayer indicated that stroke-like conditions increased its permeability. (a) The schematic representation of the *in vitro* model of BBB. (b) A BMECs monolayer was grown for 24 or 48 hours in a transwell insert, and then treated with TNF-α for 6 hours. Permeability was measured using FITC-dextran. BMECs formed a low permeability barrier after 48 hours, and permeability was increased significantly under TNF-α condition. Values represent as means ± SEM of relative ratio normalized to no cell control, set as 100%. $^{**}P < 0.01$ and $^{****}P < 0.0001$ (c) Activation of BMECs with TNF-α regulates tight junction and adherens junction

protein expressions in BMEC monolayer on coverglass. Immunofluorescence of VE-cadherin, ZO-1, and Claudin-5 showed that their expression levels were dramatically down-regulated after TNF-α treatment. DAPI was used for staining nuclei. Scale bar: 20 μm.

Exosomes cross TNF-α activated BMEC monolayer in vitro via transcellular route

To investigate whether exosomes can cross the *in vitro* BBB model under normal and stroke-like conditions, transwell assays were performed using hGluc-Lact-labeled exosomes. Exosomes were added to the luminal chamber containing a confluent layer of BMECs (**Fig. 2.5a**), and conditioned medium from both the luminal and abluminal chambers were collected at several time points from 6 hours to 24 hours. hGluc activity in the collected conditioned medium was measured immediately after addition of the CTZ substrate. In transwell assays with native (untreated) BMECs, exosomes did not significantly cross the BMEC monolayer into the abluminal chamber, as shown by the lack of hGluc signal from the abluminal chamber and high signal from the luminal chamber (**Fig. 2.5b** and **2.5c**). However, when BMECs were activated by TNF-α induction, significantly higher hGluc signals could be observed in the abluminal chamber, i.e. up to approximately 10% of exosomes crossed from the luminal to abluminal chamber after 18 hours (**Fig. 2.5b** and **2.5c**). PBS and exosomes without hGluc used as negative controls did not reveal any significant bioluminescence, as expected (**Fig. 2.5b**). Thus, exosomes were able to cross the BMEC monolayer to the abluminal chamber, but only under the stroke-like conditions with TNF-α activated BMECs. Furthermore, such exosome crossing was observed to be significantly increased for TNF-α activated BMECs after a minimum of 18 hours of incubation ($P < 0.01$, **Fig. 2.5c**).

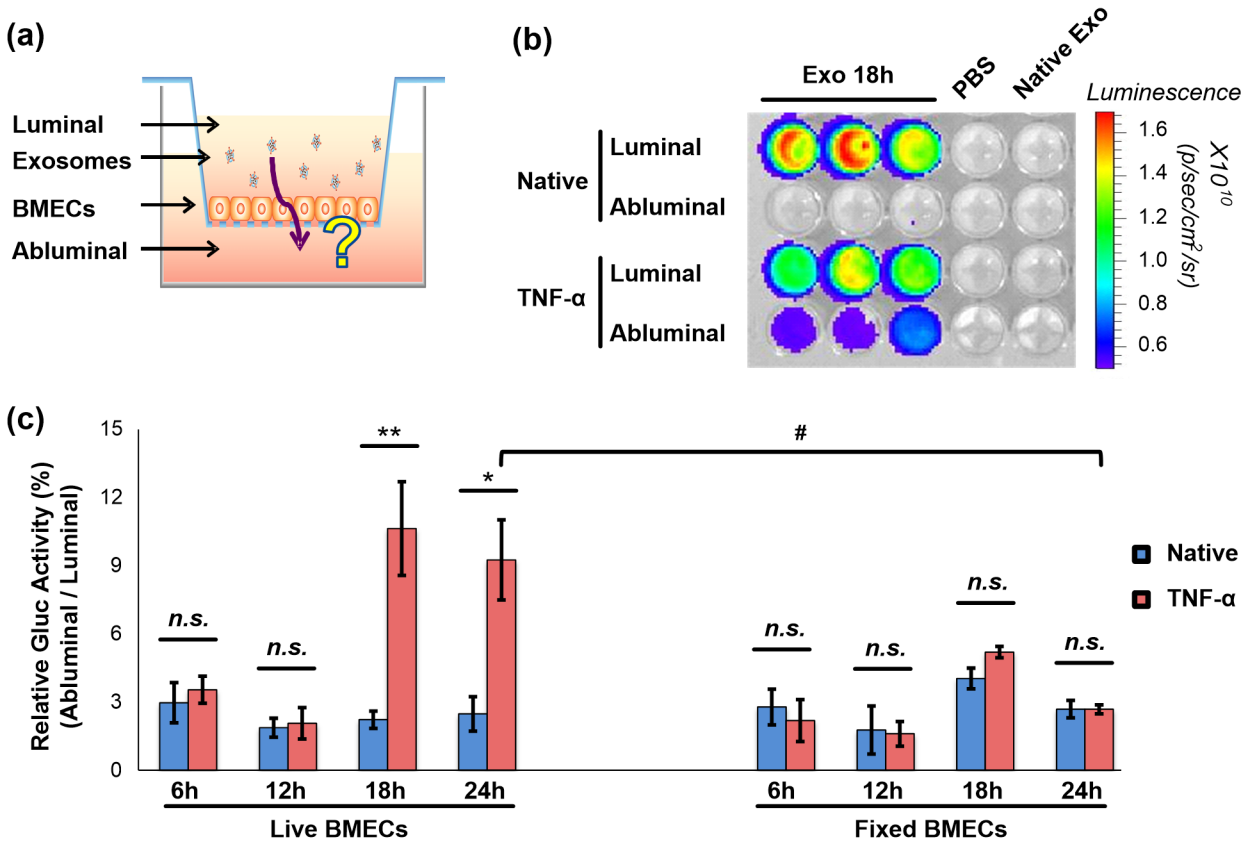

Fig. 2.5. Exosomes can cross BMEC monolayer under stroke-like conditions in a transwell assay. (a) Schematic representation of the *in vitro* model of the BBB. hGluc-Lact exosomes were added to the luminal chamber of the transwell and incubated with BMECs for various time points. Both luminal and abluminal chambers of conditioned medium were collected for bioluminescence assay. (b) and (c) Exosomes can cross BMECs in stroke-like conditions. (b) Representation of *in vitro* bioluminescence assay. Conditioned medium from both luminal and abluminal chambers were collected after exosome incubation and CTZ was added at a final concentration of 25 μM. *Gaussia* luciferase activity was measured immediately thereafter using IVIS Lumina (exposure time 0.5s). (c) Quantitative analysis of *in vitro* bioluminescence assay of hGluc-Lact exosomes crossing both live and fixed BMECs at different time points. Relative Gluc

Activity = (abluminal chamber signal – native exo signal) / (luminal chamber signal – native exo signal) × 100%. Error bar: mean ± SEM. Native vs. TNF-α: *n.s.*, not significant, $^{*}P < 0.05$ and $^{**}P < 0.01$. Live BMECs (TNF-α) vs. Fixed BMECs (TNF-α) at 24 hours: $^{\#}P < 0.05$.

As hGluc is a secreted protein with the molecular size 19kDa, it is expected to diffuse passively between the two chambers. Indeed, incubation of hGluc conditioned medium with BMECs in both native and TNF-α treated conditions revealed that hGluc can freely cross from luminal chamber to abluminal chamber in both conditions (**Fig. 2.S4**). Therefore, to confirm that the hGluc activity observed from the transwell assays came directly from the exosomes instead of free hGluc detaching off the membrane, hGluc-Lact exosomes were directly labeled with PKH67 and added to the luminal chamber of a transwell assay with TNF-α activated BMECs. Conditioned medium from abluminal chamber was collected after 18 hours as above mentioned, and then added to a plate of fresh BMECs (**Fig. 2.6a**). PKH67 signal from exosomes can be seen clearly at perinuclear regions after 6 hours of incubation with fresh BMECs, (**Fig. 2.6b**, panel iv-vi), but conditioned medium containing free hGluc labeled with PKH67 used as a control displayed no signal, as was also the case abluminal chamber conditioned medium and fresh cells, as expected (**Fig. 2.6b**, panel i-iii). This, combined with the previous assay, demonstrated that exosomes can carry at least one defined protein cargo, in this case hGluc reporter enzyme as a model system, across a BMEC monolayer under stroke-like conditions, and therefore the hGluc activity observed from the transwell system was truly from the hGluc-exosomes instead of free hGluc.

In order to test if the difference in density between exosomes and growth medium has any effects on the BMEC monolayer crossing through gravity, hGluc-Lact exosomes were added to the abluminal (lower) chamber after BMEC stimulation with TNF-α (**Fig. 2.6c**). After 18 hours of incubation, hGluc activity was measured in the

conditioned medium from the luminal (upper) chamber and was found to be significantly higher in BMECs activated with TNF-α compared to untreated (native) BMECs ($P < 0.05$, **Fig. 2.6d**). In other words, regardless of whether exosomes were added to upper or lower chambers, about 10% of them crossed the TNF-α treated BMEC monolayer, but they did not cross the untreated BMEC monolayer. Thus, the difference in exosome density and pull of gravity has little effects on their crossing, and it is equivalent to add exosomes to either upper or lower transwell chambers to study their crossing BMEC monolayers. Collectively, these results further suggest that exosomes can cross the activated, but not native, BMEC monolayer mimicking stroke-like conditions.

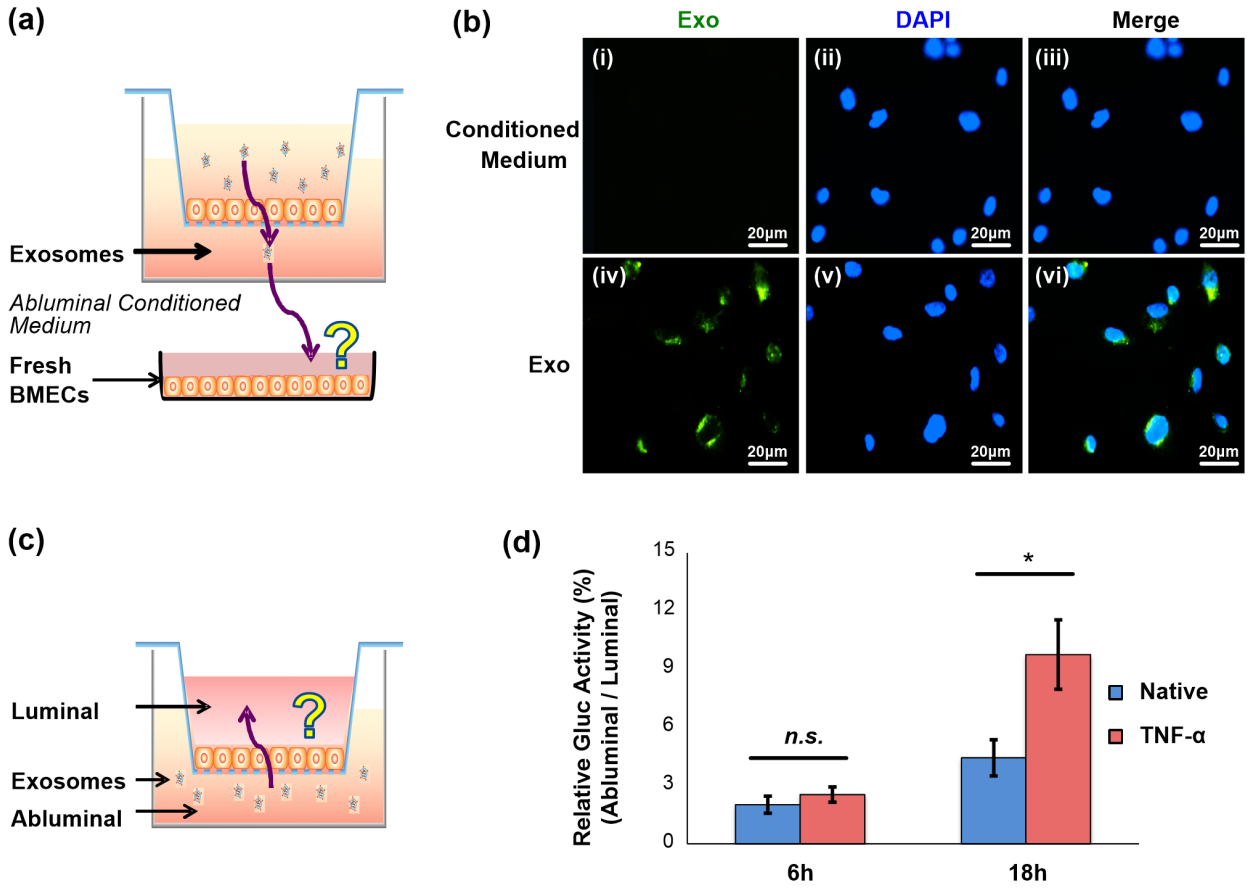

Fig. 2.6. Validation of exosome crossing BMEC monolayers. (a) Exosomes can cross the BMECs carrying hGluc *in vitro.* hGluc-Lact exosomes were labeled with the lipophilic dye PKH67, and were added to the luminal chamber of the transwell. Conditioned medium from abluminal chambers were collected and then incubated with a monolayer of BMEC on coverglass to further confirm the hGluc activity observed from bioluminescence assay was directly from exosomes. (b) Exosomes uptake by BMECs. hGluc conditioned medium of abluminal chamber stained with PKH67 was used as a control. Scale bar: 20 μm. (c) The schematic representation of exosome migration from abluminal chamber to the luminal chamber under native and TNF-α-treated conditions. (d) Quantitative analysis of exosome migration from abluminal to luminal chamber at 6

hours and 18 hours. Relative bioluminescence activity suggested that there was no significant difference between native and TNF-α-treated conditions at 6 hours, whereas the relative bioluminescence activity is significant higher in BMECs treated with TNF-α at 18 hours. Relative Gluc Activity = (luminal chamber signal – native exo signal) / (abluminal chamber signal – native exo signal) × 100%. Error bar: mean ± SEM. *N.s.*, not significant and $*P < 0.05$.

To further delineate by which mechanisms exosomes cross a BMECs monolayer, we next evaluated whether or not exosomes can also cross the *in vitro* BBB through passive diffusion of the paracellular route (i.e. though intercellular junctions between BMECs). In addition to a live BMECs transwell bioluminescence assay as in previous experiments, confluent BMEC monolayers (untreated or TNF-α activated) grown on the transwell insert were fixed with PFA, and exosomes were added for various time periods (6, 12, 18 and 24 hours) as before. Notably, no significant differences in bioluminescence activity were observed for fixed BMECs under both TNF-α activated and untreated conditions at all time points, unlike the much greater exosome crossing of the living BMECs under TNF-α compared to untreated condition. This data indicates that the paracellular diffusion route contributes little to the overall exosome crossing, i.e. no more than the background signal (e.g. native BMECs at 6 hours, Fig. 4c). Additionally, exosomes added to living BMECs treated with TNF-α showed significantly increased migration across the BMECs monolayer compared to that of exosomes added to fixed BMECs treated with TNF-α (for the 24 hour time point, $P < 0.05$, Fig. 4c). This suggested that the transcellular route, which operates only in the case of live but not fixed BMECs, likely accounts for majority of migration of exosomes across the BMEC monolayer.

Exosomes are internalized by BMECs via endocytosis

Internalization of exosomes, MVB formation and subsequent exocytosis (i.e. transcytosis) is one proposed mechanism(Svensson et al., 2013) of exosome trafficking across the BMEC monolayer. To elucidate the mechanisms of exosome crossing in our

study, microscopy experiments were performed to examine the interaction of exosomes with BMECs under both native and TNF-α activated conditions, and in the absence or presence of various endocytosis inhibitors. PKH67-labeled exosomes were incubated with CellMask-labeled BMECs (deep red) for 1, 3, 6, 12, 18 or 24 hours on coverglass. Confocal microscopy analysis was conducted to measure exosome uptake by BMECs (**Fig. 2.7a** and **2.7b**). Briefly, cells were washed to remove any membrane-bound exosomes before sample preparation and the fluorescence intensity of intracellular exosomes that were specifically associated with the cells was then quantified (**Fig. 2.7b**, see also Methods). Fluorescence intensity analysis demonstrated that BMECs uptake exosomes in a time dependent manner, as exosome internalization was increased with longer incubation time (**Fig. 2.7b**). Furthermore, cells treated with TNF-α showed more uptake than native cells at 12 and 18 hours ($P < 0.05$, **Fig. 2.7b**), consistent with previous studies in which TNF-α activation resulted in an increase in nanocarrier internalization in brain endothelial cells(Hsu et al., 2014). Therefore, these data indicated that exosomes can be robustly internalized by BMECs. Native and TNF-α activated BMECs were observed to endocytose exosomes at similar rates up to 12 hours. Then the endocytosis of native cells kept increasing ($P < 0.05$, **Fig. 2.7b**) while that of TNF-α activated BMECs remained the same ($P = 0.15$, Fig. 6b). Interestingly, discrepancy between uptake (**Fig. 2.7**) and transwell (**Fig. 2.5**) assays was observed in that 1) the transwell data showed no significant exosome bypassing BMECs, regardless native and TNF-α activated conditions, within 12 hours, while uptake data demonstrated exosomes are being internalized by both native and TNF-α activated BMECs within the same time period, and 2) exosomes only bypass TNF-α activated but not native BMECs

(at later time points (i.e., 18 h and 24 h), whereas exosomes can be uptaken by both native and TNF-α activated BMECs. The reason for these observations remains unclear, however, it could be due to the active and unregulated exocytosis processes in TNF-α activated BMECs.

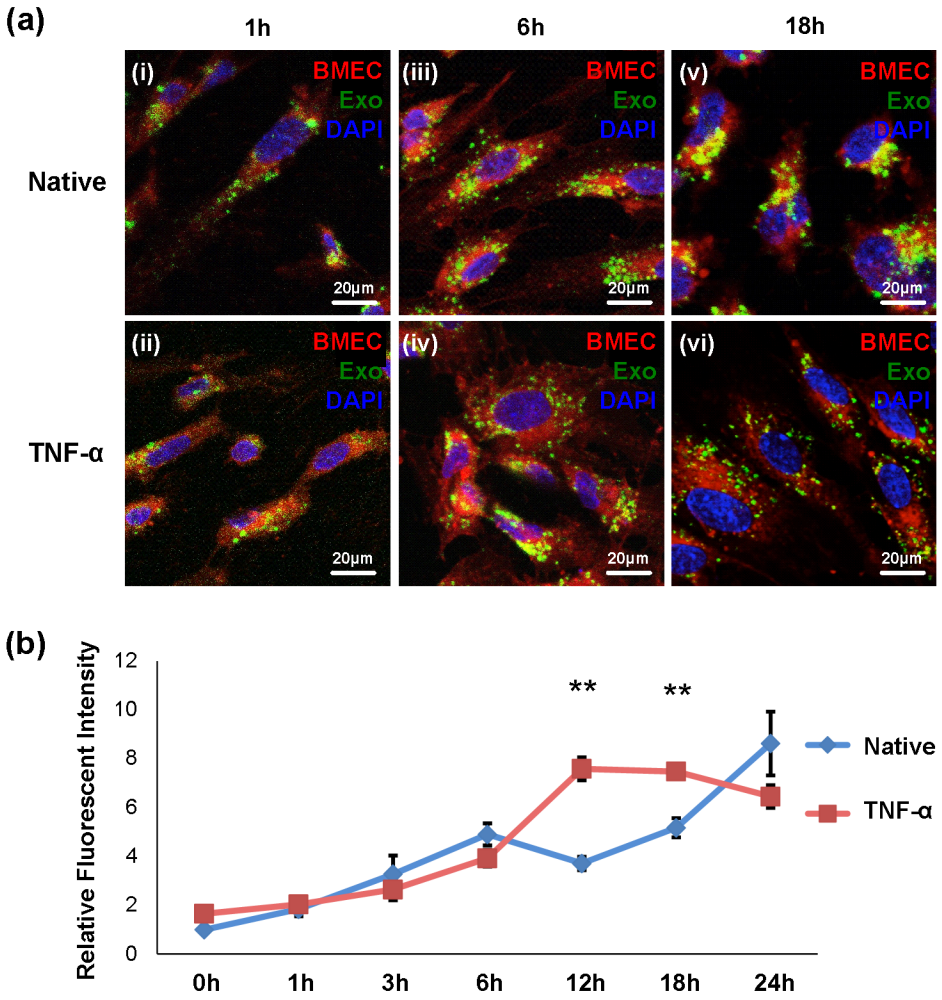

Fig. 2.7 Exosome uptake by BMECs. (a) and (b) Confocal microscopy analysis of exosome uptake by BMECs. (a) Representative pictures of exosome uptake under normal and stroke-like conditions at selected time points (1, 6 and 18 hour). Exosomes were labeled with PKH67 (green), BMECs were stained with CellMask (deep red), and DAPI (blue) was used for staining nuclei. Scale bar: 20 μm. (b) Quantitative analysis of fluorescence intensity of the PKH67-labeled exosomes. Briefly, the outline of each cell (n > 30) was drawn referring to the cell membrane labeling. The fluorescence intensity of intracellular exosomes that were specifically associated with the cells was then quantified (see Methods). Error bar: mean ± SEM. $^{**}P < 0.01$.

In order to study the intracellular trafficking of internalized exosomes in BMECs, early and late endosomal markers were used to identify endosomal trafficking machinery. BMECs were pre-incubated with cholera toxin B (CtxB), a late endosomal compartment marker, and cultured with PKH67-labeled exosomes for 1 or 3 hours. Confocal microscopy analysis revealed that colocalization of exosomes and CtxB was observed at 1 hour (**Fig. 2.8a**, panel i and ii), and accumulation of colocalization was significantly increased at 3 hours in both native and TNF-α treated BMECs ($P < 0.05$, **Fig. 2.8a**, panel iii and iv and **2.8b**), in agreement with our previous data showing the uptake of exosomes in a time-dependent manner (**Fig. 2.7a** and **2.7b**). Internalized exosomes were also observed to co-localize with transferrin (Tfn)-Texas Red, an early endosome marker, in BMECs (**Fig. 2.8c** and **2.8d**). Taken together, these data suggest that exosomes can be internalized by BMECs and subsequently trafficked via endocytic mechanisms.

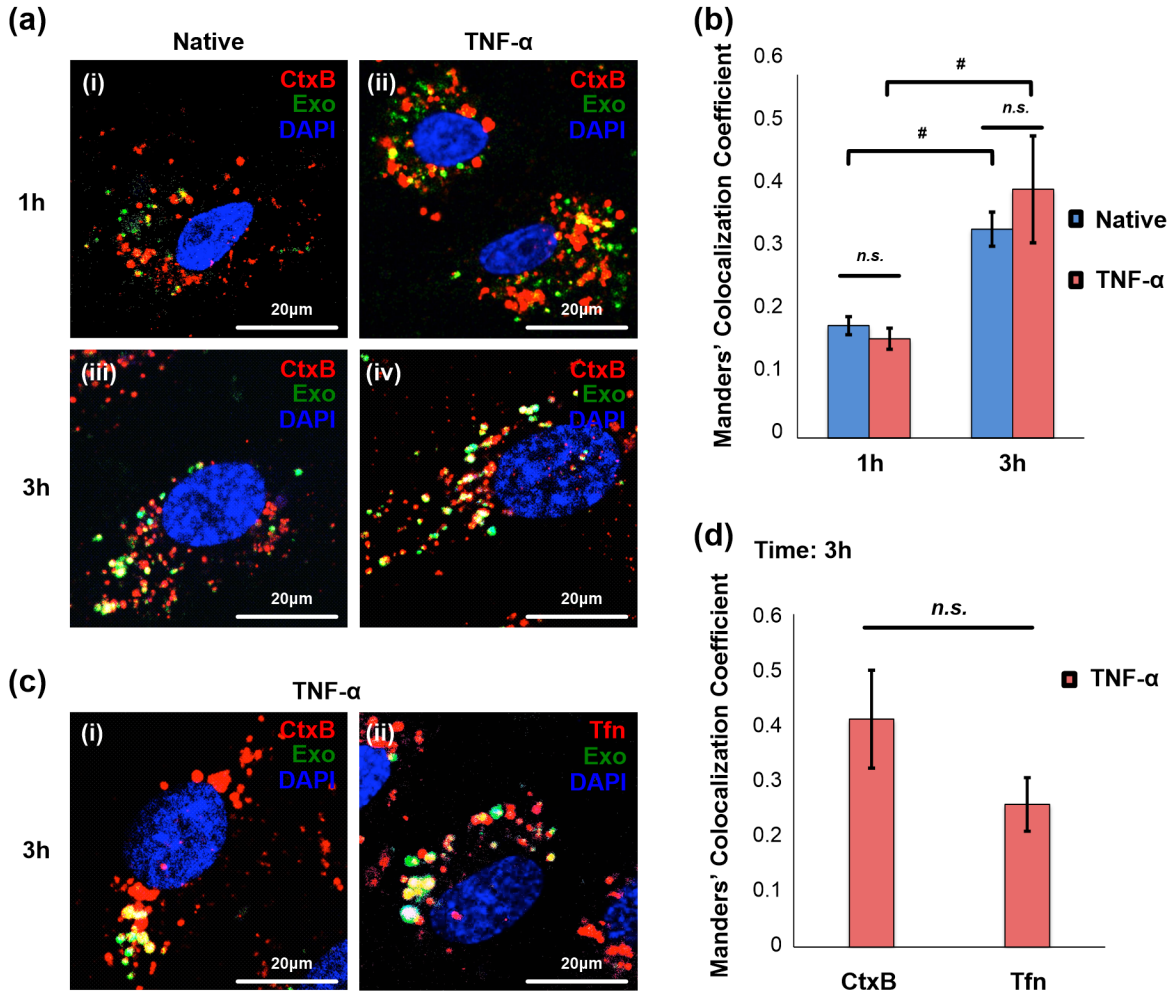

Fig. 2.8 Exosome colocalization with early and late endosomes. (a and b) Confocal microscopy analysis shows colocalization of cholera toxin B (CtxB) with exosomes. (a) Representative pictures of colocalization of CtxB with exosomes under normal and stroke-like conditions at 1 and 3 hours. Endosomes of BMECs (red, native or TNF-α stimulated) were stained with CtxB-biotin conjugated with Alexa Fluor 594-streptavidin for 30 minutes and then washed. PKH67-labeled exosomes (green) were incubated with BMECs for 1 or 3 hours. DAPI was used for staining nuclei. Scale bar: 20 μm. (b) Quantitative analysis of colocalization of CtxB with exosomes. Manders' Colocalization Coefficient denotes the fraction of endosome membrane co-localized with exosomes.

The coefficient tends to “1” if the exosomes are highly colocalized with endosomes. Error bar: mean ± SEM. Native vs. TNF-α: $^{*}P < 0.05$. Native 1 hour vs. 3 hours or TNF-α 1 hour vs. 3 hours: $^{\#}P < 0.05$. (c and d) The colocalization of early (Tfn) and late (CtxB) endosomes and exosomes. (c) Representative pictures of colocalization of (i) CtxB and (ii) Tfn with exosomes under stroke-like conditions at 3 hours. PKH67-labeled exosomes (green) were incubated with TNF-α stimulated BMECs for 3 hours, and then endosomes of BMECs (red) were stained with CtxB-Alexa Fluor 594 or Tfn-Texas Red; DAPI was used for staining nuclei. Scale bar: 20 μm. (d) Quantitative analysis of (c) to measure the association of exosomes with CtxB or Tfn. Error bar: mean ± SEM. *N.s.*, not significant.

To study the active transcellular route of exosomes across the BMEC monolayer *in vitro*, a pulse-chase analysis and transwell assay were employed. Pulse-hGluc-Lact exosomes were added to the luminal chamber and incubated with cells for 6 hours. For exosome chasing, hGluc-Lact exosomes were then removed and cells were washed prior to addition of unlabeled exosomes. Cells were then incubated with unlabeled exosomes for 6 and 18 hours (**Fig. 2.9a**). Conditioned media from both luminal and abluminal chambers were collected, and luciferase activity was measured from combined luminal and abluminal chambers (since BMECs are expected to secrete on both sides) and normalized to total hGluc-Lact exosomes at 0 h. In other words, the relative luciferase activity of secreted exosomes over total input exosomes indicated the percentage of exosomes secreted by BMECs. Bioluminescence activity was observed in both luminal and abluminal chambers, revealing the secretion of hGluc-Lact exosomes by exosome-pulsed BMECs in a time dependent manner ($P < 0.0001$ **Fig. 2.9b**). Importantly, a significant increase of exosome secretion was found in the TNF-α stimulated condition compared to unstimulated condition ($P < 0.05$, T = 6 h; $P < 0.05$, T = 12 h and $P < 0.01$, T = 24 h, **Fig. 2.9b**), which is consistent with the observation of increased exosome uptake by BMECs leading to subsequent increased exocytosis.

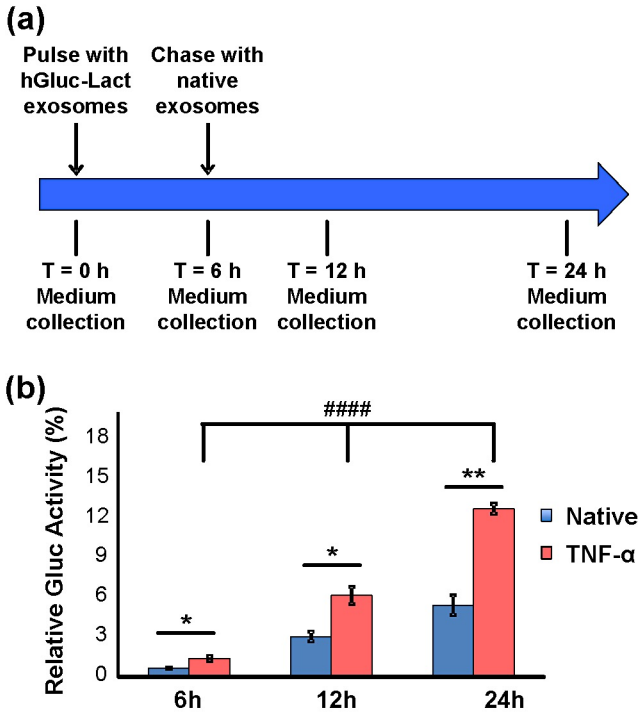

Fig. 2.9. Exosomes were exocytosed by BMECs in a transwell assay. (a) Illustration of the pulse-chase experiment to study exosome exocytosis *in vitro*. (b) Conditioned medium from BMECs pulsed for 6 hours with hGluc-labeled exosomes and chased with unlabeled exosomes (at indicated time points) was collected from both luminal and abluminal transwell chambers at indicated time points and hGluc activity was measured using IVIS Lumina (CTZ final concentration: 25 μM, exposure time: 0.5s). Error bar: mean ± SEM. Native vs. TNF-α: $^{*}P < 0.05$ and $^{**}P < 0.01$. Under TNF-α condition: $^{\#\#\#\#}P < 0.0001$, as determined by one-way ANOVA with SNK *post hoc* tests.

Exosome internalization by BMECs includes clathrin-dependent and caveolae-dependent routes

As previous studies have reported that cell uptake of exosomes includes an active endocytosis mechanism (Svensson et al., 2013), (Mulcahy et al., 2014), using uptake assay we next examined whether or not exosome uptake by BMECs and transmigrate the BMEC monolayer is an energy-requiring process or a passive membrane diffusion process (**Fig. 2.10**). Incubation of cells with exosomes at 4°C for 1 hour significantly reduced exosome uptake compared to the usual 37 °C incubation, indicating the operation of an energy–dependent process ($P < 0.05$, **Fig. 2.11c**). Exosomes can be internalized into target cells through different mechanisms, including phagocytosis, macropinocytosis, clathrin-mediated endocytosis (CME), lipid raft (caveolae)-mediated endocytosis and plasma membrane fusion(Mulcahy et al., 2014; Svensson et al., 2013; Thery et al., 2009). Therefore, we further investigated which endocytic pathways were most involved in exosome entry into BMECs. Various pharmacological inhibitors of endocytic transport, including amiloride, a Na^+/H^+ exchanger to block macropinocytosis; filipin III, methyl-β-cyclodextrin (MβCD), nystatin, to inhibit lipid raft/caveolae-mediated endocytosis; chlorpromazine (CPZ), to inhibit clathrin-dependent endocytosis, and cytochalasin D, to depolymerize actin and inhibit fluid-phase macropinocytois were used to examine exosome transcellular trafficking across the BMECs monolayer (**Fig. 2.10**).

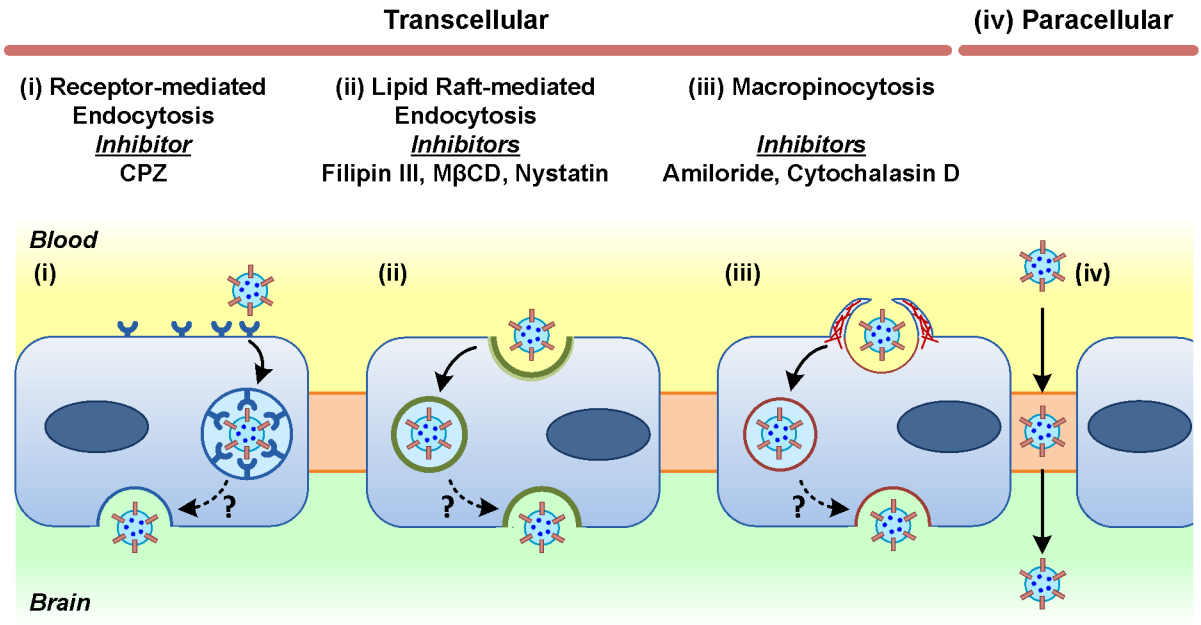

Fig. 2.10. Potential mechanisms of exosome crossing the blood-brain barrier (BBB). Schematic representation of the proposed mechanisms on how exosomes cross the BBB, and diagram of the major endocytic pathways as well as their corresponding inhibitors used in this study.

As cytotoxicity and specificity of endocytosis inhibitor were reported to be cell-type dependent(Vercauteren et al., 2010), the cellular viability of BMECs after treatment with the various concentrations of endocytosis inhibitors was measured using XTT assay. Cellular viability was significantly reduced only at high concentration of most inhibitors, and therefore the concentrations of endocytosis inhibitors used in all subsequent studies were: CPZ (15 μM), cytochalasin D (20 μM), amiloride (1 mM), methyl- β –cyclodextrin (MβCD, 5 mM), filipin III (5 μM), or nystatin (5 μM) (**Fig. 2.11a**). Next, we examined the effectiveness and specificity of endocytosis inhibitors at the concentrations determined above using endocytic markers specific for each endocytosis mechanism. Transferrin, CtxB, and dextran were shown to be internalized by CDE, caveolae-mediated endocytosis, and macropinocytosis, respectively(Svensson et al., 2013)' (Tian et al., 2014). Treatment with amiloride and cytochalasin D were shown to specifically inhibit macropinocytosis, and CPZ was revealed to significantly inhibit CDE. Treatment with filipin III, MβCD, or nystatin prior to CtxB incubation exhibited a significant reduction in dye uptake, confirming a blockage of caveolae-mediated endocytosis (**Fig. 2.11b**).

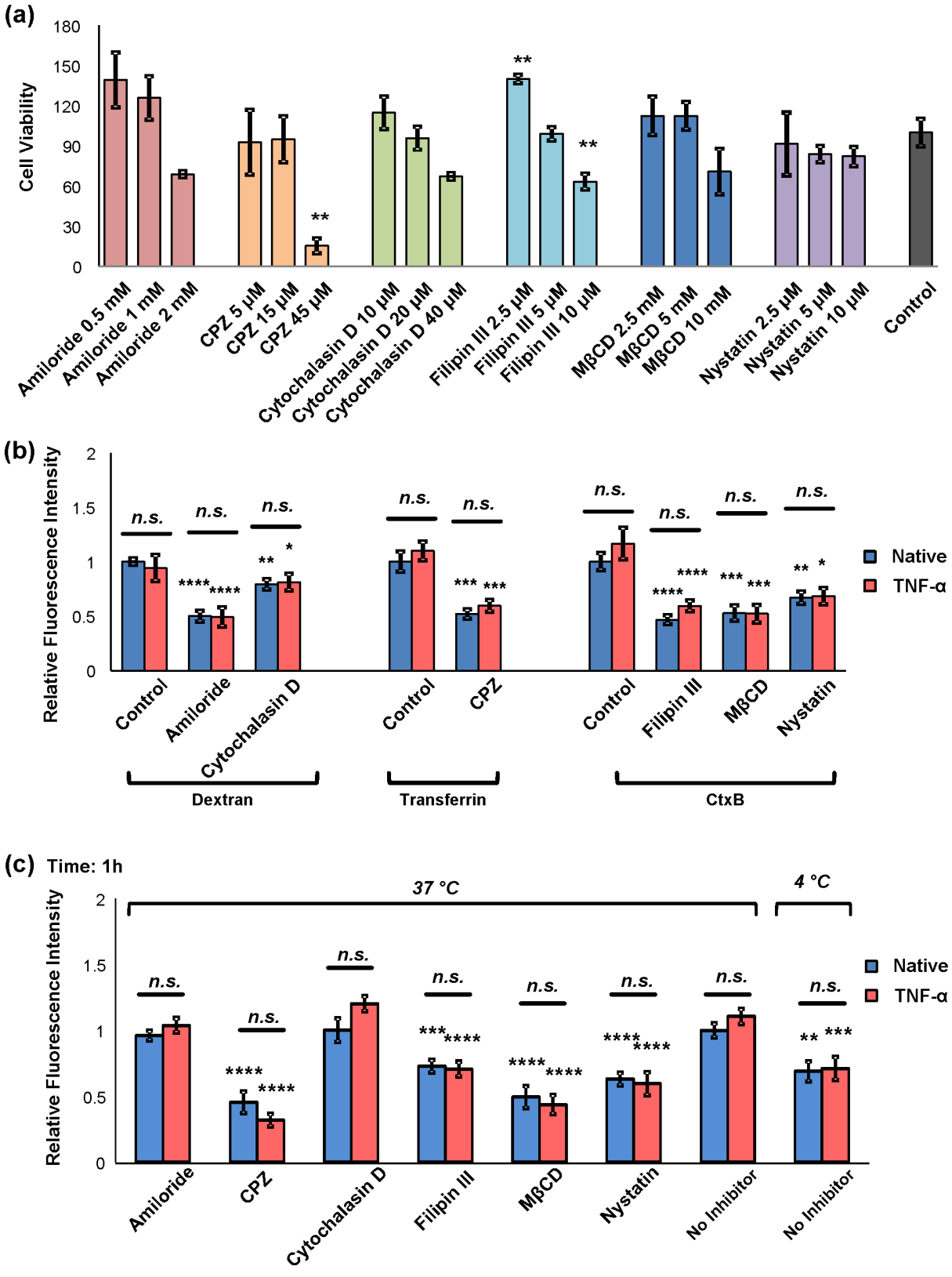
(a)
Cell Viability
180
150
120
90
60
30
0
Amiloride 0.5 mM
Amiloride 1 mM
Amiloride 2 mM
CPZ 5 μM
CPZ 15 μM
CPZ 45 μM
Cytochalasin D 10 μM
Cytochalasin D 20 μM
Cytochalasin D 40 μM
Filipin III 2.5 μM
Filipin III 5 μM
Filipin III 10 μM
MβCD 2.5 mM
MβCD 5 mM
MβCD 10 mM
Nystatin 2.5 μM
Nystatin 5 μM
Nystatin 10 μM
Control
(b)
Relative Fluorescence Intensity
2
1.5
1
0.5
0
n.s.
Control
Amiloride
Cytochalasin D
CPZ
Filipin III
MβCD
Nystatin
Dextran
Transferrin
CtxB
Native
TNF-α
(c)
Time: 1h
37 °C
4 °C
Relative Fluorescence Intensity
Amiloride
CPZ
Cytochalasin D
Filipin III
MβCD
Nystatin
No Inhibitor
No Inhibitor
Native
TNF-α

Fig. 2.11. Effects of endocytosis inhibitors on exosome internalization. (a) BMECs were treated with the indicated endocytosis inhibitors for 30 minutes, and then cell viability was determined by XTT assay. Relative cell viability was normalized to the vehicle control (no inhibitor) set as 1. Error bar: mean ± SEM.*P < 0.05 and **P < 0.01, as determined by one-way ANOVA with SNK post-hoc test. (b) BMECs were pretreated with inhibitors or vehicle (no inhibitor), followed by incubation with Texas Red-transferrin, Alexa Fluor 594-CtxB, or Alexa Fluor 594-dextran. Cellular uptake was measured by fluorescence microscopy and fluorescence intensity was quantified and displayed in the bar graphs. Error bar: mean ± SEM. *N.s.*, not significant, *P < 0.05, **P < 0.01, ***P < 0.001 and ****P < 0.0001. (c) BMECs were pretreated with indicated inhibitors: amiloride (1mM), CPZ (15 μM), cytochalasin D (20 μM), filipin III (5 μM), MβCD (5 mM), nystatin (5 μM) for 30 minutes at 37 °C. Exosomes labeled with PKH67 were incubated with BMECs at 37 °C for 1 hour, and their uptake was imaged with confocal microscopy and quantified as described in Methods. Error bar: mean ± SEM. Native vs. TNF-α: *n.s.*, not significant, **P < 0.01 and ****P < 0.0001. Conditions compared were: native (unstimulated BMECs) in the absence of inhibitors vs. In the presence of inhibitors, and native BMECs vs TNF-α-stimulated BMECs in the absence or presence of inhibitors: *P < 0.05, **P < 0.01, ***P < 0.001 and ****P < 0.0001, compared to native no inhibitor or TNF-α no inhibitor conditions, respectively.

To study which mechanisms were mostly involved in exosome endocytosis pathways, cells were pretreated with endocytosis inhibitors for 30 minutes follow by exosomes incubation for 1 hour. Exosome uptake was significantly inhibited by filipin III (73% for native, $P < 0.001$ and 64% for TNF-α, $P < 0.0001$, respectively), MβCD (49% for native, $P < 0.0001$, and 39% for TNF-α, $P < 0.0001$, respectively), and nystatin (63% for native, $P < 0.0001$, and 54% for TNF-α, $P < 0.0001$, respectively) (**Fig. 2.11c**), suggesting lipid raft disruption blocked exosome internalization. Therefore, caveolae-dependent endocytosis is one likely route of exosome internalization. Similarly, clathrin-dependent endocytosis inhibition by CPZ attenuated uptake of exosomes in BMECs (45% for native and 29% for TNF-α, $P < 0.0001$), also suggesting the involvement of this endocytic pathway. To further corroborate these data, the transwell bioluminescence assay was employed to estimate the contribution of the different endocytosis mechanisms under native and activated (TNF-α) conditions. Pretreatment of most inhibitors followed by 6 hours' incubation of exosomes showed similar results of exosome crossing in both native and TNF-α treated BMECs which are minimal in both cases (**Fig. 2.12a**). Interestingly, filipin III showed a promotional effect on exosome migration in both conditions. This is probably due to a high concentration of filipin III (5 μM) used in this study, which led to membrane permeabilization and an increase of exosome transport(Schnitzer et al., 1994). Most inhibitor treatments resulted in a significant reduction of exosome migration from luminal to abluminal chamber at 18 hours most notably in the case of TNF-α treated BMEC system while minimal exosome bypassing native BMECs was observed with or without inhibitor treatment (**Fig. 2.12b**). The attenuation of exosome crossing by inhibition of endocytosis indicated that

exosomes cross TNF-α treated BMEC monolayer largely via the transcellular route. Importantly, multiple endocytosis mechanisms (as judged by the effects on exosome crossing exerted by their corresponding inhibitors) are likely involved in exosome transcellular migration. For example, abrogation of caveolae-mediated endocytosis by cholesterol-depleting agents MβCD and filipin III resulted in significant reductions in exosome transcellular migration (**Fig. 2.12**). Likewise, inhibition of clathrin-dependent endocytosis by CPZ (which decreases the formation of clathrin-coated pits at the plasma membrane) suggested that the uptake and transport of exosomes across the BMECs is also dependent on clathrin-mediated endocytosis (**Fig. 2.12**). However, cytochalasin D, which has been reported to increase dextran uptake and decrease microparticle uptake in human brain endothelial cells(Faille et al., 2012), here altered exosome intracellular trafficking in both native and TNF-α stimulated conditions. Moreover, another inhibitor, amiloride, which has been reported to alter intracellular pH homeostasis, here also reduced exosome migration during the TNF-α activated condition. One possible explanation could be that changes in intracellular pH delayed altered lysosome acidification and subsequently diminished exosome exocytosis.

Intriguingly, a relative reduction in exosome crossing through the BMEC monolayer was observed when cells were treated with TNF-α at 4°C compared to the native BMECs at 4°C ($P < 0.01$, **Fig. 2.12**), suggesting low temperature might also attenuate TNF-α induced changes in the BBB barrier function. Additionally, exosomes were incubated at 37°C and 4°C under the complete absence of cells to determine any measurable temperature effects on the exosome diffusion rate. No significant

differences between 37°C and 4°C were observed when incubating exosomes for 6, 18, and 24 hours in the absence of a BMEC monolayer (**Fig. 2.S5**), suggesting that temperature effects did not affect the background diffusion of exosomes.

These inhibitor studies are generally consistent with clathrin and caveolae-mediated mechanisms of exosome internalization of BMECs suggested by examination of the colocalization of early and late endocytic markers. That is, colocalization of exosomes and Tfn, which is a marker of clathrin-mediated endocytosis, confirmed the exosome uptake by BMECs involves clathrin-dependent endocytosis mechanism (**Fig. 2.8c** and **2.8d**). Likewise, colocalization of exosomes and CtxB, which is a marker of caveolae-mediated endocytosis, verified that exosome internalization is associated with lipid raft-mediated endocytosis (**Fig. 2.8a** and **2.8b**). Together, these data suggested that exosomes could cross the *in vitro* BBB model through primarily transcellular routes rather than the passive paracellular route. For the transcellular crossing, both clathrin-mediated endocytosis and caveolae-mediated endocytosis likely play important roles in exosome transport.

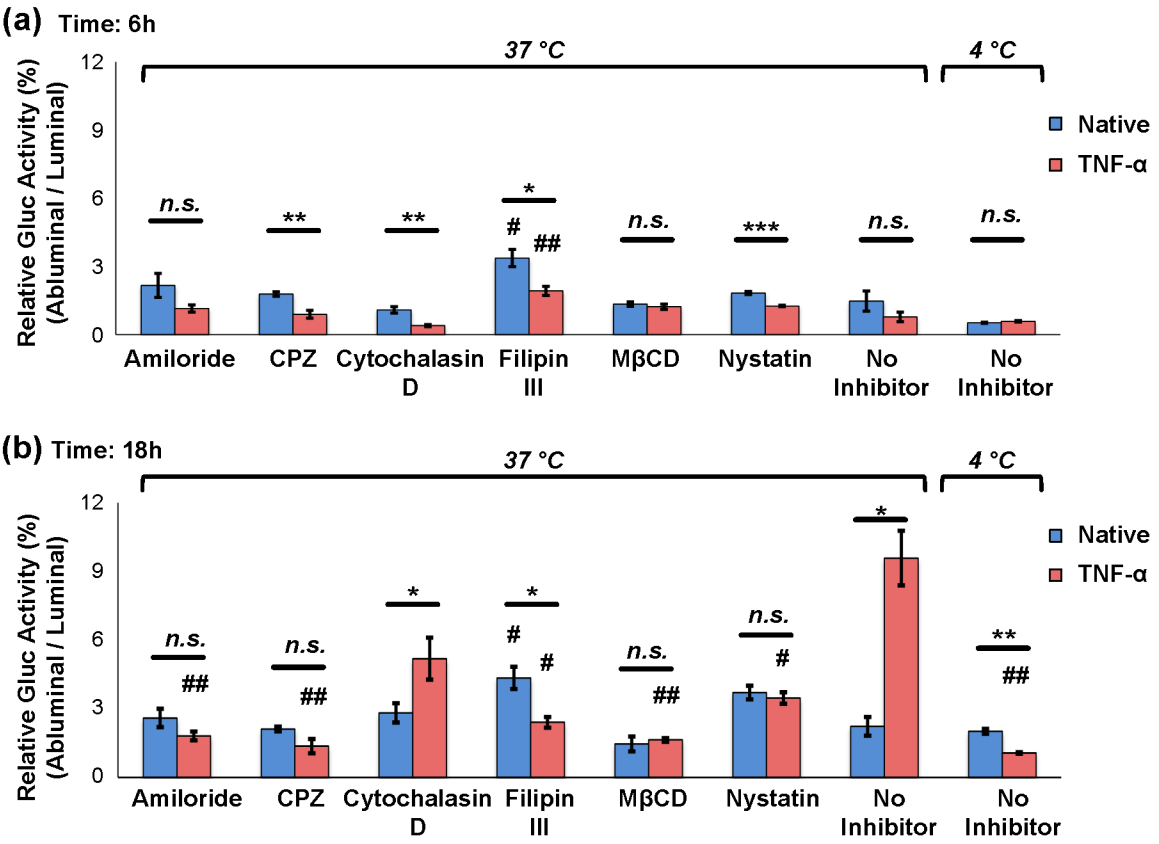

Fig. 2.12. Inhibition of endocytosis decreases exosome crossing the *in vitro* BBB. BMECs were pretreated with indicated inhibitors: amiloride (1mM), CPZ (15 μM), cytochalasin D (20 μM), filipin III (5 μM), MβCD (5 mM), nystatin (5 μM) for 30 minutes at 37 °C, respectively. hGluc-Lact exosomes were subsequently added to the luminal chamber of each transwell and incubated with BMECs for various time points (6 and 18 hours). Cells treated with vehicles (no inhibitor) alone were used as a negative control. To study the temperature effect on endocytosis, BMECs containing exosomes were incubated at either 37 °C or 4 °C for (a) 6 and (b) 18 hours, and then conditioned medium from both luminal and abluminal chambers were collected and *Gaussia* luciferase activity was measured immediately after addition of its substrate CTZ (IVIS Lumina, exposure time: 0.5s). Relative Gluc Activity = (abluminal chamber signal –

native exo signal) / (luminal chamber signal – native exo signal) × 100%. Error bar: mean ± SEM. Native vs. TNF-α: *n.s.*, not significant, **P* < 0.05 and ***P* < 0.01. $^{\#}P$ < 0.05 and $^{\#\#}P$ < 0.01, compared to native no inhibitor or TNF-α no inhibitor conditions, respectively.

2.4 Conclusions

The BBB, also referred to as the blood-brain interface(Banks, 2016), protects the brain from harmful chemicals or toxins from the systemic circulation, yet it also results in the inability of most therapeutics to cross the BBB and reach the CNS. So far, several approaches have been investigated to increase the transport of therapeutics to the brain, including local invasive intracerebroventricular (ICV) infusion, intranasal administration, induction of permeability by temporary disruption of the BBB (e.g., by ultrasound), use of prodrugs that can bypass BBB, pharmacological strategies using colloidal drug carriers such as nanoparticles or liposomes, more complex methods using endogenous transport mechanisms (either receptor mediated transport of chimeric proteins or carrier mediated transport of nutrients), and transient inhibition of drug efflux mechanisms (Banks, 2016; Dobson and Kell, 2008; Etame et al., 2012; Pardridge, 2015a, b). Nevertheless, delivering therapeutic and diagnostic agents across the BBB remains a daunting challenge.

Exosomes are involved in a variety of activities in the CNS, including neuron-glia communication, inducing neurite outgrowth and neuronal survival, transfer of toxic proteins including β-amyloid peptide that contributes to pathogenic amyloid-β deposition, mediation of neuronal development, and modulation of synaptic activity (El-Andaloussi et al., 2013; Fruhbeis et al., 2012; Kalani et al., 2014). Endogenously as well as exogenously administered exosomes may be potential therapeutic agents to mediate and treat neurological diseases (Xin et al., 2013). Moreover, under certain pathological conditions including stroke and traumatic brain injuries, exosomes were shown to have

significant therapeutic effects and neurological improvements (Xin et al., 2013; Zhang et al., 2015b). In addition, extracellular vesicles (EVs) have been found to mediate, in part, the curative effects of cell-based therapies for CNS diseases (Schiera et al., 2015; Xin et al., 2014). Thus, understanding the mechanisms of how EVs, particularly exosomes, may bypass the BBB to exert their curative effects or deliver intended cargo is a prerequisite to developing EVs as carriers of therapeutic or diagnostic agents for CNS diseases.

Here, we investigated the interactions between BMECs and exosomes trafficking *in vitro* under healthy and stroke-like conditions. Exosomes labeled with hGluc could readily be detected via bioluminescence, which allowed us to evaluate exosome trafficking quantitatively *in vitro* and will likely enable their use in future studies on EV biodistribution *in vivo* in both the healthy and pathological CNS. In particular, we observed that not only compromised TJs, but also are other cell functions including endocytosis were affected by cell activation with the inflammatory cytokine TNF-α (i.e., under stroke-like conditions)(Descamps et al., 1997). Specifically, we demonstrated that luciferase-carrying exosomes (hGluc-Lact exosomes) could be internalized by BMECs, and cross BMECs more effectively under stroke-like conditions *in vitro*. Using confocal microscopy, we demonstrated that exosomes are internalized by BMECs through endocytosis and accumulate in endosomes. In addition, the majority of exosome crossing the BMEC monolayer was via the transcellular route (i.e. endocytosis, MVB formation and exocytosis across the other side of the layer), with little via the paracellular route (i.e. via passive diffusion though intercellular gaps between BMECs).

However, as a caveat of this study, the exosome exocytosis and intracellular fate of exosomes were not investigated in this study. It is likely that a fraction of the exosomes fuse with lysosomes resulting in their digestion. Also, *de novo* generated exosomes are expected to be secreted by BMECs, in part influenced by events triggered by internalization of exogenous exosomes. A major fate of internalized exosomes is through the formation of MVBs that rely on multi-subunit endosomal sorting complex required for transport (ESCRT) machinery(Thompson et al., 2016). Internalized exosomes as well as *de novo* generated exosomes are termed intraluminal vesicles (ILVs). MVBs hosting ILVs can traffic to and fused with the plasma membrane to liberate exosomes(Ostrowski et al., 2010), in the process utilizing Rab family and small GTPases. In addition, the endosome associated proteins including soluble N-ethylmaleimide-sensitive factor attachment protein receptor (SNARE) proteins and annexins have also been proposed to involve in mediating vesicular trafficking of MVBs and regulating exosome release from the plasma membrane(Thery et al., 2002), (Colombo et al., 2014). A different possible fate of internalized exosomes is the fusion of MVBs with lysosomes to degrade the exosomes/ILVs. Furthermore, different pathways of exosome secretion can differ between different cell types, with BMECs particularly active in coupled edocytosis-exocytosis to yield efficient transcytosis of molecules such as albumin, antibodies and various growth factors (Komarova and Malik, 2010; Raposo and Stoorvogel, 2013). The intracellular trafficking of exosome secretion by BMECs after endocytosis was not examined in detail in this present study, but future studies are expected to further elucidate the exocytic trafficking of exosomes in the context of healthy and pathological BBB conditions (Thompson et al., 2016).

Our data suggest that exosomes derived from 293T cells can be internalized by multiple pathways of endocytosis, including clathrin-dependent and caveolae-dependent routes. Nonetheless, since cellular uptake of exosomes depends on specific ligand receptors or lipid rafts (Svensson et al., 2013), future studies should focus on more precisely identifying the molecular mechanisms at play on the interaction of exosomes with BMECs. For example, by using engineered exosomes from different cellular sources that carry therapeutic potential, functional antibodies to block receptor-ligand interactions, or siRNA to knockdown specific genes that involves in endocytic process for exosome uptake, their MVB formation, their exocytosis as newly released exosomes and their passive diffusion across BMEC intercellular gaps may further unravel molecular mechanisms of exosomes migration across the BBB.

This study therefore paves the way for further development of engineered exosomes as drug delivery vehicles or tracking tools for treating or monitoring neurological diseases. Although *in vitro* BMEC monolayers recapitulate many of the characteristic features of the in *vivo* BBB, incorporation of other cell types, such as primary astrocytes, pericytes, and reconstituted basement membrane may provide a more robust model. As exosome composition varies from one cell type to the other (Thery et al., 2002), the intercellular communication and cellular trafficking between exosomes and BMECs might depend on the cell source and their treatment prior to exosomes production. Although exosomes produced by the cell line HEK 293T used in this study have been engineered and used for potential drug delivery vesicles (Ohno et al., 2013), EVs derived from cell types that have been widely used in translational

applications, including MSCs and immune cells (Liu et al., 2013), are likely more ideal candidates to derive EVs for therapeutic use in clinic and will be considered in the future studies.

Moreover, additional *in vivo* and *ex vivo* assays are expected to further elucidate the physiological mechanisms of exosomes crossing the BBB and their biodistribution in the healthy and pathological CNS in animal models. While here we did not study exosomes biodistribution in the brain, it would be interesting to employ our sensitive hGluc exosomes labeling system in brain slices and in live animals *in vivo*. This system can be used to examine whether or not exosomes can be utilized to deliver therapeutic agents to specific regions of the injured brain. Taken together, our study provides insights into the development of exosomes as emerging therapeutic vehicles and diagnostic tools in the near future. The ease of bioengineering and superior biodistribution characteristics of exosomes may enable their likely therapeutic roles as drug delivery vehicles, in addition to their better-studied intrinsic curative abilities.

2.5 Materials and Methods

Cell lines and cell culture

HEK293T cells (293T, GenTarget) were cultured in high-glucose Dulbecco's modified Eagle's medium (DMEM, Corning Cellgro) supplemented with 10% fetal bovine serum (FBS, Atlanta Biologicals), 100 U/mL penicillin, and 100 µg/mL streptomycin (Life Technologies). Brain microvascular endothelial cells (BMECs) were obtained from American Type Culture Collection (ATCC) and expanded in endothelial cell growth medium (Lonza) supplemented with SingleQuot Kit Supplements and growth factors (Lonza). All cultures were maintained at 37 °C with 5% CO_2.

Generation of constructs and lentiviral transduction

The following constructs were used in this study: hGluc, hGluc-Lactadherin and hGluc-Lactadherin-GFP (Fig. S1a). The sequences of interest were obtained from pCMV-MFGE8-GFP (Origene) and LV-hGluc (Liu et al., 2015). These were cloned into a lentiviral transfer vector LV-PL4 (GenTarget) using overlap PCR(Takahashi et al., 2013). Lentivirus was packaged and 293T cells were then transduced and selected as previously described (Liu et al., 2015). Engineered cells were visualized for transduction efficiency using fluorescence microscopy (Nikon).

Exosome purification

To purify exosomes, conditioned medium was collected from 293T cells cultured for 48 hours in DMEM supplemented with 10% exosome-depleted FBS. First FBS was

depleted of bovine exosomes by centrifugation at 100,000*g* at 4 °C for 18 hours, followed by filtration through a 0.22 μm filter (Millipore). The cell supernatant was centrifuged at 300*g* for 10 minutes and 16,500*g* for 20 minutes at 4 ºC to remove cell debris and microvesicles (MVs), respectively. Next, exosomes were pelleted by ultra-centrifugation at 120,000*g* using Beckman Coulter Optima L-80 XP ultra-centrifuge (Beckman Coulter) for 2.5 hours at 4 °C and washed once in phosphate-buffered saline (PBS). Exosomes were resuspended in PBS or in lysis buffer for experimental analysis.

Nanoparticle tracking analysis

Nanoparticle tracking analysis (NTA) was performed using the NanoSight NS300 system (Malvern). Samples were diluted 1:5000 with PBS, yielding particle concentrations between 3×10^8 and 6×10^8 particles per milliliter. The size of the exosomes was determined based on both light scattering and Brownian motion, and calculated using the Stokes-Einstein equation with NTA 3.0 analytical software (Malvern). The scattering mode was used for NTA, and both acquisition and analysis settings were kept constant for all samples. Each experiment was carried out in triplicate.

Flow cytometry

Flow cytometric analysis was performed on exosomes immobilized on beads (Dynabeads 4.5 μm in diameter) bearing anti-CD63 mAb. The purified exosomes were incubated with Dynabeads overnight at 4 ºC with gentle agitation according to manufacturer's protocol (Life Technologies). After three washes in PBS with 1%

exosome-depleted FBS and 0.1% bovine serum albumin (BSA, Sigma-Aldrich), exosomes captured on beads were stained with PE conjugated CD9, CD63, or CD81 antibody, or isotype control (BD Pharmingen); beads without any antibodies were also used as an additional control. All flow cytometry data were collected on a BD LSRII flow cytometer (BD Bioscience) and analyzed with FlowJo software (FlowJo).

Immunoblotting

293T cells expressing hGluc, hGluc-Lactadherin, hGluc-Lactadherin-GFP were washed in PBS and lysed in radioimmunoprecipitation assay (RIPA) buffer (Cell Signaling) with protease inhibitors (Sigma-Aldrich). Protein concentration was determined by bicinchoninic assay (BCA) (Thermo Fisher Scientific). The total exosome or cell protein lysate from each sample was loaded on a 4-15% SDS polyacrylamide gel (Bio-Rad) and transferred onto polyvinylidene fluoride membranes (Bio-Rad). Membranes were blocked in 5% milk or 5% BSA in Tris-Buffered Saline (Thermo Fisher Scientific) with 0.1% Tween-20 (Sigma-Aldrich) for 1 hour and incubated with anti-Gluc (1:1000, Nanolight), followed by binding of goat anti-rabbit IgG horseradish peroxidase (1:10,000, Santa Cruz Biotechnology). Bands were visualized using an enhanced chemiluminescence (ECL) kit (Thermo Fisher Scientific).

For exosome characterization, the total exosomal protein content isolated from the conditioned medium was quantified using BCA as above. The primary antibodies used in this study were anti-CD63 (1:1000, System Bioscience), anti-CD9 (1:1000, System Bioscience), anti-CD81 (1:1000, System Bioscience), anti-Gluc (1:1000,

Nanolight), and anti-β-actin (1:2000, Abcam).

Exosome labeling

Purified exosomes were labeled with PKH67 or PKH26 (0.5 μg/μL in PBS) Fluorescent Cell Linker Kit for General Cell Membrane Labeling (Sigma-Aldrich) according to the manufacturer's protocol. As a control, PBS buffer alone was stained with PKH dyes. After staining, samples were washed three times with PBS, and fluorescently-labeled exosomes were concentrated using 300 kDa Vivaspin filters (Sartorius Stedim Biotech), as previously described(Lasser et al., 2011).

In vitro BBB model and permeability assays

BMECs were grown on a type I collagen (BD Biosciences)-coated 6.5 mm transwell culture inserts with pore size of 0.45 μm (Corning Life Sciences) for 48 hours until a confluent monolayer was established. For BMEC activation, cells were treated with TNF-α (50 ng/mL, BD Biosciences) for 6 hours(Liao et al., 2016). BMEC monolayer permeability was studied using Fluorescein isothiocyanate (FITC)-dextran (1 mg/mL) (Sigma-Aldrich), which was added to the upper chamber (luminal) and aliquots from the lower chamber (abluminal) were measured for their fluorescence intensity using a Biotek Synergy HT microplate reader (excitation at 485 nm and emission at 520 nm).

In vitro bioluminescence assays

BMECs were grown in a transwell insert and characterized as mentioned above. Prior to addition of exosomes and their controls, cultures were stimulated with TNF-α for

6 hours and then washed, as previously described(Liao et al., 2016). Untreated BMEC monolayers were used as an additional control. PKH67-labeled hGluc-Lact exosomes (10 μg, determined by protein content as previously described(Lai et al., 2014)) or controls (native exosomes or PBS) were then added to luminal chamber and incubated for 6 hours, 12 hours, 18 hours, and 24 hours at 37 ºC, as indicated. Conditioned medium containing exosomes collected from luminal and abluminal chambers of transwell at different time points were plated in triplicate into a white 96-well luminometer plate. 25 μM (final concentration) of *Gaussia* luciferase substrate coelenterazine (CTZ, Nanolight) was added and bioluminescence activity was measured immediately using an IVIS Lumina (Caliper LifeSciences).

Immunocytochemistry

BMECs were washed with PBS, fixed with 2% paraformaldehyde (PFA, Sigma-Aldrich) in PBS for 10 minutes at room temperature, and permeabilized with PBS containing 0.1% Triton X-100 (Sigma-Aldrich) for 10 minutes. After blocking with 1% normal donkey serum (Sigma-Aldrich) and 1% BSA in PBS containing 0.1% Triton X-100 (Sigma-Aldrich) for 1 hour, cells were subsequently incubated with anti-zonula occludens 1 (anti-ZO-1, 1:200, Life Technologies), anti-claudin-5 (1:50, Life Technologies), and anti-VE-cadherin (1:100, Santa Cruz Biotechnology) overnight at 4 ºC. The BMECs were then washed with PBS and incubated with appropriate Alexa Fluor 594 donkey anti-rabbit IgG, Alexa Fluor 488 donkey anti-mouse IgG, or Alexa Fluor 594 donkey anti-goat IgG secondary antibodies (1:500, Jackson ImmunoResearch) for 1 hour at room temperature. To stain cell nuclei, cells were

incubated in 4',6-diamidino-2-phenylindole (DAPI, Life Technologies) at 1:300 dilution in PBS at room temperature for 5 minutes.

In vitro confocal fluorescent imaging for exosome uptake and co-endocytosed localization

BMECs were grown on the coverglass coated with collagen I as described previously and stimulated with TNF-α for 6 hours. In order to image the time course of exosome uptake in BMECs, 24 hours prior to imaging, Deep Red Plasma Membrane Stain CellMask (Life Technologies) was used to label BMECs according to the manufacture protocol. Briefly, BMECs were incubated with CellMask in PBS for 5-10 minutes at 37 ºC and then washed three times. PKH67-labeled exosomes (20 μg) or the control PBS stained with PKH67 were then added to BMECs and incubated for 1 hour, 3 hours, 6 hours, 12 hours, 18 hours, and 24 hours at 37 ºC. All cells were then fixed with 2% PFA and nuclei were counterstained with DAPI. Image analysis was performed using a Zeiss LSM710 Multiphoton/Confocal microscope (Zeiss). The middle Z plane of the cell was imaged to ensure the elite imaging position. All the images were analyzed with Image J software (http://imagej.nih.gov/, NIH). For quantification, briefly, the outline of each cell (n > 30) was drawn referring to the cell membrane labeling (i.e., CellMask). The fluorescence intensity of intracellular exosomes that were specifically associated with the cells was then calculated. Triplicated samples were used for the analysis.

In order to identify the colocalization of endosomes and exosomes, BMECs grown on collagen I-coated coverglass were incubated with 10 μg/mL cholera toxin B subunit-biotin (CtxB, Sigma-Aldrich), following by Alexa Fluor 594 streptavidin (Jackson

ImmunoResearch) conjugation, or 150 μg /mL transferrin-Texas Red (Tfn-Texas Red, Life Technologies) for 30 minutes at 37 °C as previously described(Svensson et al., 2013). PKH67-labeled exosomes were subsequently incubated with cells for 1 hour or 3 hours. After incubation, excessive exosomes were washed three times with PBS. Cells were fixed with 2% PFA and nuclei were counterstained with DAPI. A Zeiss 63x1.4NA objective was used for the colocalization experiments. The images were then quantified using Image J Coloc2 plugin, which estimates the overlap coefficients in dual-color confocal images(Manders et al., 1993). Colocalization of exosomes and Tfn/CtxB was indicated as yellow (green + red) pixels in the overlay images.

In vitro cell viability and toxicity assays

BMECs were seeded at 20,000 cells/well in 96-well plates. Cells were treated with the indicated concentrations of endocytosis inhibitors or vehicle for 30 minutes, or with TNF-α or vehicle for 6 hours, to assess the cellular toxicity. Cell viability was determined using the 2,3-bis[2- Methoxy-4-nitro-5-sulfophenyl]-2H-tetrazolium-5-carboxyanilide inner salt (XTT) assay (ATCC) according to manufacture's protocol. Briefly, the XTT reagent was added to each well, incubated for 2-4 hours at 37 °C, and absorbance was measured at 450 nm with a reference wavelength 680 nm using a Biotek Synergy HT microplate reader. All samples were assayed in triplicate. The cytotoxicity of each inhibitor was compared to untreated controls.

Exosome uptake and crossing inhibition studies

To further study the mechanisms of exosome uptake by BMEC monolayer, BMECs seeded on coverglass were pretreated with the following pharmacological inhibitors at their indicated concentrations: chlorpromazine (CPZ), cytochalasin D, amiloride, methyl- β –cyclodextrin (MβCD), filipin III, or nystatin for 30 minutes at 37 °C before exosomes were added. The specificity and effective concentrations of endocytosis inhibitors were evaluated by measuring their effect on the markers for specific endocytic pathways. Specifically, Texas Red-transferrin (150 μg /mL) was used as a marker for clathrin-mediated endocytosis (CME), Alexa Fluor 594-CtxB (10 μg/mL) for lipid raft (caveolae)-mediated endocytosis, and Alexa Fluor 594-dextran (1 mg/mL) for macropinocytosis were used in this study. Inhibition was assessed by exosome uptake assay using confocal microscopy and image analysis. CellMask (Green Plasma Membrane Stain, Life Technologies)-labeled BMECs were then incubated with PKH26-labeled exosomes for 1 hour. After incubation, cells were washed with PBS, followed by fixation in PFA. Images were taken using a fluorescent microscopy (Nikon) and were analyzed with Image J software. To quantitatively measure the effects of above inhibitors on exosome crossing the *in vitro* BMEC monolayer in the transwell assay, the BMECs were pretreated with inhibitors prior to addition of exosomes, and conditioned medium from luminal and abluminal chambers were collected for bioluminescence analysis as described above.

Statistical analysis

Data were presented as means ± SEM. Statistical differences were determined using unpaired Student's *t* test when comparing between 2 independent groups, and

one- way ANOVA with Student-Newman-Keuls (SNK) *post hoc* tests when comparing across 3 or more independent groups. $P < 0.05$ was considered significant.

2.6 Supplementary Figures and Tables

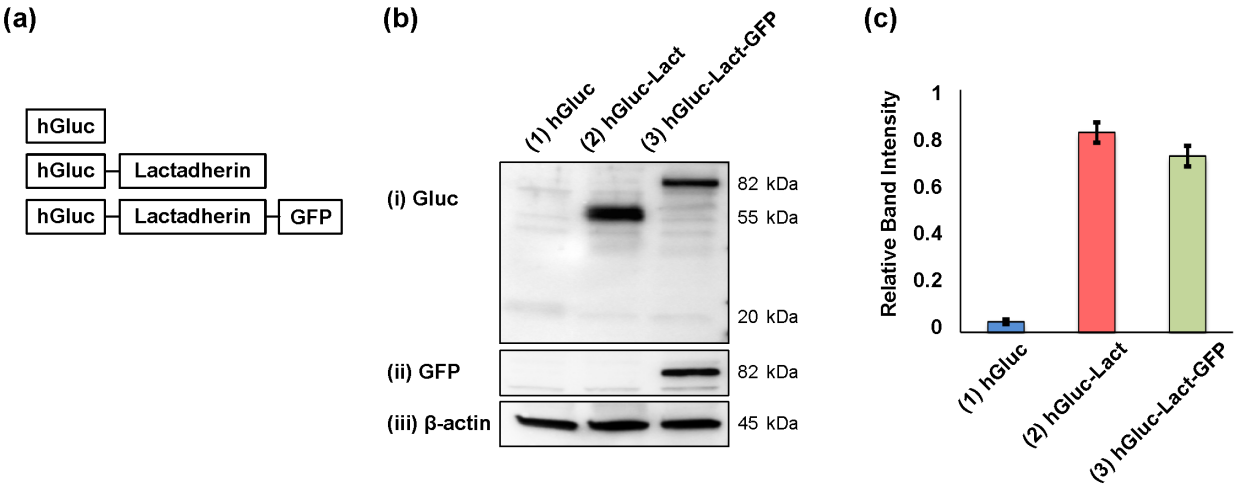

Fig. 2.S1. Membrane fusion protein hGluc-Lact is expressed in 293T cells. (a) Schematic representation of the hGluc-Lactadherin constructs engineered in this study. (b) Western blot analysis showing 293T cells expressing membrane fusion proteins hGluc-Lact and hGluc-Lact-GFP. Membranes probed with anti-Gluc antibody showed *Gaussia* luciferase (Gluc) at the expected sizes (55 kDa, and 82 kDa, respectively) compared to hGluc alone (20 kDa). Membrane was probed with anti-GFP antibody and only GFP band was detected at 82 kDa in hGluc-Lact-GFP sample. β-actin was used as a loading control. (c) Quantification of hGluc expression of (b) showing relative expression of free hGluc and tagged hGluc in lysate. The band intensity was normalized to β-actin. Relative intensities were: hGluc = 0.0437, hGluc-Lact = 0.825 and hGluc-Lact-GFP = 0.727.

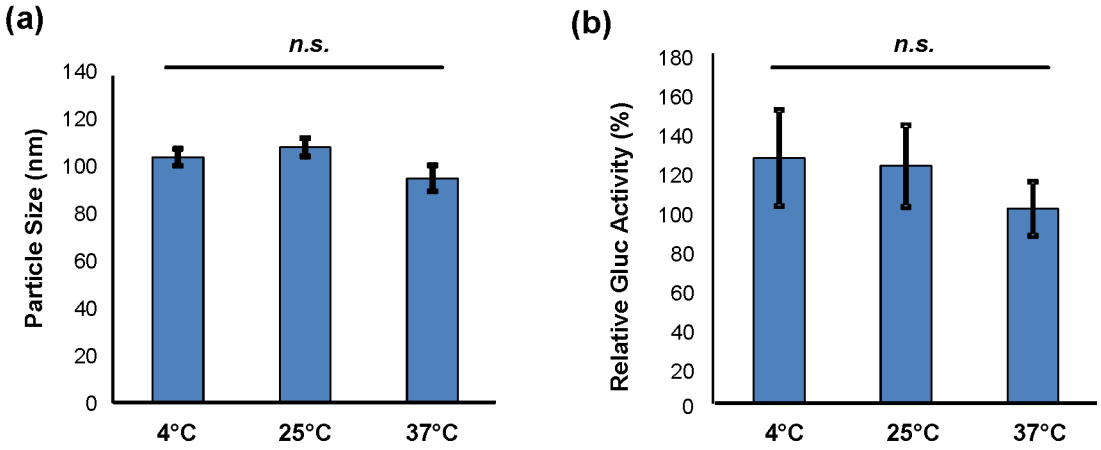

Fig. 2.S2. Stability of hGluc-Lact exosomes under various temperature conditions. (a) Nanoparticle tracking analysis (NTA) of hGluc-Lact exosomes at 37 °C, 25 °C and 4 °C. Incubation at different temperatures did not alter exosome size distribution. (b) *In vitro* bioluminescence assay of hGluc-Lact exosomes at different temperature conditions. Values are mean ± SEM of relative ratio normalized to 37 °C set as 100%. There were no significant differences in luciferase activity between 37 °C, 25 °C and 4 °C; *n.s.*, not significant.

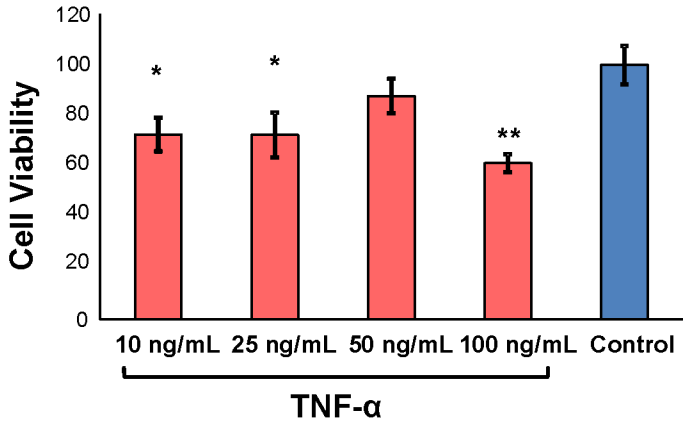

Fig. 2.S3. Effect of TNF-α on BMEC growth. Cell viability was measured after 6 hours of TNF-α activation and determined by XTT assay. Relative cell growth was normalized to the vehicle control (no TNF-α) set as 100%. Error bar: mean ± SEM.*P < 0.05 and **P < 0.01, as determined by one-way ANOVA with SNK *post hoc* tests.

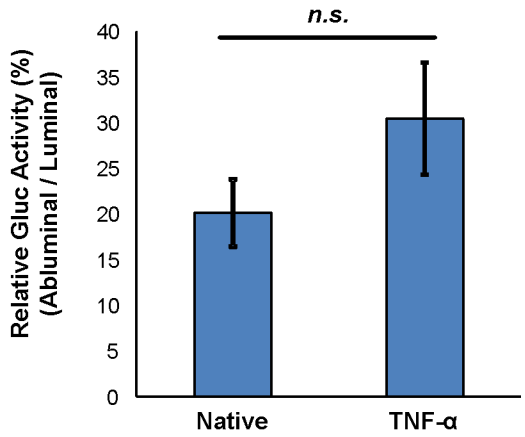

Fig. 2.S4. Diffusion of free hGluc from conditioned medium across BMEC monolayers. Secreted hGluc protein from conditioned medium can freely cross BMECs in both native and activated conditions hGluc activity was measured using IVIS Lumina (CTZ final concentration: 25 μM, exposure time: 0.5s). Relative Gluc Activity = (abluminal chamber signal **–** hGluc free conditioned medium signal) / (luminal chamber signal **–** hGluc free conditioned medium signal) × 100%. Error bar: mean ± SEM. *N.s.*, not significant.

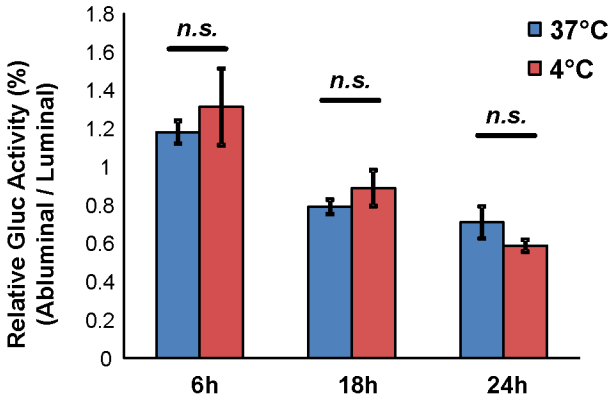

Fig. 2.S5. Measurement of temperature effects on *in vitro* transwell diffusion of exosomes in the absence of cells (free diffusion). The free diffusion rate of exosomes in the absence of live or fixed BMECs was determined by transwell and *in vitro* bioluminescence assay. Conditioned media from both luminal and abluminal chambers were collected at 6, 18, and 24 hours after addition of exosomes to the luminal chamber. Incubation of exosomes at 37 °C and 4 °C did not alter the diffusion rates of exosomes. Error bar: mean ± SEM. *n.s.*, not significant.

Table 1. Primary antibodies used in the EV-BBB study

Antigen	Company	Catalog #	Dilution
Gaussia Luciferase	Nanolight	401P	1:1,000
CD63	System Bioscience	EXOAB-CD63A-1	1:1,000
CD9	System Bioscience	EXOAB-CD9A-1	1:1,000
CD81	System Bioscience	EXOAB-CD81A-1	1:1,000
tGFP	OriGene	TA150041	1:2,000
β –actin	Abcam	ab8226	1:2,000
VE-cadherin	Santa Cruz Biotechnology, Inc.	Sc-6458	1:100
Zonula occluding-1	Life Technologies	40-2200	1:200
Claudin-5	Life Technologies	35-2500	1:100

Table 2. Secondary antibodies used in the EV-BBB study

Conjugate	Species	Company	Catalog #	Dilution
Horseradish Peroxidase	Donkey α rabbit	Santa Cruz Biotechnology, Inc.	Sc-2077	1:10,000
Horseradish Peroxidase	Goat α mouse	Santa Cruz Biotechnology, Inc.	Sc-2314	1:10,000
Alexa Fluor® 488	Donkey α rabbit	Jackson ImmunoResearch Laboratories	711-545-152	1:500
Alexa Fluor® 594	Donkey α rabbit	Jackson ImmunoResearch Laboratories	711-585-152	1:500

2.7 Acknowledgments

We thank Dr. W. Liao and M. Lu for discussion and technique training. We thank C. Deighan from Malvern Instruments for assistance with the use of NanoSight NS300 instrument for NTA analysis. This work was supported by the National Institute of Health (1DP2CA195763-01), American Heart Association (13BGIA17140099) and UC Irvine Academic Senate Council on Research, Computing, and Libraries (CORCL) Research Grant (SIIG-2013-2014-25). CCC was supported by National Science Foundation Graduate Research Fellowship (NSF GRFP). SXZ was supported by a Cardiovascular Applied Research and Entrepreneurship fellowship (NIH/NHLBI T32).

2.8 References

1. Abbott, N.J., L. Ronnback, and E. Hansson. Astrocyte-endothelial interactions at the blood-brain barrier. *Nat Rev Neurosci*. 7: 41-53, 2006.
2. Alvarez-Erviti, L., Y. Seow, H. Yin, C. Betts, S. Lakhal, and M.J. Wood. Delivery of siRNA to the mouse brain by systemic injection of targeted exosomes. *Nat Biotechnol*. 29: 341-5, 2011.
3. Andreone, B.J., B. Lacoste, and C. Gu. Neuronal and vascular interactions. *Annu Rev Neurosci*. 38: 25-46, 2015.
4. Banks, W.A. From blood-brain barrier to blood-brain interface: new opportunities for CNS drug delivery. *Nat Rev Drug Discov*. 2016.
5. Chen, J., Z.G. Zhang, Y. Li, L. Wang, Y.X. Xu, S.C. Gautam, M. Lu, Z. Zhu, and M. Chopp. Intravenous administration of human bone marrow stromal cells induces angiogenesis in the ischemic boundary zone after stroke in rats. *Circ Res*. 92: 692-9, 2003.
6. Colombo, M., G. Raposo, and C. Thery. Biogenesis, secretion, and intercellular interactions of exosomes and other extracellular vesicles. *Annu Rev Cell Dev Biol*. 30: 255-89, 2014.
7. Deli, M.A., L. Descamps, M.P. Dehouck, R. Cecchelli, F. Joo, C.S. Abraham, and G. Torpier. Exposure of tumor necrosis factor-alpha to luminal membrane of bovine brain capillary endothelial cells cocultured with astrocytes induces a delayed increase of permeability and cytoplasmic stress fiber formation of actin. *J Neurosci Res*. 41: 717-26, 1995.

8. Dendrou, C.A., L. Fugger, and M.A. Friese. Immunopathology of multiple sclerosis. *Nat Rev Immunol*. 15: 545-58, 2015.

9. Descamps, L., R. Cecchelli, and G. Torpier. Effects of tumor necrosis factor on receptor-mediated endocytosis and barrier functions of bovine brain capillary endothelial cell monolayers. *J Neuroimmunol*. 74: 173-84, 1997.

10. Dobson, P.D. and D.B. Kell. Carrier-mediated cellular uptake of pharmaceutical drugs: an exception or the rule? *Nat Rev Drug Discov*. 7: 205-20, 2008.

11. Dulamea, A.O. The potential use of mesenchymal stem cells in stroke therapy-From bench to bedside. *Journal of the Neurological Sciences*. 352: 1-11, 2015.

12. El-Andaloussi, S., I. Mager, X.O. Breakefield, and M.J. Wood. Extracellular vesicles: biology and emerging therapeutic opportunities. *Nat Rev Drug Discov*. 12: 347-57, 2013.

13. Etame, A.B., R.J. Diaz, C.A. Smith, T.G. Mainprize, K. Hynynen, and J.T. Rutka. Focused ultrasound disruption of the blood-brain barrier: a new frontier for therapeutic delivery in molecular neurooncology. *Neurosurg Focus*. 32: E3, 2012.

14. Faille, D., F. El-Assaad, A.J. Mitchell, M.C. Alessi, G. Chimini, T. Fusai, G.E. Grau, and V. Combes. Endocytosis and intracellular processing of platelet microparticles by brain endothelial cells. *J Cell Mol Med*. 16: 1731-8, 2012.

15. Fischer, S., M. Wiesnet, H.H. Marti, D. Renz, and W. Schaper. Simultaneous activation of several second messengers in hypoxia-induced hyperpermeability of brain derived endothelial cells. *J Cell Physiol*. 198: 359-69, 2004.

16. Fruhbeis, C., D. Frohlich, and E.M. Kramer-Albers. Emerging roles of exosomes in neuron-glia communication. *Front Physiol*. 3: 119, 2012.

17. Gabathuler, R. Approaches to transport therapeutic drugs across the blood-brain barrier to treat brain diseases. *Neurobiol Dis*. 37: 48-57, 2010.

18. Ge, Q.Y., Y.X. Zhou, J.F. Lu, Y.F. Bai, X.Y. Xie, and Z.H. Lu. miRNA in Plasma Exosome is Stable under Different Storage Conditions. *Molecules*. 19: 1568-1575, 2014.

19. Hsu, J., J. Rappaport, and S. Muro. Specific binding, uptake, and transport of ICAM-1-targeted nanocarriers across endothelial and subendothelial cell components of the blood-brain barrier. *Pharm Res*. 31: 1855-66, 2014.

20. Imai, T., Y. Takahashi, M. Nishikawa, K. Kato, M. Morishita, T. Yamashita, A. Matsumoto, C. Charoenviriyakul, and Y. Takakura. Macrophage-dependent clearance of systemically administered B16BL6-derived exosomes from the blood circulation in mice. *J Extracell Vesicles*. 4: 26238, 2015.

21. Kalani, A., A. Tyagi, and N. Tyagi. Exosomes: mediators of neurodegeneration, neuroprotection and therapeutics. *Mol Neurobiol*. 49: 590-600, 2014.

22. Komarova, Y. and A.B. Malik. Regulation of endothelial permeability via paracellular and transcellular transport pathways. *Annu Rev Physiol*. 72: 463-93, 2010.

23. Kourembanas, S. Exosomes: vehicles of intercellular signaling, biomarkers, and vectors of cell therapy. *Annu. Rev. Physiol.* 77: 13-27, 2015.

24. Lai, C.P., O. Mardini, M. Ericsson, S. Prabhakar, C.A. Maguire, J.W. Chen, B.A. Tannous, and X.O. Breakefield. Dynamic Biodistribution of Extracellular Vesicles in Vivo Using a Multimodal Imaging Reporter. *Acs Nano*. 8: 483-494, 2014.

25. Lasser, C. Exosomes in diagnostic and therapeutic applications: biomarker, vaccine and RNA interference delivery vehicle. *Expert Opin. Biol. Ther.* 15: 103-117, 2015.

26. Lasser, C., S.E. O'Neil, L. Ekerljung, K. Ekstrom, M. Sjostrand, and J. Lotvall. RNA-containing exosomes in human nasal secretions. *Am J Rhinol Allergy*. 25: 89-93, 2011.

27. Lee, C.C., J.A. MacKay, J.M. Frechet, and F.C. Szoka. Designing dendrimers for biological applications. *Nat Biotechnol*. 23: 1517-26, 2005.

28. Lee, R.H., A.A. Pulin, M.J. Seo, D.J. Kota, J. Ylostalo, B.L. Larson, L. Semprun-Prieto, P. Delafontaine, and D.J. Prockop. Intravenous hMSCs improve myocardial infarction in mice because cells embolized in lung are activated to secrete the anti-inflammatory protein TSG-6. *Cell Stem Cell*. 5: 54-63, 2009.

29. Liao, W., V. Pham, L. Liu, M. Riazifar, E.J. Pone, S.X. Zhang, F. Ma, M. Lu, C.M. Walsh, and W. Zhao. Mesenchymal stem cells engineered to express selectin ligands and IL-10 exert enhanced therapeutic efficacy in murine experimental autoimmune encephalomyelitis. *Biomaterials*. 77: 87-97, 2016.

30. Liu, L., M.A. Eckert, H. Riazifar, D.K. Kang, D. Agalliu, and W. Zhao. From blood to the brain: can systemically transplanted mesenchymal stem cells cross the blood-brain barrier? *Stem Cells Int*. 2013: 435093, 2013.

31. Liu, L., S.X. Zhang, R. Aeran, W. Liao, M. Lu, G. Polovin, E.J. Pone, and W. Zhao. Exogenous marker-engineered mesenchymal stem cells detect cancer and metastases in a simple blood assay. *Stem Cell Res Ther*. 6: 181, 2015.

32. Manders, E.M.M., F.J. Verbeek, and J.A. Aten. Measurement of Colocalization of Objects in Dual-Color Confocal Images. *Journal of Microscopy-Oxford*. 169: 375-382, 1993.

33. Mathivanan, S., H. Ji, and R.J. Simpson. Exosomes: extracellular organelles important in intercellular communication. *J Proteomics*. 73: 1907-20, 2010.

34. Mulcahy, L.A., R.C. Pink, and D.R. Carter. Routes and mechanisms of extracellular vesicle uptake. *J Extracell Vesicles*. 3: 2014.

35. Obermeier, B., R. Daneman, and R.M. Ransohoff. Development, maintenance and disruption of the blood-brain barrier. *Nat Med*. 19: 1584-96, 2013.

36. Ohno, S., M. Takanashi, K. Sudo, S. Ueda, A. Ishikawa, N. Matsuyama, K. Fujita, T. Mizutani, T. Ohgi, T. Ochiya, N. Gotoh, and M. Kuroda. Systemically injected exosomes targeted to EGFR deliver antitumor microRNA to breast cancer cells. *Mol Ther*. 21: 185-91, 2013.

37. Ostrowski, M., N.B. Carmo, S. Krumeich, I. Fanget, G. Raposo, A. Savina, C.F. Moita, K. Schauer, A.N. Hume, R.P. Freitas, B. Goud, P. Benaroch, N. Hacohen, M. Fukuda, C. Desnos, M.C. Seabra, F. Darchen, S. Amigorena, L.F. Moita, and C. Thery. Rab27a and Rab27b control different steps of the exosome secretion pathway. *Nat Cell Biol*. 12: 19-30; sup pp 1-13, 2010.

38. Pardridge, W.M. Targeted delivery of protein and gene medicines through the blood-brain barrier. *Clin Pharmacol Ther*. 97: 347-61, 2015.

39. Pardridge, W.M. Blood-brain barrier endogenous transporters as therapeutic targets: a new model for small molecule CNS drug discovery. *Expert Opin Ther Targets*. 19: 1059-72, 2015.

40. Pardridge, W.M. Drug transport across the blood-brain barrier. *J Cereb Blood Flow Metab*. 32: 1959-72, 2012.

41. Pardridge, W.M. The blood-brain barrier: bottleneck in brain drug development. *NeuroRx*. 2: 3-14, 2005.

42. Peer, D., J.M. Karp, S. Hong, O.C. Farokhzad, R. Margalit, and R. Langer. Nanocarriers as an emerging platform for cancer therapy. *Nat Nanotechnol*. 2: 751-60, 2007.

43. Petros, R.A. and J.M. DeSimone. Strategies in the design of nanoparticles for therapeutic applications. *Nat. Rev. Drug. Discov.* 9: 615-627, 2010.

44. Pols, M.S. and J. Klumperman. Trafficking and function of the tetraspanin CD63. *Exp Cell Res*. 315: 1584-92, 2009.

45. Raposo, G. and W. Stoorvogel. Extracellular vesicles: Exosomes, microvesicles, and friends. *Journal of Cell Biology*. 200: 373-383, 2013.

46. Ridder, K., S. Keller, M. Dams, A.K. Rupp, J. Schlaudraff, D. Del Turco, J. Starmann, J. Macas, D. Karpova, K. Devraj, C. Depboylu, B. Landfried, B. Arnold, K.H. Plate, G. Hoglinger, H. Sultmann, P. Altevogt, and S. Momma. Extracellular vesicle-mediated transfer of genetic information between the hematopoietic system and the brain in response to inflammation. *Plos Biology*. 12: 2014.

47. Rochfort, K.D., L.E. Collins, R.P. Murphy, and P.M. Cummins. Downregulation of blood-brain barrier phenotype by proinflammatory cytokines involves NADPH oxidase-dependent ROS generation: consequences for interendothelial adherens and tight junctions. *PLoS One*. 9: e101815, 2014.

48. Rubin, L.L. and J.M. Staddon. The cell biology of the blood-brain barrier. *Annu Rev Neurosci*. 22: 11-28, 1999.

49. Sandoval, K.E. and K.A. Witt. Blood-brain barrier tight junction permeability and ischemic stroke. *Neurobiol Dis*. 32: 200-19, 2008.

50. Schiera, G., C.M. Di Liegro, and I. Di Liegro. Extracellular membrane vesicles as vehicles for brain cell-to-cell interactions in physiological as well as pathological conditions. *Biomed Research International*. 2015.

51. Schnitzer, J.E., P. Oh, E. Pinney, and J. Allard. Filipin-sensitive caveolae-mediated transport in endothelium: reduced transcytosis, scavenger endocytosis, and capillary permeability of select macromolecules. *J Cell Biol*. 127: 1217-32, 1994.

52. Shlosberg, D., M. Benifla, D. Kaufer, and A. Friedman. Blood-brain barrier breakdown as a therapeutic target in traumatic brain injury. *Nature Reviews Neurology*. 6: 393-403, 2010.

53. Song, J. Ischemic apoplexy-induced sequelae treated by penetrating puncture with long needles. *J Tradit Chin Med*. 22: 200-2, 2002.

54. Sordi, V., M.L. Malosio, F. Marchesi, A. Mercalli, R. Melzi, T. Giordano, N. Belmonte, G. Ferrari, B.E. Leone, F. Bertuzzi, G. Zerbini, P. Allavena, E. Bonifacio, and L. Piemonti. Bone marrow mesenchymal stem cells express a restricted set of functionally active chemokine receptors capable of promoting migration to pancreatic islets. *Blood*. 106: 419-27, 2005.

55. Svensson, K.J., H.C. Christianson, A. Wittrup, E. Bourseau-Guilmain, E. Lindqvist, L.M. Svensson, M. Morgelin, and M. Belting. Exosome uptake depends

on ERK1/2-heat shock protein 27 signaling and lipid Raft-mediated endocytosis negatively regulated by caveolin-1. *J Biol Chem*. 288: 17713-24, 2013.

56. Takahashi, Y., M. Nishikawa, H. Shinotsuka, Y. Matsui, S. Ohara, T. Imai, and Y. Takakura. Visualization and in vivo tracking of the exosomes of murine melanoma B16-BL6 cells in mice after intravenous injection. *J Biotechnol*. 165: 77-84, 2013.

57. Takeshita, Y., B. Obermeier, A. Cotleur, Y. Sano, T. Kanda, and R.M. Ransohoff. An in vitro blood-brain barrier model combining shear stress and endothelial cell/astrocyte co-culture. *J Neurosci Methods*. 232: 165-72, 2014.

58. Tannous, B.A., D.E. Kim, J.L. Fernandez, R. Weissleder, and X.O. Breakefield. Codon-optimized Gaussia luciferase cDNA for mammalian gene expression in culture and in vivo. *Mol Ther*. 11: 435-43, 2005.

59. Thery, C., S. Amigorena, G. Raposo, and A. Clayton. Isolation and characterization of exosomes from cell culture supernatants and biological fluids. *Curr Protoc Cell Biol*. Chapter 3: Unit 3 22, 2006.

60. Thery, C., M. Ostrowski, and E. Segura. Membrane vesicles as conveyors of immune responses. *Nat Rev Immunol*. 9: 581-93, 2009.

61. Thery, C., L. Zitvogel, and S. Amigorena. Exosomes: composition, biogenesis and function. *Nat Rev Immunol*. 2: 569-79, 2002.

62. Thompson, A.G., E. Gray, S.M. Heman-Ackah, I. Mager, K. Talbot, S.E. Andaloussi, M.J. Wood, and M.R. Turner. Extracellular vesicles in neurodegenerative disease - pathogenesis to biomarkers. *Nat Rev Neurol*. 12: 346-57, 2016.

63. Tian, T., Y.L. Zhu, Y.Y. Zhou, G.F. Liang, Y.Y. Wang, F.H. Hu, and Z.D. Xiao. Exosome uptake through clathrin-mediated endocytosis and macropinocytosis and mediating miR-21 delivery. *J Biol Chem*. 289: 22258-67, 2014.

64. Torchilin, V.P. Multifunctional, stimuli-sensitive nanoparticulate systems for drug delivery. *Nat. Rev. Drug Discov.* 13: 813-827, 2014.

65. Torchilin, V.P. Recent advances with liposomes as pharmaceutical carriers. *Nat Rev Drug Discov*. 4: 145-60, 2005.

66. Trumpp, A., M. Essers, and A. Wilson. Awakening dormant haematopoietic stem cells. *Nat Rev Immunol*. 10: 201-9, 2010.

67. Upadhyay, R.K. Drug delivery systems, CNS protection, and the blood brain barrier. *Biomed Res Int*. 2014: 869269, 2014.

68. Valadi, H., K. Ekstrom, A. Bossios, M. Sjostrand, J.J. Lee, and J.O. Lotvall. Exosome-mediated transfer of mRNAs and microRNAs is a novel mechanism of genetic exchange between cells. *Nat Cell Biol*. 9: 654-9, 2007.

69. Vercauteren, D., R.E. Vandenbroucke, A.T. Jones, J. Rejman, J. Demeester, S.C. De Smedt, N.N. Sanders, and K. Braeckmans. The use of inhibitors to study endocytic pathways of gene carriers: optimization and pitfalls. *Mol Ther*. 18: 561-9, 2010.

70. Wajant, H., K. Pfizenmaier, and P. Scheurich. Tumor necrosis factor signaling. *Cell Death Differ*. 10: 45-65, 2003.

71. Whalen, G.F., Y. Shing, and J. Folkman. The fate of intravenously administered bFGF and the effect of heparin. *Growth Factors*. 1: 157-64, 1989.

72. Wolburg, H. and A. Lippoldt. Tight junctions of the blood-brain barrier: development, composition and regulation. *Vascul Pharmacol*. 38: 323-37, 2002.

73. Xin, H., Y. Li, and M. Chopp. Exosomes/miRNAs as mediating cell-based therapy of stroke. *Front Cell Neurosci*. 8: 377, 2014.

74. Xin, H., Y. Li, Y. Cui, J.J. Yang, Z.G. Zhang, and M. Chopp. Systemic administration of exosomes released from mesenchymal stromal cells promote functional recovery and neurovascular plasticity after stroke in rats. *J Cereb Blood Flow Metab*. 33: 1711-5, 2013.

75. Yang, T., P. Martin, B. Fogarty, A. Brown, K. Schurman, R. Phipps, V.P. Yin, P. Lockman, and S. Bai. Exosome delivered anticancer drugs across the blood-brain barrier for brain cancer therapy in Danio rerio. *Pharm Res*. 32: 2003-14, 2015.

76. Zhang, Y., M. Chopp, Y. Meng, M. Katakowski, H. Xin, A. Mahmood, and Y. Xiong. Effect of exosomes derived from multipluripotent mesenchymal stromal cells on functional recovery and neurovascular plasticity in rats after traumatic brain injury. *J Neurosurg*. 122: 856-67, 2015.

77. Zhuang, X., X. Xiang, W. Grizzle, D. Sun, S. Zhang, R.C. Axtell, S. Ju, J. Mu, L. Zhang, L. Steinman, D. Miller, and H.G. Zhang. Treatment of brain inflammatory diseases by delivering exosome encapsulated anti-inflammatory drugs from the nasal region to the brain. *Mol Ther*. 19: 1769-79, 2011.

Chapter 3: Role of the CPEB3 Ribozyme in Regulation of Activity-Dependent Gene Expression in Primary Cortical Neurons

3.1 Introduction

Molecular mechanisms of synaptic plasticity in learning and memory

Neuroplasticity is a reflection of changes in the strength of neural communication between axons and dendrites at synapses. Alternations in synaptic functions and synaptic transmission are critical to the storage of information in the central nervous system, thereby contributing to memory formation and consolidation. To better understand activity-dependent synaptic plasticity of learning and memory in neural circuits, LTP and LTD are two model systems that have been extensively characterized in the mammalian brain. LTP is characterized by a persistent enhancement in synaptic transmission that is induced by high-frequency stimulation in the hippocampus. Conversely, LTD is expressed as a decrease in postsynaptic strength by low-frequency stimulation (Bailey et al., 2015; Bear and Malenka, 1994; Bliss and Collingridge, 1993; Bliss et al., 2014). There are two phases of LTP. An early-phase LTP (E-LTP), which is dependent on its alternation of preexisting proteins, can last 1-3 hours. The long-lasting or late-phase LTP (L-LTP), which is dependent on transcription and new protein synthesis, may last for several hours *in vitro* and days to weeks *in vivo* (Costa-Mattioli et al., 2009; Lynch, 2004). This biological mechanism is evolutionary conserved. In

Aplysia, one train of stimuli induces short-term facilitation. Conversely, repeat trains of stimuli induce long-term facilitation (LTF), which shares similar features with the late phase of LTP in the mammalian hippocampus (Kandel, 2001). There is compelling evidence to suggest that the cellular and molecular mechanisms of LTP require *de novo* protein synthesis and new synaptic connections, leading to memory consolidation (Bailey et al., 2015; Bear and Malenka, 1994; Bliss and Collingridge, 1993; Costa-Mattioli et al., 2009). Importantly, treatment with transcription or translation inhibitors in CA1 region dendrites was shown to block the induction of L-LTP (Bradshaw et al., 2003; Nguyen et al., 1994; Sutton and Schuman, 2006). In fact, more studies have suggested that *N*-methyl-D-aspartate receptors (NMDARs) and α-amino-3-hydroxy-5-methyl-4-isoxazolepropionic receptors (AMPARs) are involved in LTP induction. This occurs when the release of glutamate at the presynaptic terminal binds to NMDARs, and postsynaptic depolarization for the activation of NMDARs by extracellular magnesium ion (Mg^{2+}) blockage allows the entry of calcium ion (Ca^{2+}) into the postsynaptic cell. Ca^{2+} acts as a second messenger to activate intracellular signaling in dendritic protein-synthesis machinery, and it activates calcium/calmodulin-dependent protein kinase II (CaMKII) and protein kinase C (PKC). This results in phosphorylation of AMPARs or activation of translation factors that are required for mRNA stabilization, thereby increasing dendritic spine formation and facilitating LTP induction (Bear and Malenka, 1994; Lynch, 2004; Malinow and Malenka, 2002). Another pathway involves in AMPARs trafficking during synaptic plasticity so that AMPARs can be recycled and reinserted to the plasma membrane in an activity-dependent manner. This rapid movement between postsynaptic density and cytosolic compartment of AMPARs is regulated by AMPAR

subunit composition and incorporated into synapses followed by NMDARs stimulation, and thereby strengthening the spine for subsequent potentiation (Collingridge et al., 2004; Derkach et al., 2007; Malinow and Malenka, 2002; Shepherd and Huganir, 2007). Moreover, several kinases have been implicated in L-LTP. Activation of cyclic adenosine 3', 5'-monophosphate (cAMP)–dependent protein kinase A (PKA) has been suggested to transform short-term memory to long-term memory (LTM). The activation of PKA can recruit mitogen-activated protein kinase (MAPK) to the nucleus, and phosphorylate cAMP-responsive element-binding protein (CREB) to activate transcription of plasticity-associated genes (Kandel, 2001, 2012; Waltereit and Weller, 2003). Collectively, this evidence indicates that mRNA transcription and *de novo* protein synthesis in the postsynaptic neurons are an essential determinant for maintaining LTP and memory formation.

In contrast with LTP, LTD is characterized by a decrease in the synaptic response of neurons to prolonged periods of low frequency stimulation (LFS). LTD involves alterations in NMDAR-dependent and metabotropic glutamate receptor (mGluR)-dependent synaptic transmission (Collingridge et al., 2010). Weak stimulation at presynaptic neurons can lead to moderate membrane depolarization, and calcium influx via NMDAR can activate protein phosphatase 2B (PP2B, also known as calcineurin) and protein phosphatase 1 (PP1) that dephosphorylates AMPA receptors, thereby promoting AMPAR internalization (Lisman, 1989; Mulkey et al., 1993). Group 1 mGluR-dependent LTD is the second type of LTD (Luscher and Huber, 2010). Stimulation of mGluR initiates a signaling cascade, including phospholipase C (PLC)

activation, Inositol 1, 4, 5 – triphosphate (IP_3) production, intracellular Ca^{2+} release, and PKC activation. This leads to endocytosis of ionotropic AMPAR, and a decrease in the number of postsynaptic surface AMPAR (Gladding et al., 2009; Luscher and Huber, 2010; Moult et al., 2006).

Changes in synaptic transmission contribute to dendritic spine morphology, and have been suggested to underlie memory consolidation. Induction of LTP is associated with the preexisting spine enlargement, growth of new dendritic spines, and increased size of the postsynaptic densities (PSDs). In contrast, induction of LTD is associated with spine shrinkage or loss of the dendritic spines (Bosch and Hayashi, 2012; Malenka and Bear, 2004; Yuste and Bonhoeffer, 2001; Zhou et al., 2001). Growing evidence has suggested that regulation of activity-dependent protein synthesis at the stimulated spines is tightly coupled with dynamic reorganization of actin cytoskeleton (Basu and Lamprecht, 2018; Bosch et al., 2014; Nakahata and Yasuda, 2018). Filamentous actin (F-actin), a major component of the cytoskeletal element in dendritic spines, is dynamically remodeling at excitatory synapses upon synaptic activity (Cingolani and Goda, 2008). Furthermore, the actin filament serves a role in protein trafficking in dendritic spine. Studies have suggested the actin cytoskeleton is involved in the distribution of AMPARs. Hippocampal neuronal cultures treated with jasplakinolide, a macrocyclic peptide that promotes actin polymerization, exhibited an inhibition in APMAR internalization. In contrast, treatment with latrunculin A, an inhibitor of actin polymerization, resulted in depolymerization of F-actin, and this led to a reduction of NMDAR and AMPAR internalization in dendritic spines (Allison et al., 1998; Zhou et al.,

2001). Together, this highlights the dynamic molecular and structural mechanisms of synaptic plasticity underlying learning and memory.

Cytoplasmic polyadenylation element binding protein 3 (CPEB3) modulates synaptic plasticity and memory consolidation

Several mechanisms have been proposed to elucidate the regulation of synaptic plasticity, with cytoplasmic polyadenylation-induced translation as a key step for regulating protein synthesis and synaptic plasticity in hippocampal dendrites (Atkins et al., 2004; Wu et al., 1998). The cytoplasmic polyadenylation element-binding proteins (CPEBs) are sequence-specific RNA binding proteins that bind to 3′ untranslated region (UTR) of cytoplasmic mRNAs, facilitate cytoplasmic polyadenylation, and regulate specific mRNA translation (Hake and Richter, 1994). In hippocampal neurons, upon activation of polyadenylation by CPEB, synaptic protein synthesis can be upregulated, thereby strengthening synaptic activity and memory formation (Du and Richter, 2005; Si et al., 2003a; Wu et al., 1998). CPEB is found in several invertebrate and vertebrate neurons, and 4 *CPEB* genes (*CPEB1–4*) have been identified in mammals (Richter, 2007; Si et al., 2003a; Theis et al., 2003). All CPEB proteins have two RNA recognition domain (RRM motifs) and two zinc-finger motifs in the C-terminal region, yet CPEB2, CPEB3, and CPEB4 are more closely related to each other than to CPEB1(Hake and Richter, 1994; Huang et al., 2006; Ivshina et al., 2014). *Aplysia* CPEB (ApCPEB) and *Drosophil*a Orb2A, and mouse CPEB3 have two distinct functional conformations in which they can convert from soluble monomers to amyloidogenic oligomers; this aggregated conformation is physiologically active, which it enables to mediate the

target mRNA translation at activated synapses (Fioriti et al., 2015; Khan et al., 2015; Kruttner et al., 2012; Rayman and Kandel, 2017; Si et al., 2010). In particular, application of repeated pulses of 5-HT in the sensory-motor neuron coculture induces ApCPEB multimerzation at the stimulated synapses and long-term facilitation (LTF), which is a form of learning-related synaptic plasticity that is widely studied in *Aplysia* (Si et al., 2010; Si et al., 2003b). Treatment with ApCPEB antisense oligonucleotides 24 hours after repeated pulses of 5-HT abrogates the persistence of LTF, and results in a significant reduction of newly formed sensory neuron varicosities induced by 5-HT (Miniaci et al., 2008).

In mammals, CPEB3 is suggested to be most similar to *Aplysia* CPEB, where it possesses N terminal prion-like domain and can convert from monomer to oligomers to mediate translational machinery upon neuronal stimulation. CPEB3 is highly expressed in the brain and heart, weakly expressed in the liver, kidney, embryo, and ovary, and not expressed in the lung, spleen, and thymus (Theis et al., 2003; Wang and Cooper, 2009). CPEB3 protein is found in the postsynaptic density (PSD) and is unique in that it represses the translation of AMPARs subunit GluR2 in the basal state (Huang et al., 2006). Experiments with hippocampal neurons stimulated with glycine showed that when CPEB3 is activated, it can promote the translation of AMPARs, highlighting the importance of CPEB3 in regulating mRNA translation (Drisaldi et al., 2015). CPEB3 also acts as a translational modulator for long-term synaptic plasticity. SUMOylation of CPEB3 was observed in unstimulated neuronal cultures of naïve animals, whereas deSUMOylated and the aggregated form of CPEB3 was observed in glycine stimulated

hippocampal neuronal cultures and contextual fear conditioning mice (Drisaldi et al., 2015). Moreover, SUMOylation regulates CPEB3 distribution and oligomerization, in which CPEB3 is localized to cytoplasmic processing bodies (P bodies) under the basal state, and redistributed to polysomes upon chemical induced LTP (Ford et al., 2019).

In cerebellar stellate cells, Ca^{2+} entry during action potential enhances CPEB3 protein expression at proximal dendrites *via* protein kinase C (PKC) activation, and this signaling results in a suppression of GluA2 protein synthesis and increase in GluA2-lacking AMPARs protein synthesis (Savtchouk et al., 2016). In addition, CPEB3 plays a novel role in regulating transcription. CPEB3 shuttles from the cytoplasm to the nucleus upon NMDA stimulation, and the nuclear CPEB3 can interact with signal transducer activated transcription (Stat) 5b and suppress Stat5b-dependent epidermal growth factor receptor (EGFR) transcription, which in turn influences spatial learning and memory performance (Peng et al., 2010). Activation of CPEB3 translation is induced by the calpain 2 mediated cleavage mechanism through NMDAR signaling. The influx of calcium via NMDAR triggers calpain 2 proteolysis of CPEB3 repressor fragment, and subsequently activates activity-dependent translation of CPEB3 (Wang, 2011). CPEB2, CPEB3 and CPEB4 are regulated by miR-92 and miR-26 in paralog positions of 3′-UTRs, and the target motif is evolutionary conserved in vertebrates (Morgan et al., 2010).

Studies of CPEB3 in memory formation revealed that the local protein synthesis and long-term memory storage are regulated by the prion-like CPEB3 aggregates: the

aggregation of CPEB3 is thought to strengthen synaptic plasticity in the hippocampus; and *CPEB3* conditional knockout mice display impairments in memory consolidation, object placement recognition, and long-term memory maintenance (Drisaldi et al., 2015). However, a different *CPEB3* KO mouse model has produced substantially the opposite results with respect to memory formation, where the total knockout mice exhibit better spatial memory consolidation in Morris water maze and short-term memory in contextual fear conditioning (Chao et al., 2013). This suggests that CPEB3 might have multiple roles in memory formation and that a different experimental approach may be necessary to decipher the biological role(s) of this gene.

The Hepatitis delta virus (HDV) ribozyme: A RNA enzyme that exerts a self-cleaving action

Ribozymes are small RNA molecules that exhibit catalytic properties. These self-cleaving ribozymes, ranging from 40 to 200 nucleotides in length, have complex folded secondary and three-dimensional structure (Serganov and Patel, 2007). There are five major classes of ribozymes that catalyze self-cleavage including hammerhead, hairpin, hepatitis delta virus (HDV), Neurospora Varkud satellite (VS) motif, and the bacterial 97ainite-amine-6-phosphate synthase (glmS) ribozyme. In addition, there are other classes recently identified including the group I intron-like ribozyme (GIR 1), twister, twister sister, pistol, hatchet motif, murine B2 and human ALU from short interspersed nuclear element (SINE) retrotransposons (Hernandez et al., 2020; Jimenez et al., 2015; Serganov and Patel, 2007; Weinberg et al., 2015). The HDV ribozyme was discovered in the human genome through *in vitro* selection, and it was found in genomic and

antigenomic RNA strands through rolling-circle replication (Ferre-D'Amare et al., 1998; Riccitelli and Luptak, 2013; Sharmeen et al., 1988). The self-cleaving process catalyzed by HDV ribozyme occurs via phosphodiester-cleavage reaction, in which 2'-hydroxyl (OH) nucleophile attacks the adjacent phosphate phosphodiester backbone of the RNA, and yields a 2′,3′-cyclic phosphate and 5′-OH termini (Murray et al., 1998). Both genomic and antigenomic HDV ribozymes are folded into a unique secondary structure. It is composed of five helical stems (P1, P2, P3, P1.1, and P4), linked by joining (J) strands J1/2 and J4/2, and folded into a nested double pseudoknot. Structural and mechanistic studies showed that the active-site cytosine (C75) possesses a direct role as a general base to deprotonate the 2′-OH of the nucleotide from the cleavage site in the reaction (Ferre-D'Amare et al., 1998). Furthermore, evidence suggested that divalent metal ions promote ribozyme self-scission reaction, in which a Mg^{2+} ion was observed in the ribozyme active site. The interaction between Mg^{2+} ion and active site residues suggests Mg^{2+} ion is involved in catalysis by facilitating deprotonation and stabilizing the transition state in the active site (Nakano et al., 2001; Riccitelli and Luptak, 2013; Shih and Been, 1999).

More recently, HDV-like ribozymes have been found in diverse organisms through *in vitro* genomic selection and bioinformatics searches, including insects, plants, fish, fungi, and mammals (Riccitelli and Luptak, 2013; Webb and Luptak, 2011; Webb et al., 2009). These HDV-like ribozymes exert a variety of biological functions in self-cleavage, retrotransposition processing, and regulation of mRNA translation. In particular, *in vitro* selection of the human genomic library revealed a highly conserved

mammalian sequence sharing the secondary structure and catalytic mechanism with the HDV ribozymes in the *CPEB3* gene (**Fig. 3.1**) (Salehi-Ashtiani et al., 2006; Webb and Luptak, 2011). The CPEB3 ribozyme is conserved among mammals and its self-scission is modulated both by mutations in the catalytic core (Salehi-Ashtiani et al., 2006) and by upstream sequences that interfere with folding of the rest of the ribozyme (Chadalavada et al., 2010), a well-known effect in HDV ribozymes (Chadalavada et al., 2000; Jeong et al., 2003; Nishikawa et al., 1999; Ruminski et al., 2011). Moreover, expressed sequence tags (ESTs), 5′ rapid amplification of cDNA ends (5′ RACE), and RT–PCR experiments of human and mouse tissues showed that the CPEB3 ribozyme is expressed *in vivo*, and the self-cleavage activity is tissue-specific (Chadalavada et al., 2010; Salehi-Ashtiani et al., 2006). The CPEB3 ribozyme has been hypothesized to play a role in regulating CPEB3 translation, whereby the higher rate of ribozyme self-cleavage leads to lower expression of the full-length CPEB mRNA and consequently protein expression (Salehi-Ashtiani et al., 2006). The mouse ribozyme is located 14 kbp upstream of the third exon of the *CPEB3* gene (**Fig. 3.1**). In humans, a single nucleotide polymorphism (SNP) at the ribozyme cleavage site, resulting in 3-fold higher rate of *in vitro* self-scission, is associated with episodic memory (Salehi-Ashtiani et al., 2006; Vogler et al., 2009). As a result, these findings demonstrate that HDV-like ribozymes are evolved to serve distinct biological roles in nature.

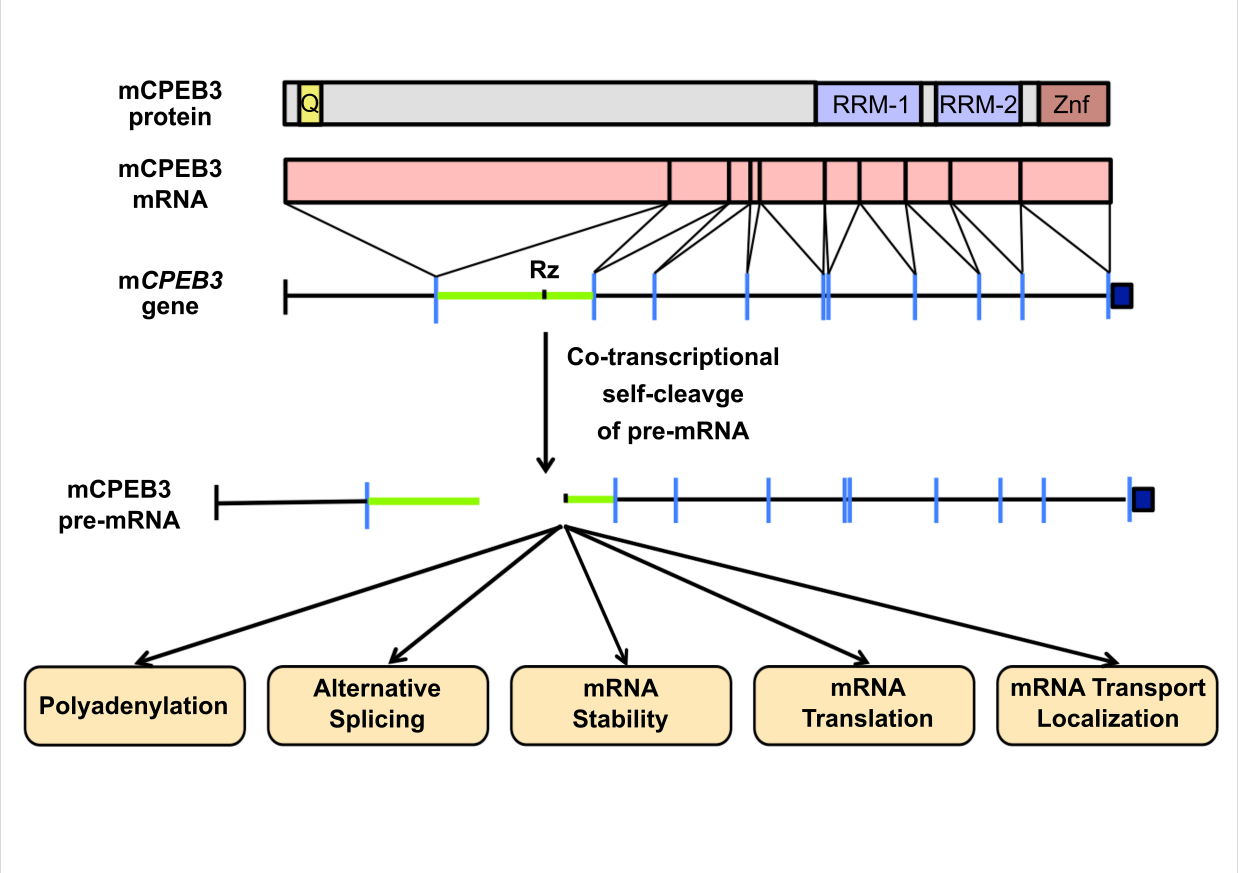

Figure 3.1. Schematic representation of mouse mRNA of *CPEB3* gene. Rz denotes the ribozyme location. The ribozyme is located in the second intron between the 2nd and 3rd exon.

Antisense oligonucleotides (ASOs)

The genomic revolution has helped us expand our knowledge of the biological mechanisms of brain disease. Nucleic acid-based therapies have been recognized as a novel drug discovery paradigm that has translated into gene therapy, precision medicine, and molecular targeted therapy. Several types of nucleic-based therapies have been investigated and developed including antisense oligonucleotides (ASOs), small interfering RNA (siRNA), microRNA, non-coding RNA, aptamers, RNA decoys, splice-witching oligonucleotides, gene-editing CRISPR-Cas, and immune modulating oligonucleotides (Burnett and Rossi, 2012; Smith and Zain, 2019; Sridharan and Gogtay, 2016). In particular, we are interested in exploring the potential of ASO technologies in treating CNS diseases. ASOs are short synthetic single-strand DNA, typically 8 to 50 base pairs in length, designed to bind to a sequence-specific region of RNA through Watson-Crick base pairing. Upon hybridization to the target RNA, ASOs can inhibit RNA and promote or reduce translation of target protein via different mechanisms, and therefore, alter disease pathophysiology.

In order to deliver ASOs effectively to target cells, modifications of backbone and sugar have been studied to improve ASOs stability and specificity. The first generation of ASOs is the ASOs with phosphorothioate (PS) backbone modification. The replacement of nonbridging oxygen atoms in the phosphodiester linkage with sulfur significantly enhances nuclease resistance and increases plasma protein binding, leading to slower excretion by glomerular filtration and longer half-lives in serum (Eckstein, 2000; Juliano, 2016; Wahlestedt et al., 2000). These ASOs are designed to

activate the RNase H cleavage mechanism. RNase H is a ubiquitous enzyme that hydrolyzes the RNA-DNA heteroduplex and cleaves the RNA, and therefore, ASOs worked with RNase H-dependent activity can robustly degrade the target RNA (Bennett and Swayze, 2010; Crooke, 2004; Wu et al., 2004). While promising, a major disadvantage of PS-ASO is the nonspecific side effects such as complement cascade activation and immune stimulation (Mansoor and Melendez, 2008).The second generation of ASOs involves modifications of sugar moieties at the 2' ribose position such as 2′-O-methyl (2′-Ome) and 2′-O-methoxy-ethyl (2′-MOE). However, ASOs with fully 2′-Ome and 2′-MOE modifications are not substrates for RNase H and do not support RNase H-dependent cleavage. To circumvent this challenge, the "gapmer" strategy as the second generation ASOs was developed, where chimeric ASOs have a core region of PS-ASO and are flanked by 2′-O-Me or 2′-MOE modifications at each end. This development considerably improves hybridization affinity of the targeted RNA, increases nuclease resistance, and decreases PS-ASO induced immunostimulatory toxicity (Bennett and Swayze, 2010; Juliano, 2016; Shen and Corey, 2018).

More recently, the third generation of ASOs was developed to enhance target affinity, pharmacological properties, and pharmacokinetic properties. This includes peptide nucleic acid (PNA), phosphoroamidate morpholino oligomer (PMO), 2′-deoxy-2′-fluoro-b-D-arabino nucleic acid (FANA), cyclohexene nucleic acids (CeNAs) and 102ainite102-DNA (tcDNA), locked nucleic acid (LNA), and 2'-O,4'-C-ethylene-bridged nucleic acid (ENA) (Kurreck, 2003; Shen and Corey, 2018; Smith and Zain, 2019).PNA contains a pseudopeptide polymer (N-(2-aminoethyl)glycine)N-2-aminoethylglycine

backbone and has good Watson–Crick hybridization properties. It also provides high resistance to nuclease and protease degradation. Similarly, PMO has phosphoroamidate linkage backbone and the ribose sugar replaced by a morpholino ring (Evers et al., 2015; Summerton and Weller, 1997). PMO has been shown to target translation inhibition and alternative splicing modification of pre-mRNA, in which ICV administration of PMO extended survival and improved neuromuscular phenotype in spinal muscular atrophy (SMA) mice (Porensky et al., 2012). Both PNA and PMO are nonpolyanion oligomers and they do not activate RNase H for RNA cleavage. The mechanism of PNA and PMO is featured by steric hindrance of translation machinery (Summerton, 2003). A major disadvantage of PNA and PMO is poor cellular uptake and poor pharmacokinetics. Strategies utilizing cell-penetrating peptide conjugation to ASOs were investigated to facilitate intracellular delivery of PNA and PMO (Amantana et al., 2007; Shiraishi and Nielsen, 2011). Furthermore, some off-target effects were observed in PMOs studies (Eisen and Smith, 2008). Minimization of off-target effects has to be considered when delivering PMO *in vivo*. LNA, a conformationally restrained ribose ring that contains O2'-C4'-methylene linkage, elicits unprecedented binding affinity compared to a DNA-RNA duplex, enhances specificity, and improves biostability (Evers et al., 2015; Wahlestedt et al., 2000). Like any PNA and PMO, LNA does not induce RNase H-mediated cleavage; therefore, gapmers were incorporated with LNA to recruit RNase H (Bennett et al., 2017). However, studies reported LNA induced significant hepatotoxicity (Swayze et al 2007; Burdick et al. 2014). Subsequently, several LNA analogs have evolved via structure modifications to address toxicity profiles (Seth et al., 2009; Soler-Bistue et al., 2019). ENA, a second generation of LNA,

has been studied in lymphoma and non-small cell lung cancer (NSCLC) phase I studies (Hong et al., 2015).

With promising progress of ASOs as a therapeutic agent, there are 182 clinical studies registered at ClinicalTrials.gov and currently there are 8 ASO therapies approved by the FDA (Levin, 2019; Yin and Rogge, 2019). Nusinersen, a phosphorothioate 2′-O-methoxyethoxy ASO, was the first drug approved to treat SMA in 2016. This ASO binds to intronic splicing silencer N1 (ISS-N1) that is located at downstream of exon 7 in *Survival Motor Neuron 2* (*SMN2*) gene and restores inclusion of *SMN2* exon 7 (Singh et al., 2017).

The CNS drug development is always challenging. With clinical efficacy, Nusinersen has a significant impact on ASO as a drug therapeutic platform for the treatment of CNS diseases. Currently ASO therapies are studied in clinical trials for various treatments including AD, ALS, HD, MS, and Duchenne's muscular dystrophy (DMD) (Bennett et al., 2017; Khorkova and Wahlestedt, 2017). In our study, we use the most recent ASO technology to examine the effect of CPEB3 ribozyme on memory formation.

3.1 Results and Discussion

CPEB3 mRNA expression and ribozyme activity are upregulated in response to neuronal stimulation

The neuronal activity-dependent gene regulation is essential for synaptic plasticity (Neves et al., 2008). To investigate the effect of the CPEB3 ribozyme on the *CPEB3* gene expression, and measure its effect on mRNA maturation and protein expression, primary cortical neurons were stimulated by glutamate or potassium chloride (KCl). Expression of the *CPEB3* gene was examined at various time points post stimulation. First, levels of the CPEB3 mRNA were analyzed with specific primers that amplified across the exon-exon splice junctions (exons 2–3, 3–6, 6–9; **Fig. 3.1**). Glutamate stimulation resulted in an increase of exons 2–3 mRNA expression at 2 hours, and downregulation at prolonged time points (**Fig. 3.2A**; one-way ANOVA with Sidak's *post hoc* tests, $F_{(5,21)} = 5.826$, $P = 0.0016$). Increased levels of exons 3–6 were observed up to 4 hours after treatment (**Fig. 3.2A**; unpaired *t* test, $t = 4.564$, $df = 4.879$, $P = 0.0064$), and a slight increase in CPEB3 exons 6–9 was observed at 6 hours (**Fig. 3.2A**; unpaired *t* test, $t = 2.916$, $df = 3.143$, $P = 0.0583$). To examine CPEB3 ribozyme activity, total and uncleaved ribozyme expressions were determined by qRT-PCR and fraction cleaved was calculated as [(total ribozyme – uncleaved ribozyme)/total ribozyme]. An increase of total ribozyme expression was observed in response to glutamate, correlating with CPEB3 mRNA expression (**Fig. 3.2B**; one-way ANOVA with Sidak's *post hoc* tests, $F_{(5,26)} = 4.657$, $P = 0.0036$). Similarly, membrane depolarization by KCl induced an up-regulation of CPEB3 mRNA at 2 hours compared with non-

stimulated cultures (**Fig. 3.2C**; exons 3–6: one-way ANOVA with Sidak's *post hoc* tests, $F_{(5,12)}$ = 25.48, P < 0.0001. exons 6–9: one-way ANOVA with Sidak's *post hoc* tests, $F_{(5,12)}$ = 4.376, P = 0.0168). Ribozyme activity showed an increase at 1 hour following KCl treatment, indicating that the ribozyme is concomitantly self-cleaving in an activity-dependent manner (**Fig. 3.2D**; one-way ANOVA with Sidak's *post hoc* tests, $F_{(5,17)}$ = 12.96, P < 0.0001). This finding is supported by previous studies showing that synaptic stimulation by glutamate leads to an increase in CPEB3 protein expression in hippocampal neurons (Fioriti et al., 2015) and treatment with 106ainite likewise induces CPEB3 expression in the hippocampus (Theis et al., 2003). Taken together, these data suggest that the self-cleaving ribozyme is both expressed and activated by neuronal activity, and it is likely involved in *cis* regulation of the (pre-)mRNA, translation of which in turn contributes to learning and memory.

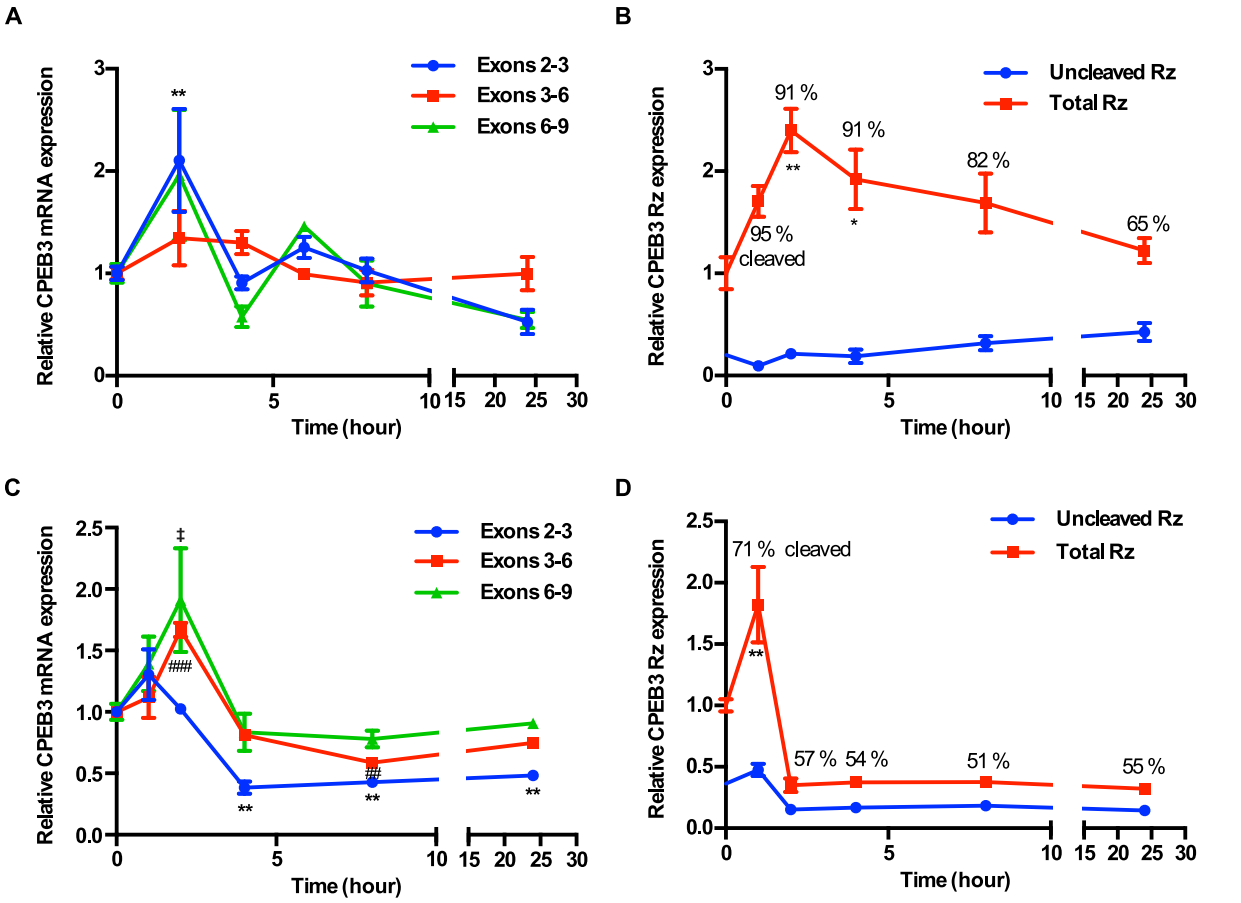

Fig. 3.2. Neuronal stimulation profile of the *CPEB3* gene in embryonic cortical neurons. (A) CPEB3 mRNA exons 2–3 expression is upregulated 2 hours after glutamate stimulation (one-way ANOVA with Sidak's *post hoc* tests. ***P* < 0.01). (B) CPEB3 total ribozyme expression is upregulated 2 hours after glutamate treatment (one-way ANOVA with Sidak's *post hoc* tests. **P* < 0.05, ***P* < 0.01). % cleaved was calculated as [(total ribozyme – uncleaved ribozyme)/total ribozyme]. (C) CPEB3 mRNA expression is significantly increased after membrane depolarization by KCl at early time points and reduced at 24 hours (one-way ANOVA with Sidak's *post hoc* tests. **P* < 0.05, ***P* < 0.01, ##*P* < 0.01, ###*P* < 0.001, ‡*P* < 0.05). (D) CPEB3 total ribozyme expression is upregulated at 1 hour after KCl induction (one-way ANOVA with Sidak's *post hoc* tests. ***P* < 0.01). Data are presented as mean ± SEM.

Co-transcriptional cleavage of CPEB3 ribozyme at different Mg^{2+} concentrations

To study the self-scission activity of CPEB3 ribozyme, genomic region containing mouse CPEB3 ribozyme was amplified, and *in vitro* co-transcriptional kinetics was performed to mimic ribozyme self-cleavage *in vivo*. Previous diffusion ordered spectroscopy (DOSY) NMR studies identified eight Mg^{2+} binding sites, some of which are important for functional folding and catalysis (Skilandat et al., 2016). As Mg^{2+} is a cofactor for ribozyme catalysis, different concentrations of Mg^{2+} were introduced in the kinetic reaction to study the role of Mg^{2+} in the CPEB3 ribozyme. Aliquots were collected at indicated time points and terminated by addition of quench solution. The self-cleaving activity of CPEB3 ribozyme is dependent on Mg^{2+} concentration, where minimal RNA self-cleavage products were observed at 0 mM of Mg^{2+}, and ~60% of CPEB3 ribozyme was cleaved at 10 mM of Mg^{2+} (**Fig. S3.1 A** and **B**). Indeed, Nakano and colleagues have shown that low concentrations of Mg^{2+} promote ribozyme folding, particularly in the inner catalytic core and the nested double pseudoknot structure. At high concentrations of Mg^{2+}, Mg^{2+} ions have been shown to facilitate catalysis by interacting directly with 2′-OH and coordinating with bridging and nonbridging oxygen of the scissile phosphodiester (Frederiksen and Piccirilli, 2009; Nakano and Bevilacqua, 2001). In line with these observations, our data showed distinct cleavage products of CPEB3 ribozyme in higher concentrations of Mg^{2+}, suggesting higher concentration of Mg^{2+} is necessary for efficient self-cleavage. Together, this demonstrates that the presence of Mg^{2+} is essential for catalysis of newly transcribed RNA.

Antisense oligonucleotides (ASOs) inhibit CPEB3 ribozyme self-cleaving activity

Given that the rate of transcription by RNA polymerase II is around 2000 nucleotides/min, and that the CPEB3 ribozyme is located at 14 kb upstream of the third exon, the estimated time for RNA polymerase II to reach exon 3 after ribozyme synthesis is ~7 minutes (Salehi-Ashtiani et al., 2006; Ucker and Yamamoto, 1984). Our *in vitro* measurements of the co-transcriptional ribozyme self-scission showed a $t_{1/2}$ of ~7 minutes, suggesting that the ribozyme activity is tuned to the co-transcriptional processing of the CPEB3 pre-mRNA. To modulate the activity of the ribozyme, we used antisense oligonucleotides (ASO) spanning the CPEB3 ribozyme cleavage site (**Fig. 3.3**). ASOs are synthetic single-stranded nucleic acids that can bind to pre-mRNA or mature RNA through Watson-Crick base-pairing, and typically trigger RNA degradation machinery by RNase H. ASOs have previously been used to modulate alternative splicing, suggesting that they act co-transcriptionally (e.g. to correct *SMN2* gene (Hua et al., 2010)). ASOs were designed to block co-transcriptional self-scission, and screened to identify promising candidates that exhibit the highest inhibitory effect of ribozyme self-cleavage. Ribozymes were inhibited in the presence of ASOs that block the ribozyme cleavage site: as the CPEB3 ribozyme was synthesized, 80% of it remained uncleaved in the presence of ASOs, compared to 50% in the presence of a control, sense oligonucleotides at the 10-min time point (**Fig. S3.2C**; unpaired *t* test, $t = 3.031$, $df = 4.619$, $P = 0.0321$). Similarly, another ASO targeting at the upstream ribozyme leader sequence results in a reduction of ribozyme self-scission activity (**Fig. S3.2D**; unpaired *t* test, $t = 4.785$. $df = 3.987$ $P = 0.0088$). These results illustrate that ASOs designed to base–pair with the ribozyme can prevent it from self-cleaving. Percent of inhibition was calculated by normalizing fraction cleaved of each ASO to its corresponding sense

oligonucleotides at 10-min reaction time-point, and we found that top candidates ASOs inhibit CPEB3 ribozyme self-cleavage by 50% and 25% (**Fig. S3.2; C** and **D**). The most effective ASO constructs were selected for the use *in vitro* and *in vivo*. To improve ASOs specificity and stability *in vivo*, the lead ASO used in the study were chemically modified and synthesized by Ionis Pharmaceuticals.

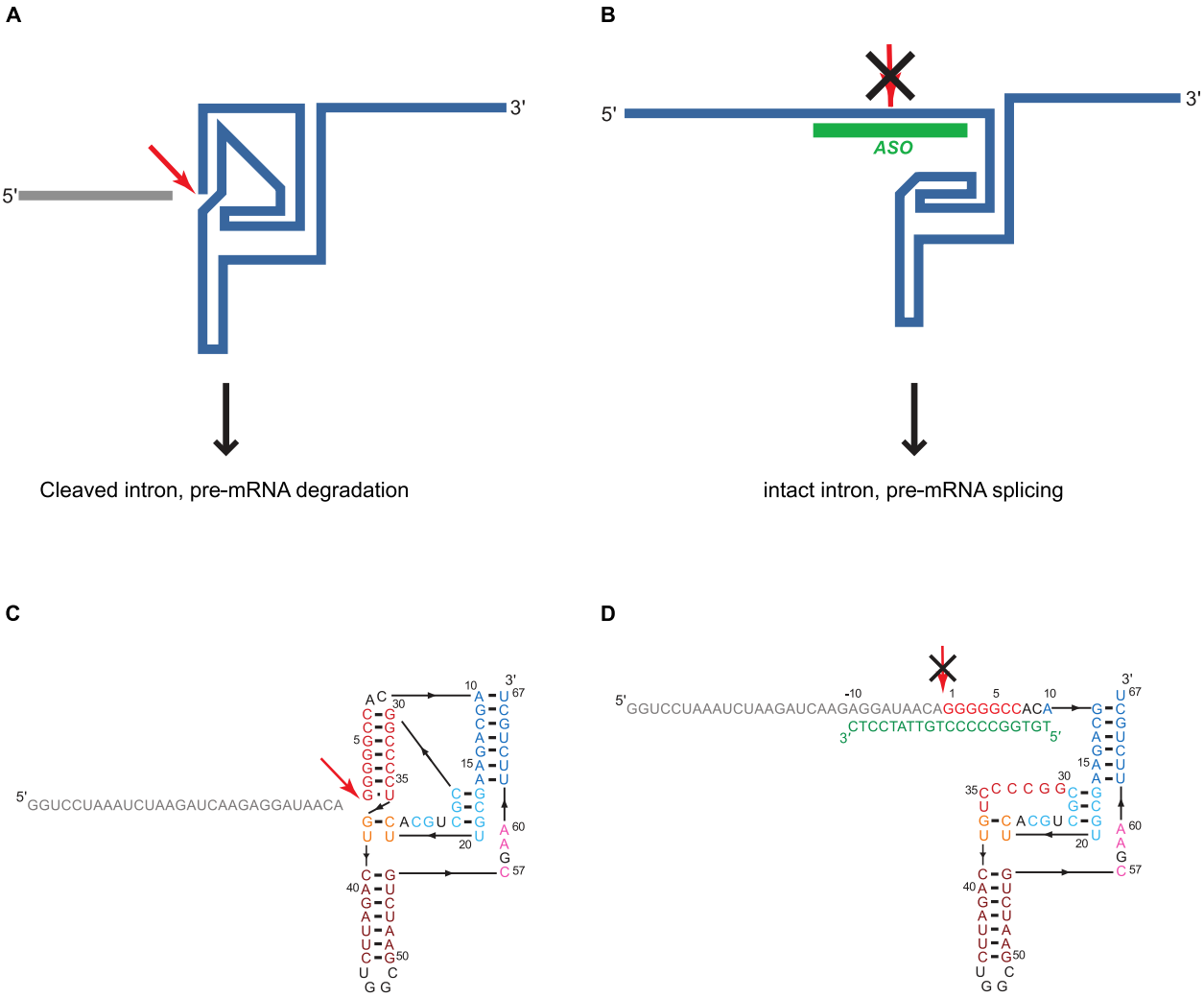

Fig. 3.3. Inhibition of the CPEB3 ribozyme by an ASO targeting its cleavage site. (A) and (B) Model of CPEB3 ribozyme inhibition. Intron cleavage (red arrow) results in liberation of the upstream sequence (gray) and pre-mRNA degradation, whereas binding by the ASO (green line) inhibits the ribozyme activity, leading to higher levels of mature CPEB3 mRNA. (C) Secondary structure of the ribozyme. Sequence upstream of the ribozyme is indicated by gray color and the site of self-scission is shown with the red arrow. (D) Model of the ribozyme inhibited by the ASO (green letters) showing base-pairing between the ASO and 10 nucleotides upstream and downstream of the ribozyme cleavage site. Inhibition of self-scission is indicated by crossed arrow.

CPEB3 mRNA is upregulated in primary neuronal cultures treated with ASO

Emerging evidence suggests that regulation of gene expression in dendrites is pivotal in synaptic plasticity, in which synapses undergo structural and functional changes in response to synaptic signals (Neves et al., 2008). In neurons, CPEB3 plays dual roles in regulating mRNA translation (Du and Richter, 2005; Stephan et al., 2015). A post-translational modification of CPEB3 can convert it from a repressor to an activator: a monoubiquitination by Neuralized1 leads to activation of CPEB3, which promotes subsequent polyadenylation and translation of GluA1 and GluA2 (Pavlopoulos et al., 2011). Our data suggest that CPEB3 ribozyme activity is correlated with mRNA expression. We hypothesize that regulation of self-cleaving CPEB3 ribozyme may modulate CPEB3 mRNA splicing. To test this hypothesis, we used the lead ASO from co-transcriptional analysis to inhibit the ribozyme activity. To study the effect of CPEB3 ribozyme on its mRNA expression, neuronal cultures were pretreated with either ASO or scrambled control ASO, followed by a 5-minute KCl membrane depolarization. To evaluate whether CPEB3 ribozyme activity is activity-dependent, cultures at different time points were collected after neuronal stimulation. First, we tested whether the lead ASO can inhibit CPEB3 ribozyme expression. In the absence of ASO, KCl induced a rapid and robust increase in ribozyme expression at 2-hour time point compared to the scrambled ASO, whereas this activity was blocked in the presence of ASO (**Fig. 3.4A**; one-way ANOVA with Sidak's *post hoc* tests, $F_{(3,19)} = 8.259$. $P = 0.0010$). These results indicate that the ASO can bind to CPEB3 ribozyme, and inhibit the expression of CPEB3 ribozyme effectively. Next, we tested whether ASO treatment affects CPEB3 gene expression. At the early time point (2 hours post KCl induction), ASO resulted in

an increase of CPEB3 mRNA expression (**Fig. 3.4 B and C**; exons 2–3: one-way ANOVA with Sidak's *post hoc* tests, $F_{(3,20)}$ = 7.330, P = 0.0017; Exons 3–6: one-way ANOVA with Sidak's *post hoc* tests, $F_{(3,19)}$ = 4.906, P = 0.0109). This suggests that ASO prevents CPEB3 ribozyme from cleaving CPEB3 pre-mRNA, which promotes mRNA maturation. Intriguingly, we did not observe any difference in CPEB3 mRNA exons 6–9 between ASO and control groups (**Fig. 3.4D**; one-way ANOVA with Sidak's *post hoc* tests, $F_{(3,19)}$ = 1.788, P = 0.2202). At the later time point (24 hours post KCl induction), there were no significant differences in CPEB3 ribozyme expression between groups (**Fig. 3.4E**; one-way ANOVA with Sidak's *post hoc* tests, $F_{(3,18)}$ = 0.5720, P = 0.6406). Likewise, CPEB3 mRNA exons 2–3 level returned to the basal level (**Fig. 3.4F**; one-way ANOVA with Sidak's *post hoc* tests, $F_{(3,19)}$ = 1.179, P = 0.3441), while exons 3–6 remained slightly elevated in the ASO treatment groups (**Fig. 3.4G**; one-way ANOVA with Sidak's *post hoc* tests, $F_{(3,19)}$ = 4.427, P = 0.0160). The mRNA expression of CPEB3 exons 6–9 remained stable over time, and was not affected by ASO treatment or KCl stimulation (**Fig. 3.4H**; one-way ANOVA with Sidak's *post hoc* tests, $F_{(3,19)}$ = 0.7121, P = 0.5567). Combined, these data suggest that CPEB3 ribozyme plays a key role in modulating its mRNA processing.

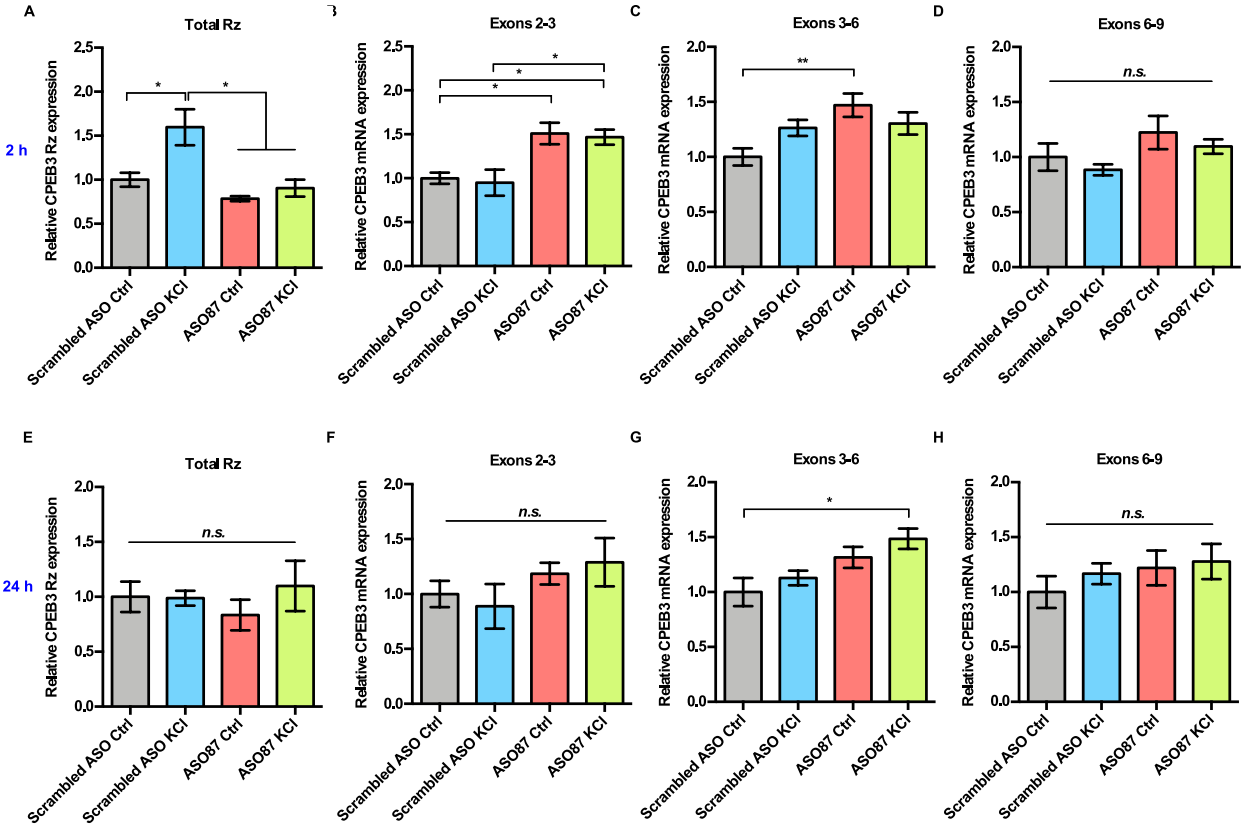

Fig. 3.4. Effect of CPEB3 ribozyme ASO on mRNA expression in embryonic cortical neurons. Primary cortical neurons were pretreated with ASO or scrambled ASO prior to KCl depolarization. Cells were harvested at 2-hour and 24-hour time points after KCl induction. (A) CPEB3 ribozyme activity was inhibited in the presence of ASO at 2 hours (one-way ANOVA with Sidak's *post hoc* tests, $*P < 0.05$). (B) Inhibition of the CPEB3 ribozyme by ASO resulted in upregulation of CPEB3 mRNA exons 2–3 expression at 2 hours (one-way ANOVA with Sidak's *post hoc* tests, $*P < 0.05$). (C) Inhibition of CPEB3 ribozyme by ASO resulted in upregulation of CPEB3 mRNA exons 3–6 expression at 2 hours (one-way ANOVA with Sidak's *post hoc* tests, $**P < 0.01$). (D) There was no significant difference in CPEB3 mRNA exons 6–9 expression between groups at 2 hours (one-way ANOVA with Sidak's *post hoc* tests, *n.s.* not significant). (E) There was no significant difference in CPEB3 ribozyme expression

between groups at 24 hours post KCl induction (one-way ANOVA with Sidak's *post hoc* tests, *n.s.* not significant). (F) There was no significant difference in mRNA exons 2–3 expression between groups at 24 hours (one-way ANOVA with Sidak's *post hoc* tests, *n.s.* not significant). (G) Pretreatment of ASO and KCl stimulation led to an increase in CPEB3 mRNA exons 3–6 expression at 24 hours (one-way ANOVA with Sidak's *post hoc* tests, $*P < 0.05$). (H) There was no significant difference in mRNA exons 6–9 expression between groups at 24 hours (one-way ANOVA with Sidak's *post hoc* tests, *n.s.* not significant). Data are presented as mean ± SEM.

The lead ASO is sequence specific and does not induce cytotoxicity in neuronal cultures

Similar to other small molecules and antibody drug discovery platforms, one of potential risks of antisense oligonucleotide technologies is the off-target effects, in which ASOs partially hybridize to sequences that are not their intended targets. This sometimes can result in unexpected toxicities such as innate immunostimulatory effects and hepato/nephrotoxicity, or alter the expression of other genes (Frazier, 2015; Shen and Corey, 2018). To mitigate hybridization-dependent off-target effects, our designed ASOs were chemically modified with bridged-nucleic acid, also known as locked nucleic acid (LNA), that was shown to have higher binding affinity against RNA with tremendous discriminatory properties (Rahman et al., 2008). To evaluate whether the lead ASO is specific targeting CPEB3 ribozyme, quantitative PCR of CPEB3 4^{th} intron was measured. No significant differences in the 4^{th} intron expression between groups were observed (**Fig. S3.2A**; one-way ANOVA with Sidak's *post hoc* tests, $F_{(3,18)} = 1.752$, $P = 0.1924$). This demonstrates that the lead ASO does not have a broad non-specific effect on the stability of other introns.

Previous studies reported that some second generation of ASOs lead to sequence dependent cytotoxicity and inhibit cell proliferation (Drygin et al., 2004). To assess whether the lead ASO induces cytotoxicity *in vitro*, neuronal cultures were treated with ASO or scrambled ASO, and XTT assay was performed to measure the cell viability. Relative cell viability was normalized to the vehicle control. No significant differences in cell viability were found in either ASO or scrambled ASO compared to untreated cells (**Fig. S3.2B**; Scrambled ASO: unpaired *t* test, $t = 0.1257$, $df = 2.986$, $P =$

0.9079. ASO: unpaired *t* test, $t = 0.5869$, $df = 5.437$, $P = 0.5808$), suggesting that the ASOs used in this study did not induce cytotoxic effects in cultured neurons.

CPEB3 ribozyme ASO treatment leads to an increase in CPEB3 protein expression

In primary hippocampal neurons, the level of CPEB3 protein expression is positively regulated by neuronal activity (Fioriti et al., 2015). We first examined whether inhibition of CPEB3 ribozyme modulates CPEB3 protein expression. Consistent with the previous study, CPEB3 protein level was upregulated in primary cortical neurons stimulated with KCl (**Fig. 3.5 A** and **B**; unpaired *t* test, $t = 2.756$, $df = 6.00$, $P = 0.0330$). Remarkably, treatment with ASO induced a significant increase in CPEB3 expression in both the basal state and the KCl-stimulated conditions (**Fig. 3.5 A** and **B;** one-way ANOVA with Sidak's *post hoc* tests, $F_{(3,24)} = 7.591$, $P = 0.0007$),, indicating a coordination of activity-dependent transcription and translation upon regulation of CPEB3 ribozyme activity.

Effect of CPEB3 ribozyme ASO on transcriptional and translational regulation of plasticity-related proteins in embryonic cortical neurons

In neurons, mRNA are transported to dendrites and translated to protein in response to synaptic stimulation (Martin and Zukin, 2006). To test whether inhibition of CPEB3 ribozyme affect plasticity-related protein translation, we examined mRNA levels and protein expression of GluA1 and GluA2 following pretreatment of ASO and KCl stimulation. Both GluA1 and GluA2 mRNA levels remained unchanged between groups.

(**Fig. 3.6A**; GluA1: one-way ANOVA with Sidak's *post hoc* tests, $F_{(3,35)}$ = 1.333, P = 0.2793. GluA2: one-way ANOVA with Sidak's *post hoc* tests, $F_{(3,35)}$ = 1.879, P = 0.1511). Yet we found that under transient depolarization by KCl, CPEB3 ribozyme ASO treatment led to an increase in GluA1 protein expression (**Fig. 3.5 A and C**; one-way ANOVA with Sidak's *post hoc* tests, $F_{(3,24)}$ = 3.040, P = 0.0485). In contrast, only a slight increase of GluA2 expression in ASO treatment groups was observed (**Fig. 3.5 A and C**; one-way ANOVA with Sidak's *post hoc* tests, $F_{(3,24)}$ = 2.523, P = 0.0817). PSD-95, a major synaptic plasticity regulator, has been shown to regulate AMPAR trafficking in the hippocampus and cortex (Ehrlich et al., 2007). It also promotes synaptic strengthening and synapse maturation, and mediates AMPAR synaptic potentiation (Ehrlich and Malinow, 2004; El-Husseini et al., 2000). Moreover, acute knockdown of PSD-95 results in decreased AMPA-mediated excitatory postsynaptic currents (EPSCs) in CA1 pyramidal neurons (Ehrlich et al., 2007). In fact, Chao and colleagues demonstrated the role of CPEB3 in the translational regulation of PSD95 expression (Chao et al., 2013). Here, we found that there were no differences in PSD-95 mRNA level between groups (**Fig. 3.6A**; one-way ANOVA with Sidak's *post hoc* tests, $F_{(3,34)}$ = 0.04508, P = 0.9871). Nevertheless, PSD-95 protein expression was elevated in cultures treated with ASO (**Fig. 3.5 A and C**; one-way ANOVA with Sidak's *post hoc* tests, $F_{(3,44)}$ = 3.729, P = 0.0209), indicating CPEB3 might facilitate PSD-95 translation in neurons. Similarly, NMDAR signaling has been suggested to regulate nucleocytoplasmic redistribution of CPEB3 to control gene expression and synaptic plasticity (Chao et al., 2012). We investigated whether NMDAR is regulated by the translation of CPEB3 resulting from ribozyme activity inhibition, and we found that ASO treatment led to up-regulation of one

of NMDAR subunits, NR2B protein expression (**Fig. 3.5 D and E**; one-way ANOVA with Sidak's *post hoc* tests, $F_{(3,19)} = 4.015$, $P = 0.0227$), while NR2B mRNA levels remained unchanged between groups (**Fig. 3.6A**; one-way ANOVA with Sidak's *post hoc* tests, $F_{(3,34)} = 0.1786$, $P = 0.9102$). This suggests that translational up-regulation of NMDAR is mediated by CPEB3.

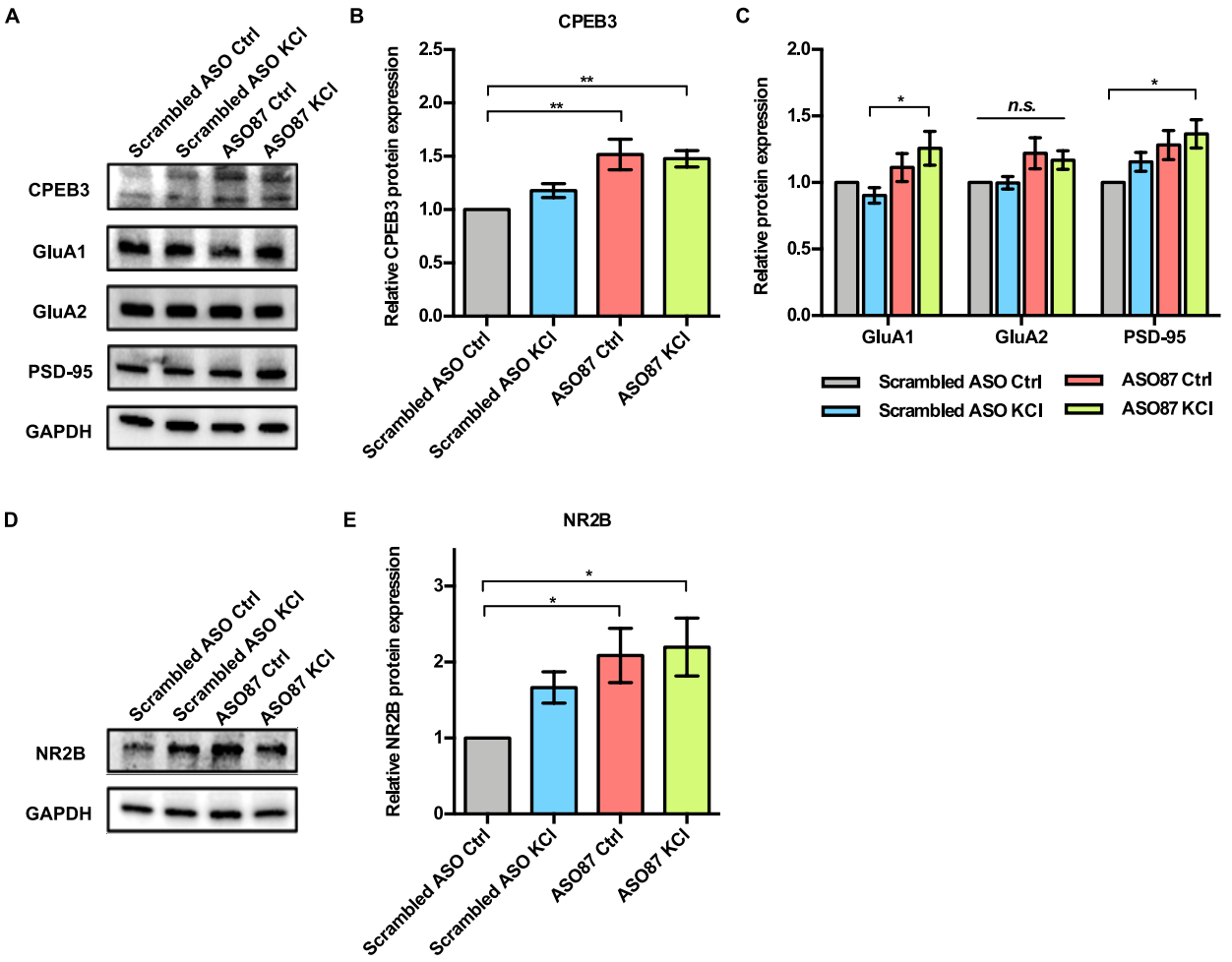

Fig. 3.5. Effect of CPEB3 ribozyme ASO on protein expression in embryonic cortical neurons. Primary neuronal cultures were pretreated with ASO or scrambled ASO followed by KCl stimulation. Cells were harvested 8 hours after KCl induction. CPEB3 and PRPs protein expression levels were analyzed by immunoblotting. (A) Representative image of CPEB3, GluA1, GluA2, and PSD-95 protein expression. GAPDH is used as a loading control. (B) Quantification of CPEB3 protein expression. Treatment of ASO followed by KCl stimulation led to an increase of CPEB3 expression (one-way ANOVA with Sidak's *post hoc* tests, $^{**}P < 0.01$). (C) Quantification of PRPs protein expression (one-way ANOVA with Sidak's *post hoc* tests, $^{*}P < 0.05$, *n.s.* not

significant). (D) Representative image of immunoblotting analysis showing NR2B protein expression. GAPDH is used as a loading control. (E) Quantification of NR2B protein level. ASO treatment led to an increase in NR2B expression (one-way ANOVA with Sidak's *post hoc* tests, $*P < 0.05$). Data are presented as mean ± SEM.

Effect of CPEB3 ribozyme ASO on polyadenylation in embryonic cortical neurons

Given the fact that 3′ UTR is necessary for mRNA processing, stability, transport, localization, and gene regulation, there has been increasing evidence to suggest the role of alternative polyadenylation (APA) in the CNS system (Mayr, 2017; Miura et al., 2014). In mammalian cells, most genes contain multiple polyadenylation sites (PAS) that can undergo alternative cleavage and polyadenylation machinery, resulting in different mRNA isoforms. Specifically, in neurons, distinct 3′ UTR preferentially selects distal rather than proximal 3′ UTR sites, and it undergoes significant 3′ UTR shortening in response to LTP (Fontes et al., 2017; Lau et al., 2010; Miura et al., 2014). Previous studies have suggested that the regulation of polyadenylation is governed by CPEB via Aurora A kinase phosphorylation, which in turn, initiates polyadenylation and mRNA translation (Mendez et al., 2000; Mendez and Richter, 2001). With an increase in CPEB3 protein production by CPEB3 ribozyme ASO, we investigated whether CPEB3 further changes polyadenylation of genes that are associated with synaptic function. 3′ RACE was carried out to study the regulation of polyadenylation in neurons. Total RNA isolated from primary cortical neurons was reverse transcribed using the oligo-dT adapter primer. Amplification was performed using gene-specific primers. Changes in exons-poly(A) tail or polyadenylation site (PAS)-poly(A) tail were determined by a nested qPCR approach. In this study, we focus on PRPs (i.e., AMPAR, NMDAR, and PSD-95). First, we measured exon-poly(A) level of each target gene among control or ASO treatment group, and we did not observe any significant difference in GluA1, GluA2, PSD-95, and NR2B expression between scrambled ASO and ASO groups (**Fig. 3.6B**; GluA1: unpaired *t* test, $t = 0.4868$, $df = 11.94$, $P = 0.6352$. GluA2: unpaired *t* test, *t*

= 1.089, *df* = 10.86, *P* = 0.2998. PSD-95: unpaired *t* test, *t* = 0.8342, *df* = 9.375, *P* > 0.4249. NR2B: unpaired *t* test, *t* = 0.4008, *df* = 14.73, *P* = 0.6943). Next, we measured whether there is any effect in poly(A) length based on the known polyadenylation sites. In these 3′ RACE experiments, to identify whether there is a change in polyadenylation sites, primer walking strategies were employed to screen across 3′ UTR PAS of each gene of interest. In non-stimulated cultures, CPEB3 ribozyme ASO treatment did not change poly(A) length of GluA1, GluA2, PSD-95, and NR2B (**Fig. 3.6C**; GluA1: unpaired *t* test, *t* = 1.382, *df* = 13.12, *P* = 0.1902. GluA2: unpaired *t* test, *t* = 0.9097, *df* = 11.32, *P* = 0.3819. PSD-95: unpaired *t* test, *t* = 0.7055, *df* = 14.37, *P* = 0.4918. NR2B: unpaired *t* test, *t* = 0.6918, *df* = 15.90, *P* = 0.4990). These results suggest that in the basal state, changes in CPEB3 protein expression by ribozyme inhibition did not affect AMPAR or NMDAR polyadenylation. Recent evidence suggests that neuronal activity promotes alternative polyadenylation, where hundreds of activity-dependent genes switched their polyadenylation sites from distal to proximal sites upon neuronal stimulation (Flavell et al., 2008). In addition, Du and Richter identified 6 mRNA targets including ABP, ELK2, δCaMKII, Map2, RCM3, and αCaMKII that can undergo activity-dependent polyadenylation in hippocampal neurons (Du and Richter, 2005). To further elucidate whether CPEB3 ribozyme is involved in APA process, future studies are expected to focus on neuronal activity-regulated polyadenylation site profiling.

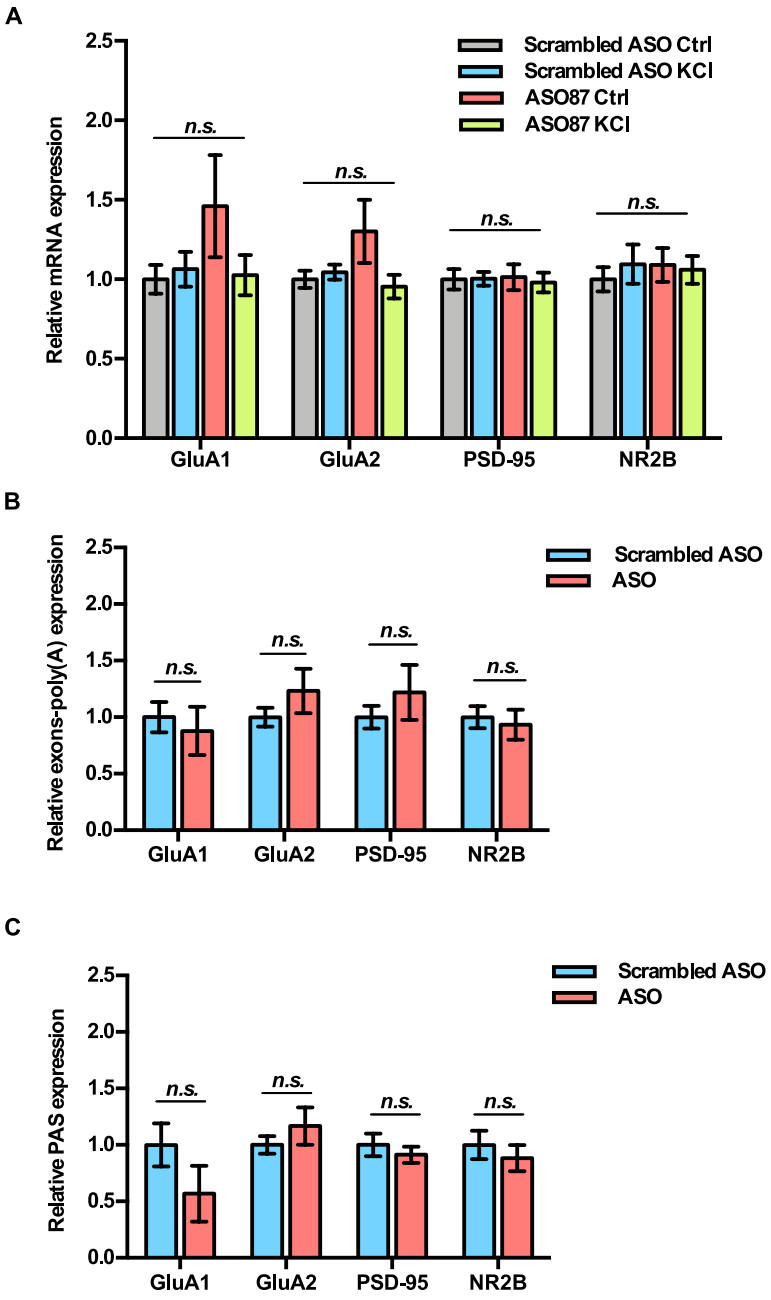

Fig. 3.6. Effect of CPEB3 ribozyme ASO on transcription and polyadenylaton of plasticity-related genes in embryonic cortical neurons. (A) Inhibition of CPEB3 ribozyme did not affect transcription of GluA1, GluA2, PSD-95, and NR2B (one-way ANOVA with Sidak's *post hoc* tests, *n.s.* not significant). (B) Effect of CPEB3 ribozyme ASO on polyadenylation of plasticity-related genes. 3′ RACE analysis revealed that

CPEB3 ribozyme ASO did not affect polyadenylation of plasticity related genes in the basal state (unpaired *t* test, *n.s.* not significant). (C) Specific polyadenylation sites of plasticity-related genes were identified based on the UCSC genome browser. Nested qPCR was performed using primers in close proximity to the known poly(A) site of each gene. In non-stimulated neuronal cultures, there was no significant difference in PAS between scrambled ASO and ASO groups (unpaired *t* test, *n.s.* not significant). Data are presented as mean ± SEM.

Dynamic regulation of activity-dependent nascent CPEB3 RNA in primary cortical neurons

The regulation of gene expression and underlying molecular mechanisms are typically measured on the global RNA expression level. Studying the dynamics of RNA transcription, processing, and degradation can provide insights into temporal RNA regulation. Conventional methods used radiolabeled nucleoside (3H-uridine) and autoradiography to study RNA synthesis (Olea and Nagata, 1992). Recent studies used uridine analogs including 4-thiouridine (4sU), 5-etyniluridine (5EU) and 5′-bromo-uridine (5BrU) to label *de novo* RNA transcripts in mammalian cells (Tani and Akimitsu, 2012). 4sU can be rapidly taken up by cells and thiolated RNAs can be isolated using organomercurial agarose affinity chromatography, or using thiol-specific biotinylation and streptavidin magnetic beads separation (Kenzelmann et al., 2007; Russo et al., 2017; Woodford et al., 1988). Similar to 4sU, 5EU can be incorporated into cellular RNA by transcription machinery. EU-labeled RNA can be separated from pre-existing RNA via biotinylation in a copper(I)-catalyzed azide alkyne cycloaddition (CuAAC) reaction, also known as click chemistry, followed by streptavidin purification (Jao and Salic, 2008). 5BrU is another nucleoside analog that can be incorporated into cells with high efficiency. 5BrU-labeled nascent RNAs can be immunoprecipitated using anti-bromodeoxyuridine (BrdU) antibody (Haider et al., 1997). The newly transcribed RNA can be analyzed by qPCR, microarray, and RNA-sequencing. These methodologies allow us to study the kinetics of transcription and RNA decay.

It is well recognized that L-LTP depends on gene transcription and protein synthesis (Igaz et al., 2002; Kandel, 2001; Nguyen et al., 1994). To further dissect whether CPEB3 ribozyme activity is involved in activity-dependent gene expression through gene transcription, cytoplasmic mRNA translation, or mRNA stability, metabolic labeling of nascent RNA with 5EU was performed to examine the transcriptional activity in primary cortical neurons. During the last hour of ASO pretreatment prior to synaptic stimulation (KCl 35 mM, 5 minutes), 5EU was added to the culture medium to label newly synthesized RNA. Cells were harvested at the indicated time points after neuronal stimulation. 5EU-labeled RNA was biotinylated and isolated from total RNA through streptavidin capture and subjected to qPCR analysis (**Fig. 3.7A**). Nascent transcripts of CPEB3 ribozyme and CPEB3 mRNA (exons 2–3) expression were evaluated at 1, 2, and 4 hours after KCl induction. In this study, we focused on activity-dependent transcriptional dynamics of CPEB3 ribozyme and its mRNA. Pretreatment of ASO with neuronal stimulation led to an increase in nascent CPEB3 ribozyme expression compared to the control at 1 hour (**Fig. 3.7B**; Scrambled ASO Ctrl vs ASO87 KCl; unpaired *t* test, $t = 3.185$, $df = 4.511$, $P = 0.0282$), whereas nascent CPEB3 mRNA (exons 2–3) remained unchanged (**Fig. 3.7C**; Scrambled ASO Ctrl vs ASO87 KCl: unpaired *t* test, $t = 0.1414$, $df = 4.347$, $P = 0.8939$). We observed a significant increase in CPEB3 ribozyme expression in ASO + KCl-induced group compared to scrambled ASO control and ASO non-stimulated control. (**Fig. 3.7D**; Scrambled ASO Ctrl vs ASO87 KCl: unpaired *t* test, $t = 4.248$, $df = 3.824$, $P = 0.0145$; ASO87 Ctrl vs ASO87 KCl: $t = 3.293$, $df = 5.708$, $P = 0.0178$, respectively). Similarly, we also found that newly synthesized CPEB3 mRNA (exons 2–3) transcripts were elevated in ASO + KCl

treatment cultures compared to scrambled ASO control at 2-hour time point (**Fig. 3.7E**; Scrambled ASO Ctrl vs ASO87 KCl: unpaired *t* test, $t = 2.526$, $df = 5.488$, $P = 0.0485$). At the 4-hour time point, no significant differences were observed in both CPEB3 nascent CPEB3 ribozyme expression and CPEB3 mRNA transcripts, implying that the nascent transcription might return to the basal level (**Fig. 3.7 F and G**; CPEB3 Rz Scrambled ASO Ctrl vs ASO87 KCl: unpaired *t* test, $t = 0.03682$, $df = 3.001$, $P = 0.9729$. CPEB3 mRNA, Scrambled ASO Ctrl vs ASO87 KCl: unpaired *t* test, $t = 0.9011$, $df = 4.956$, $P = 0.4092$). Together, these data suggest the combination of ASO treatment and neuronal activity might lead to a dynamic transcriptional response of CPEB3 ribozyme and mRNA, which might further regulate RNA processing and translation.

Previous studies have demonstrated mRNA are transported to dendrites and translated locally at activated synapses. An immediate early gene (IEG) *Arc* mRNA, for example, has been investigated extensively to elucidate RNA transcription, stability, and downstream LTP/LTD (Das et al., 2018; Farris et al., 2014). In hippocampal neurons, *Arc* mRNA transcripts were observed at nucleus at 30 minutes, and at cytoplasm at 2-hour after stimulation (Das et al., 2018). Though CPEB3 is suggested as an IEG that its mRNA transcripts are activated in the hippocampus after kainite injection (Theis et al., 2003), how CPEB3 transports to dendrites and affects local translation at the temporal scale remains to be elucidated.

Here we found newly transcribed CPEB3 mRNA is elevated at 2-hour time point and returned back to the basal level after 4 hours. It is unclear whether ASO treatment

or KCl induction alone could alter temporal dynamics of gene expression. Interestingly, primary neuronal cultures and HeLa cell lines exhibit similar transcription rate (~3 kb/min in primary neuronal culture, and 3.7 kb/min in HeLa cells), and the metabolic labeling time is dependent on the metabolic state (Duffy et al., 2018). A recent study by Akbalik *et al*. suggests that 5 mM of 5EU labeling resulted in a stronger signal in hippocampal distal dendrites. An increasing dendritic RNA signal is correlated with an increasing concentration as well as the labeling incubation time (Akbalik et al., 2017). Alternatively, a bioorthongonal metabolic labeling of newly synthesized RNA using the salvage enzyme uracil phophoribosyltransferase (UPRT)− 5EUracil system has been demonstrated to profile the transcriptome in specific cell population under activity-dependent conditions (Zajaczkowski et al., 2018). To fully elucidate the dynamic regulation of CPEB3 gene expression, further optimization of nascent RNA labeling method such as increasing labeling time, higher concentration of 5EU, and different time windows might be considered as future work.

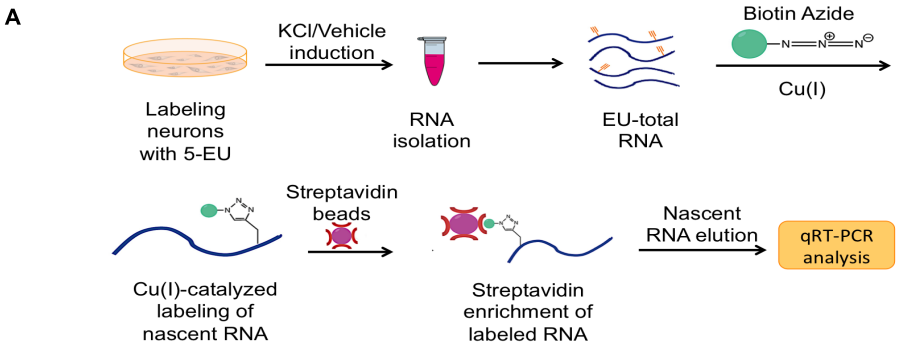
A
KCl/Vehicle induction
Biotin Azide
Cu(I)
Labeling neurons with 5-EU
RNA isolation
EU-total RNA
Streptavidin beads
Nascent RNA elution
qRT-PCR analysis
Cu(I)-catalyzed labeling of nascent RNA
Streptavidin enrichment of labeled RNA

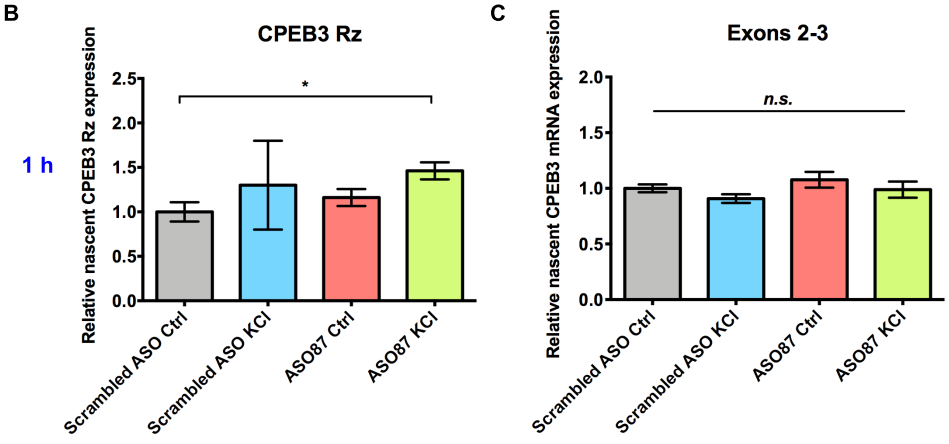
B
CPEB3 Rz
Relative nascent CPEB3 Rz expression
1 h
*
Scrambled ASO Ctrl
Scrambled ASO KCl
ASO87 Ctrl
ASO87 KCl

C
Exons 2-3
Relative nascent CPEB3 mRNA expression
n.s.
Scrambled ASO Ctrl
Scrambled ASO KCl
ASO87 Ctrl
ASO87 KCl

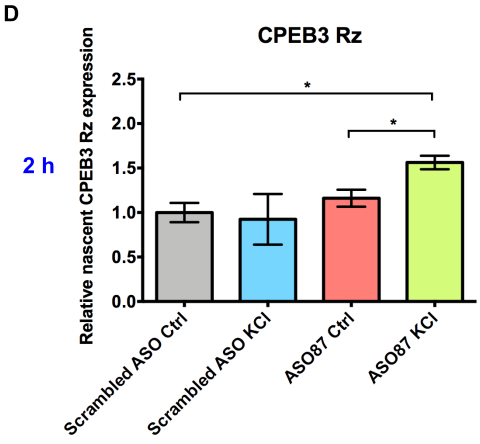
D
CPEB3 Rz
Relative nascent CPEB3 Rz expression
2 h
*
*
Scrambled ASO Ctrl
Scrambled ASO KCl
ASO87 Ctrl
ASO87 KCl

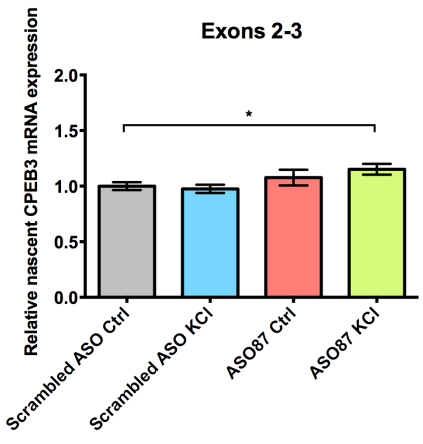
E
Exons 2-3
Relative nascent CPEB3 mRNA expression
*
Scrambled ASO Ctrl
Scrambled ASO KCl
ASO87 Ctrl
ASO87 KCl

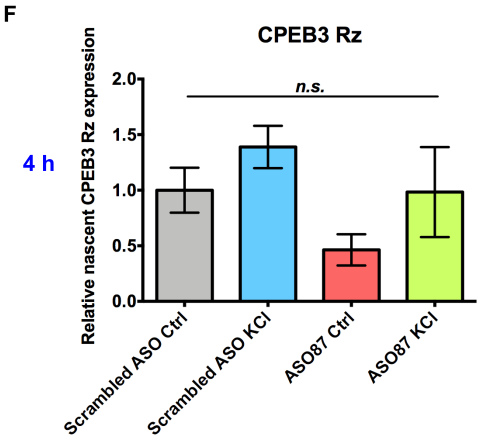
F
CPEB3 Rz
Relative nascent CPEB3 Rz expression
4 h
n.s.
Scrambled ASO Ctrl
Scrambled ASO KCl
ASO87 Ctrl
ASO87 KCl

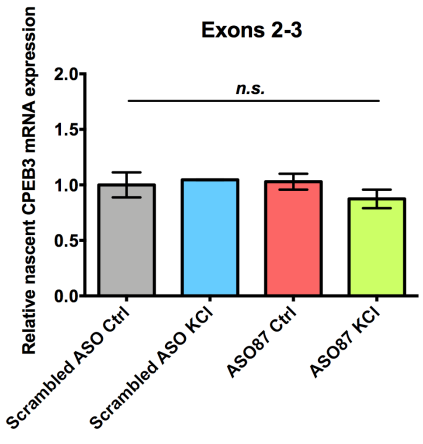
G
Exons 2-3
Relative nascent CPEB3 mRNA expression
n.s.
Scrambled ASO Ctrl
Scrambled ASO KCl
ASO87 Ctrl
ASO87 KCl

Fig. 3.7. Dynamic regulation of activity-dependent nascent CPEB3 RNA in primary cortical neurons. (A) Schematic of RNA synthesis monitoring with 5EU. Primary embryonic cortical neurons were pretreated with ASO and labeled with 5EU prior to KCl induction. Cells were harvested at 1, 2, and 4-hour time points after neuronal stimulation. The newly synthesized RNAs were captured by click reactions and analyzed by qRT-PCR. Relative nascent CPEB3 ribozyme expression or CPEB3 mRNA (exons 2–3) were normalized to scrambled ASO no induction control. (B) Relative nascent CPEB3 ribozyme expression at 1 hour after KCl induction. CPEB3 ribozyme nascent expression is upregulated in the presence of ASO treatment (unpaired *t* test, $*P < 0.05$). (C) There was no significant difference in CPEB3 nascent mRNA (exons 2–3) expression between groups at 1 hour post KCl induction (unpaired *t* test, *n.s.* not significant). (D) ASO treatment resulted in upregulaton of CPEB3 nascent ribozyme expression at 2 hours post KCl induction (unpaired *t* test, $*P < 0.05$). (E) In the presence of ASO, KCl stimulation induced an increase of CPEB3 nascent mRNA (exons 2–3) expression at 2 hours (unpaired *t* test, $*P < 0.05$). (F) No significant difference was observed in CPEB3 nascent ribozyme expression between groups at 4 hours post KCl induction (unpaired *t* test, *n.s.* not significant). (G) No significant difference was observed in CPEB3 nascent mRNA (exons 2–3) expression between groups at 4 hours post KCl induction (unpaired *t* test, *n.s.* not significant). Data are presented as mean ± SEM.

3.3 Conclusions

Regulation of transcription and translation is essential for LTP and synaptic plasticity. Therefore, in this study, we investigated the role of the CPEB3 ribozyme in regulating its mRNA expression in response to neuronal stimulation. We used KCl to evoke membrane depolarization and release endogenous glutamate from presynaptic terminals, which has shown to lead to activation of PSD (Nicholls and Sihra, 1986). We demonstrated that synaptic stimulation by glutamate or KCl resulted in an upregulation of CPEB3 mRNA and ribozyme expression in primary cortical neurons. Using ASO targeting the CPEB3 ribozyme, we found that inhibition of CPEB3 ribozyme led to an increase in CPEB3 mRNA 2 hours after KCl induction. We also studied activity-dependent gene regulation by the CPEB3 ribozyme in neurons, including GluA1, GluA2, PSD-95, and NR2B. Our results strongly suggest that the CPEB3 ribozyme modulates several processes, particularly mRNA maturation, cytoplasmic mRNA translation, and expression of PRPs, including AMPAR and NMDAR mRNA translation.

Metabolic labeling of nascent RNA revealed a dynamic regulation of activity-dependent CPEB3 ribozyme as well as its mRNA in primary cortical neurons. This highlights the role of the CPEB3 ribozyme in transcription and RNA processing. Collectively, these synaptic changes are important for neuroplasticity and LTM consolidation.

3.4 Materials and Methods

Antisense oligonucleotides (ASOs)

The ASOs used in co-transcriptional analysis were obtained from Integrated DNA Technologies, Inc (IDT). Lead ASOs used *in vitro* and *in vivo* were described in table 3, and were provided by Ionis Pharmaceuticals. ASOs used in this study are 20 nucleotides in length and chemically modified with 2′-O-methoxyethyl (MOE) and/or 2′-4′ constrained ethyl (cEt). All internucleoside linkages are modified with phosphorothioate linkages to improve nuclease resistance. All chemical modified ASOs were synthesized as previously described (Seth et al., 2009). ASOs were solubilized in sterile phosphate-buffered saline (PBS).

Co-transcription kinetics and gel analysis

In vitro ribozyme self-cleavage reactions were performed using DNA containing the T7 RNA polymerase promoter, 5 mM dithiothreitol, 40 mM Tris-HCl, 6 mM $MgCl_2$, 2 mM spermidine, 1mM rNTPs, and T7 RNA polymerase. For Mg^{2+}-dependent studies, reactions were incubated with different Mg^{2+} concentrations (0 mM to 10 mM). For ASO inhibition studies, ASOs or sense oligonucleotides (1 μM) were added to the reaction mixture. The reaction was incubated at 37 ºC, aliquots were collected at indicated times and quenched by mixing with equal volume of stop solution (20 mM EDTA, 8 M urea). Aliquots were resolved on 2% agarose gels and analyzed using imageJ software.

Primary cortical neuronal culture

Pregnant female C57BL/6 mice were euthanized at E18 and embryos were collected into an ice-cold Neurobasal medium (Invitrogen). Embryonic cortices were dissected, meninges were removed, and tissues were minced. Cells were mechanically dissociated, passed through a 40 μm cell strainer, counted, and plated at a density of 0.5 x 10^6 cells per well in six-well plates coated with poly-D-lysine (Sigma-Aldrich). Neuronal cultures were maintained at 37 °C with 5% CO_2, and grown in Neurobasal medium containing 2% B27 supplement (Invitrogen), 1% penicillin/streptomycin (Invitrogen), and 1% GlutaMAX (Invitrogen) for 7-10 days *in vitro* (DIV), with 50% of the medium being replaced every 3 days. All experimental procedures were performed according to the National Institutes of Health Guide for the Care and Use of Laboratory Animals and approved by the Institutional Animal Care and Use Committee of the University of California, Irvine.

Neurons were treated with ASO or scrambled ASO (1 μM) for 18 hours prior to neuronal stimulation. To study activity-dependent gene regulation, neuronal cultures were treated with vehicle, 5 μM glutamate (10 minutes), or 35 mM KCl (5 minutes). After stimulation, cultures were washed with Hank's buffered salt solution (HBSS, Invitrogen), and then replaced with fresh medium.

Quantitative RT-PCR analysis

Total RNA was isolated from primary cortical neurons using TRIZOL reagent

(Invitrogen) according to the manufacturer's protocol. RNA concentration was measured using a NanoDrop ND-1000 spectrophotometer (Thermo Fisher Scientific). Total RNA was reverse transcribed using random decamers and M-MLV reverse transcriptase (Promega)/Superscript II RNase H reverse transcriptase (Invitrogen). Quantitative RT-PCR was performed on a BioRad CFX Connect system using iTaq Universal SYBR® Green Supermix (BioRad). Designed primers were acquired from Integrated DNA Technologies, Inc. and provided in table 4. Desired amplicons were verified by melting curve analysis and followed by gel electrophoresis. The starting quantity of DNA from each sample was determined by interpolation of the threshold cycle (Ct) from a standard curve of each primer set. Relative gene expression levels were normalized to the endogenous gene *GAPDH*.

Immunoblotting

Primary cortical neurons were washed with HBSS buffer and collected by mechanical scraping. Cells were lysed in lysis buffer with protease inhibitor and phosphatase inhibitor (Santa Cruz Biotechnology). Cell lysates were sonicated, centrifuged at 13,000 g for 10 minutes at 4 °C, and the supernatant was collected. Protein concentrations were measured using bicinchonic acid (BCA) protein assay (Pierce Biotechnology). Protein samples were loaded on 10% sodium dodecyl sulfate polyacrylamide (SDS-PAGE) gels and separated by electrophoresis. Gels were electro-transferred onto polyvinylidene fluoride (PVDF) membranes using a semi-dry transfer system (BioRad). Membranes were either blocked with 5% nonfat milk or 5% bovine serum albumin (BSA) in Tris-buffered saline/Tween 20 (0.1% [vol/vol]) (TBST) for 1 hour at room

temperature. Membranes were incubated with primary antibodies (Table 5) overnight at 4 °C. After primary antibody incubation, membranes were washed three times with TBST and then incubated with secondary antibodies (Table 6) for 1 hour at room temperature. Bands were detected using an enhanced chemiluminescence (ECL) kit (Thermo Fisher Scientific), visualized using BioRad Chemidoc MP imaging system, and analyzed by Image Lab software (BioRad). GAPDH was used as a loading control.

In vitro XTT cell viability assay

Primary cortical neurons (10,000 to 20,000 cells/well) were plated onto 96-well plates coated with poly-D-lysine. After 7-14 days, ASOs, scrambled ASOs, or vehicle were added and incubated for 18 hours. Cell viability was determined using the 2,3-bis [2-Methoxy-4-nitro-5-sulfophenyl]-2H -tetrazolium-5-carboxyanilide inner salt (XTT) assay according to the manufacture's protocol (Biotium). The assay utilizes the ability of viable cells with active metabolism to reduce the yellow tetrazolium salt to the soluble orange formazan product by mitochondrial dehydrogenase enzymes(Gerlier and Thomasset, 1986; Scudiero et al., 1988). The XTT reagent was added to each well, incubated for 2–4 hours at 37 °C and 5% CO_2, and absorbance was measured at 450 nm with a reference wavelength 680 nm using a Biotek Synergy HT microplate reader. Results were normalized to control and all samples were assayed in triplicate.

Metabolic labeling of nascent RNA

5-ethynyl uridine (5EU, Berry & Associates), an alkyne-modified nucleoside analog, was added to culture medium from 200 mM DMSO stocks with a final concentration of 200 μM (<1% DMSO), and incubated for 1 hour prior to neuronal stimulation.

Biotinylation via CuAAC and strepdavidin enrichment of 5EU-labeled RNA

Total RNA was isolated using TRI reagent (Sigma-Aldrich) according to the manufacturer's instructions. 5EU-labeled RNA was biotinylated using biotin azide (PEG4 carboxamide-6-Azidohexanyl biotin, Sigma-Aldrich). Click reactions were performed by mixing 1-2 μg of 5EU-labeled total RNA, 0.5 mM biotin azide (Sigma-Aldrich), freshly prepared THPTA (tris(hydroxypropyltriazolyl)methylamine (THPTA, Sigma-Aldrich) with a final concentration of 2.5 mM, fresh sodium ascorbate (NaASc, Sigma-Aldrich) with a final concentration of 2.5 mM, and $CuSO_4$ with a final concentration of 0.5 mM. The reaction was incubated for 30 minutes at room temperature with gentle shaking. Following the incubation, biotinylated RNA was recovered by precipitation with 0.1 volume of 3 M sodium acetate and 2.5-3 volumes of ice-cold 100% ethanol overnight at -80 °C. The pellet was washed with ice-cold 75% ethanol, and 5EU-labeled RNA was resuspended in RNase-free water. Following CuAAC biotinylation, biotinylated RNA was enriched using Dynabeads MyOne™ Streptavidin C1 beads (Invitrogen) following the manufacturer's protocols. Briefly, beads were washed with 1x Dynabeads binding & washing buffer (5 mM Tris-HCl, pH 7.5, 0.5 mM EDTA, 1 M NaCl). Biotinylated RNA with 20 units of ribonuclease (RNase) inhibitor (New England Biolabs) was incubated with prewashed Dynabeads with gentle rotation for 15 minutes at room temperature. After incubation, beads were captured on a magnet

and washed with 1x Dynabeads binding & washing buffer. 5EU-labeled RNA was eluted with elution buffer (95% formamide + 10 mM EDTA, pH 8.2) for 2 minutes at 90 °C, and purified using the RNA clean & concentrator-5 kit (Zymo Research).

3′ RACE

Total RNA was extracted from primary cortical neurons. 3′ rapid amplification of cDNA ends (3′ RACE) was performed to study the alternative polyadenylation. cDNA was synthesized using oligo(dT) primers with *3′* RACE adapter primer sequence at the 5′ ends. This cDNA library results in a universal sequence at 3′ end. A gene-specific primer (GSP) and an anchor primer that targets the poly(A) tail region were used for the first PCR using the following protocol: 95 °C for 3 minutes, followed by 30 cycles of 95 °C for 30 seconds, 55 °C for 30 seconds, and 72 °C for 3 minutes, with a final extension of 72 °C for 5 minutes. To improve specificity, a nested PCR was then carried out using nested primers. Upon amplification condition optimization, a quantitative PCR was performed on the first diluted PCR product, and a standard curve of the primer set was generated to determine the effect of relative expression of 3′-mRNA and alternative polyadenylation. All primers used in this study are listed in table 7.

Statistical analysis

Data were presented as means ± SEM. Statistical differences were determined using unpaired Student's *t* test when comparing between 2 independent groups, and one- way

ANOVA with Sidak's *post hoc* tests when comparing across 3 or more independent groups. $P < 0.05$ was considered significant.

3.5 Supplement Figures and Tables

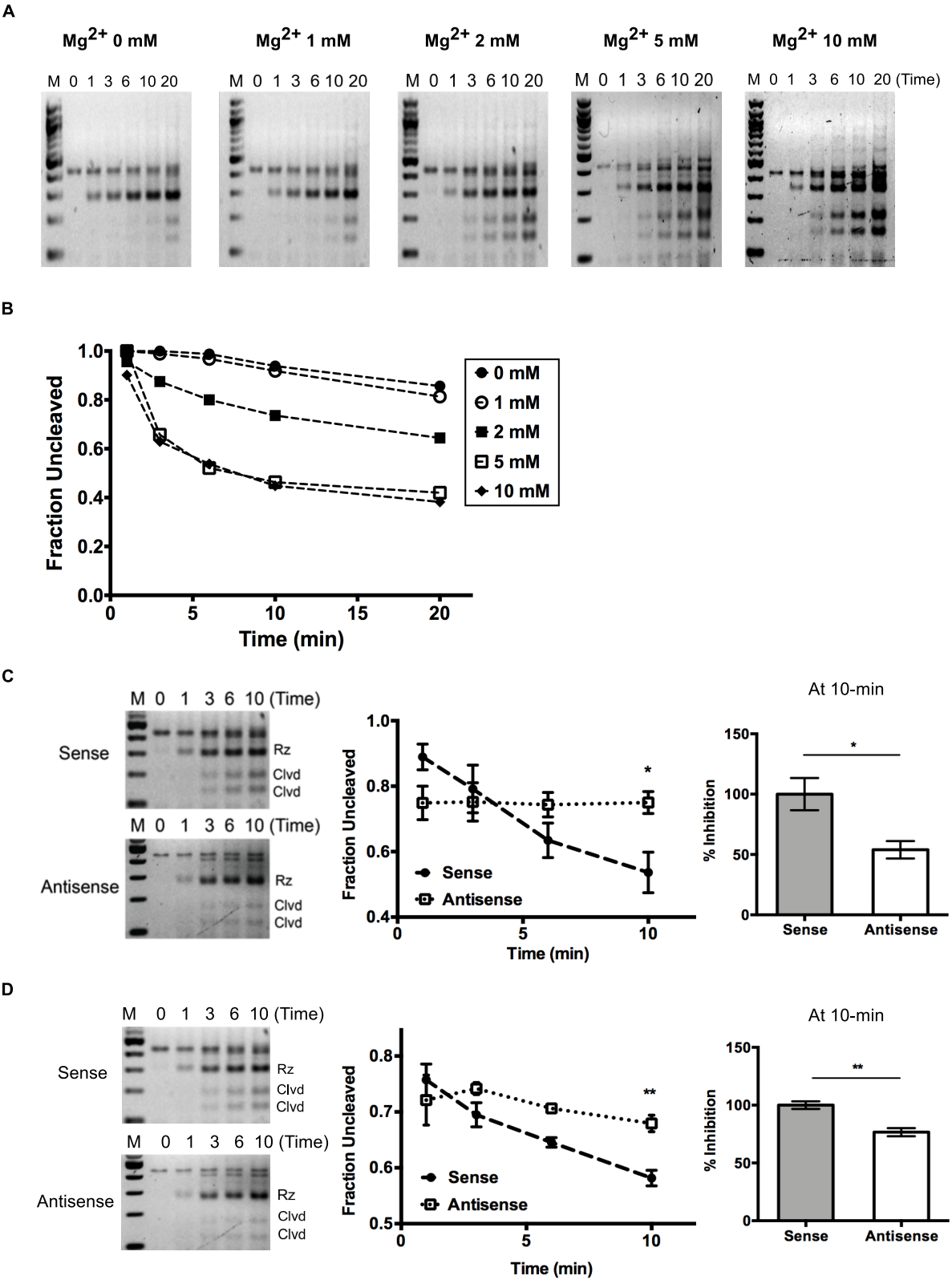

Fig. S3.1. Effect of Mg^{2+} and ASOs on the self-cleaving activity of CPEB3 ribozyme. (A) Co-transcriptional self-cleavage reactions were performed at 37 °C at different Mg^{2+} concentrations (0 – 10 mM). Aliquots were collected at indicated time points and terminated by addition of quench solution. Reactions were resolved by 2% agarose gel electrophoresis. (B) Quantification of CPEB3 ribozyme self-cleavage reactions. Fraction uncleaved values were calculated and plotted vs. time. (C) and (D) CPEB3 ribozyme self-cleaving activity was inhibited in the presence of ASOs. Sense or antisense oligonucleotides (1 μM) were added during co-transcriptional self-cleavage reactions under 2 mM Mg^{2+} condition. % of inhibition was normalized to the respective sense oligonucleotides at the end point (unpaired *t* test, $*P < 0.05$ and $**P < 0.01$). Data are presented as mean ± SEM.

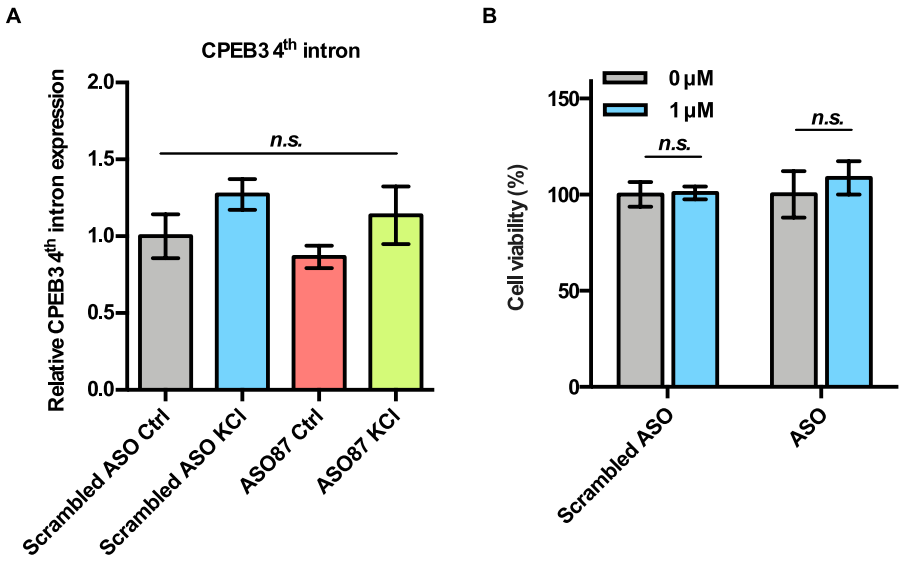

Fig. S3.2. Characterization of the lead ASO specificity and toxicity. (A) qRT-PCR analysis of CPEB3 4th intron expression revealed that the lead ASO is sequence specific (one-way ANOVA with Sidak's *post hoc* tests, *n.s.* not significant). (B) Effect of ASOs treatment on cell viability. XTT assay was performed after 18 hours of incubation with ASOs. Relative cell viability was normalized to the vehicle control (unpaired *t* test, *n.s.* not significant). Data are presented as mean ± SEM.

Table 3. ASO sequences

ID	Sequence
AL3049	5′-TGTGGCCCCCTGTTATCCTC-3′
AL3050	5′-ACGCTTCTGCTGTGGCCCCC-3′
AL3058	5′-GAGGATAACAGGGGGCCACA-3′
AL3059	5′-GGGGGCCACAGCAGAAGCGT-3′
1227287	5′-TGTGGmCmCmCmCmCTGTTATmCmCTmC-3′
1259490	5′-mCmCTTmCmCmCTGAAGGTTmCmCTmCmC-3′

Table 4. Primers used in qPCR

Target		Sequence	Note
CPEB3 exons 2–3	Forward	CGATAATGGTAACAATCTGTTGCC	
	Reverse	CCTTATCATATCCATTAAGGAGTTCTCC	
CPEB3 exons 3–6	Forward	GACCGGAGTAGGCCCTATGA	
	Reverse	CCAGACGATAAGGCCTGATCA	
CPEB3 exons 6–9	Forward	ACTCTAGAAAGGTGTTTGTTGGAGG	
	Reverse	TCGAAGGGGTCGTGGAACT	
CPEB3 ribozyme cleaved	Forward	GTTCACGTCGCGGCC	
	Reverse	GTGATATAGTGTGTTCTTCAGTGACTCCT	
CPEB3 ribozyme uncleaved	Forward	CCAAGCAGCAGCACAGGTC	
	Reverse	GTGATATAGTGTGTTCTTCAGTGACTCCT	
CPEB3 4th intron	Forward	CACTCTAGCCTAACTGGTGAGCTC	
	Reverse	AGTCATTCCAACAGAAATGAAGTACC	
GluA1	Forward	GTCCGCCCTGAGAAATCCAG	(Pignataro et al., 2007)
	Reverse	CTCGCCCTTGTCGTACCAC	
GluA2	Forward	TGGTACGACAAAGGAGAGTGC	(Wen et al., 2014)
	Reverse	ACCAGCATTGCCAAACCAAG	
PSD-95	Forward	TGAGATCAGTCATAGCAGCTACT	(He et al., 2014)
	Reverse	CTTCCTCCCCTAGCAGGTCC	
NR2B	Forward	GCCATGAACGAGACTGACCC	(Agudelo et al., 2014)
	Reverse	GCTTCCTGGTCCGTGTCATC	
GAPDH	Forward	TGACCACAGTCCATGCCATC	
	Reverse	GACGGACACATTGGGGGTAG	

Table 5. Primary antibodies used in the CPEB3 ribozyme study

Antigen	Company	Catalog #	Dilution
CPEB3	Abcam	ab18833	1:1,000
GluA1	UC Davis/NIH NeuroMab Facility	75-327	1:1,000
GluA2	Proteintech	11994-1-AP	1:2,000
PSD-95	Proteintech	20665-1-AP	1:2,000
NR2B	Proteintech	21920-1-AP	1:2,000
GAPDH	Proteintech	60004-1-Ig	1:10,000

Table 6. Secondary antibodies used in the CPEB3 ribozyme study

Conjugate	Species	Company	Catalog #	Dilution
Horseradish Peroxidase	Donkey α rabbit	Thermo Fisher Scientific	A16023	1:10,000
Horseradish Peroxidase	Goat α mouse	R&D system	HAF007	1:1,000

Table 7 Primers used in 3′RACE

Target	Sequence	Note
3′RACE adaptor	CCAGTGAGCAGAGTGACGAGGACTCGAGCTC AAGCTTTTTTTTTTTTTTTTTTT	
3′RACE outer primer	CCAGTGAGCAGAGTGACG	
3′RACE inner primer	GAGGACTCGAGCTCAAGC	
GluA1	GGTCCGCCCTGAGAGGTCCC	
GluA1 nested	CCTGAGCAATGTGGCAGGCGT	
GluA2	GCTACGGCATCGCCACACCT	
GluA2 nested	ATCCTTGTCGGGGGCCTTGGT	
PSD-95	GGCCACGAAGCTGGAGCAGG	
PSD-95 nested	GGCCTGGACTCACCCTGCCT	
NR2B	GAGACGAAGGCTGCAAGCTGGT	
NR2B nested	CGCCAGGTGGACCTTGCTATCC	
GluA1 PAS	GAAATGAGGGTCTTGCTGGGAGGG	(Pavlopoulos et al., 2011)
GluA2 PAS	GGAAAGACCAAAATAATT ATGAACT	(Pavlopoulos et al., 2011)
PSD-95 PAS	GGGCCTCTGCCCTCCCCATT	
NR2B PAS	GAGACGAAGGCTGCAAGCTGGT	
NR2B PAS nested	CGCCAGGTGGACCTTGCTATCC	

3.6 References

Agudelo, L.Z., Femenia, T., Orhan, F., Porsmyr-Palmertz, M., Goiny, M., Martinez-Redondo, V., Correia, J.C., Izadi, M., Bhat, M., Schuppe-Koistinen, I.*, et al.* (2014). Skeletal muscle PGC-1alpha1 modulates kynurenine metabolism and mediates resilience to stress-induced depression. Cell *159*, 33-45.

Akbalik, G., Langebeck-Jensen, K., Tushev, G., Sambandan, S., Rinne, J., Epstein, I., Cajigas, I., Vlatkovic, I., and Schuman, E.M. (2017). Visualization of newly synthesized neuronal RNA in vitro and in vivo using click-chemistry. RNA Biol *14*, 20-28.

Allison, D.W., Gelfand, V.I., Spector, I., and Craig, A.M. (1998). Role of actin in anchoring postsynaptic receptors in cultured hippocampal neurons: differential attachment of NMDA versus AMPA receptors. J Neurosci *18*, 2423-2436.

Amantana, A., Moulton, H.M., Cate, M.L., Reddy, M.T., Whitehead, T., Hassinger, J.N., Youngblood, D.S., and Iversen, P.L. (2007). Pharmacokinetics, biodistribution, stability and toxicity of a cell-penetrating peptide-morpholino oligomer conjugate. Bioconjug Chem *18*, 1325-1331.

Atkins, C.M., Nozaki, N., Shigeri, Y., and Soderling, T.R. (2004). Cytoplasmic polyadenylation element binding protein-dependent protein synthesis is regulated by calcium/calmodulin-dependent protein kinase II. J Neurosci *24*, 5193-5201.

Bailey, C.H., Kandel, E.R., and Harris, K.M. (2015). Structural Components of Synaptic Plasticity and Memory Consolidation. Cold Spring Harb Perspect Biol *7*, a021758.

Basu, S., and Lamprecht, R. (2018). The Role of Actin Cytoskeleton in Dendritic Spines in the Maintenance of Long-Term Memory. Front Mol Neurosci *11*, 143.

Bear, M.F., and Malenka, R.C. (1994). Synaptic plasticity: LTP and LTD. Curr Opin Neurobiol *4*, 389-399.

Bennett, C.F., Baker, B.F., Pham, N., Swayze, E., and Geary, R.S. (2017). Pharmacology of Antisense Drugs. Annu Rev Pharmacol Toxicol *57*, 81-105.

Bennett, C.F., and Swayze, E.E. (2010). RNA Targeting Therapeutics: Molecular Mechanisms of Antisense Oligonucleotides as a Therapeutic Platform. Annual Review of Pharmacology and Toxicology *50*, 259-293.

Bliss, T.V., and Collingridge, G.L. (1993). A synaptic model of memory: long-term potentiation in the hippocampus. Nature *361*, 31-39.

Bliss, T.V., Collingridge, G.L., and Morris, R.G. (2014). Synaptic plasticity in health and disease: introduction and overview. Philos Trans R Soc Lond B Biol Sci *369*, 20130129.

Bosch, M., Castro, J., Saneyoshi, T., Matsuno, H., Sur, M., and Hayashi, Y. (2014). Structural and molecular remodeling of dendritic spine substructures during long-term potentiation. Neuron *82*, 444-459.

Bosch, M., and Hayashi, Y. (2012). Structural plasticity of dendritic spines. Curr Opin Neurobiol *22*, 383-388.

Bradshaw, K.D., Emptage, N.J., and Bliss, T.V.P. (2003). A role for dendritic protein synthesis in hippocampal late LTP. European Journal of Neuroscience *18*, 3150-3152.

Burnett, J.C., and Rossi, J.J. (2012). RNA-based Therapeutics- Current Progress and Future Prospects. Chem Biol *19*, 60-71.

Chadalavada, D.M., Gratton, E.A., and Bevilacqua, P.C. (2010). The human HDV-like CPEB3 ribozyme is intrinsically fast-reacting. Biochemistry-Us *49*, 5321-5330.

Chadalavada, D.M., Knudsen, S.M., Nakano, S., and Bevilacqua, P.C. (2000). A role for upstream RNA structure in facilitating the catalytic fold of the genomic hepatitis delta virus ribozyme. J Mol Biol *301*, 349-367.

Chao, H.W., Lai, Y.T., Lu, Y.L., Lin, C.L., Mai, W., and Huang, Y.S. (2012). NMDAR signaling facilitates the IPO5-mediated nuclear import of CPEB3. Nucleic Acids Res *40*, 8484-8498.

Chao, H.W., Tsai, L.Y., Lu, Y.L., Lin, P.Y., Huang, W.H., Chou, H.J., Lu, W.H., Lin, H.C., Lee, P.T., and Huang, Y.S. (2013). Deletion of CPEB3 enhances hippocampus-dependent memory via increasing expressions of PSD95 and NMDA receptors. J Neurosci *33*, 17008-17022.

Cingolani, L.A., and Goda, Y. (2008). Actin in action: the interplay between the actin cytoskeleton and synaptic efficacy. Nature Reviews Neuroscience *9*, 344-356.

Collingridge, G.L., Isaac, J.T., and Wang, Y.T. (2004). Receptor trafficking and synaptic plasticity. Nat Rev Neurosci *5*, 952-962.

Collingridge, G.L., Peineau, S., Howland, J.G., and Wang, Y.T. (2010). Long-term depression in the CNS. Nat Rev Neurosci *11*, 459-473.

Costa-Mattioli, M., Sossin, W.S., Klann, E., and Sonenberg, N. (2009). Translational control of long-lasting synaptic plasticity and memory. Neuron *61*, 10-26.

Crooke, S.T. (2004). Antisense strategies. Curr Mol Med *4*, 465-487.

Das, S., Moon, H.C., Singer, R.H., and Park, H.Y. (2018). A transgenic mouse for imaging activity-dependent dynamics of endogenous Arc mRNA in live neurons. Sci Adv *4*, eaar3448.

Derkach, V.A., Oh, M.C., Guire, E.S., and Soderling, T.R. (2007). Regulatory mechanisms of AMPA receptors in synaptic plasticity. Nat Rev Neurosci *8*, 101-113.

Drisaldi, B., Colnaghi, L., Fioriti, L., Rao, N., Myers, C., Snyder, A.M., Metzger, D.J., Tarasoff, J., Konstantinov, E., Fraser, P.E.*, et al.* (2015). SUMOylation Is an Inhibitory Constraint that Regulates the Prion-like Aggregation and Activity of CPEB3. Cell Rep *11*, 1694-1702.

Drygin, D., Barone, S., and Bennett, C.F. (2004). Sequence-dependent cytotoxicity of second-generation oligonucleotides. Nucleic Acids Res *32*, 6585-6594.

Du, L., and Richter, J.D. (2005). Activity-dependent polyadenylation in neurons. RNA *11*, 1340-1347.

Duffy, E.E., Canzio, D., Maniatis, T., and Simon, M.D. (2018). Solid phase chemistry to covalently and reversibly capture thiolated RNA. Nucleic Acids Res *46*, 6996-7005.

Eckstein, F. (2000). Phosphorothioate Oligodeoxynucleotides: What Is Their Origin and What Is Unique About Them? Antisense Nucleic Acid Drug Dev *10*.

Ehrlich, I., Klein, M., Rumpel, S., and Malinow, R. (2007). PSD-95 is required for activity-driven synapse stabilization. Proc Natl Acad Sci U S A *104*, 4176-4181.

Ehrlich, I., and Malinow, R. (2004). Postsynaptic density 95 controls AMPA receptor incorporation during long-term potentiation and experience-driven synaptic plasticity. J Neurosci *24*, 916-927.

Eisen, J.S., and Smith, J.C. (2008). Controlling morpholino experiments: don't stop making antisense. Development *135*, 1735-1743.

El-Husseini, A.E., Schnell, E., Chetkovich, D.M., Nicoll, R.A., and Bredt, D.S. (2000). PSD-95 involvement in maturation of excitatory synapses. Science *290*, 1364-1368.

Evers, M.M., Toonen, L.J., and van Roon-Mom, W.M. (2015). Antisense oligonucleotides in therapy for neurodegenerative disorders. Adv Drug Deliv Rev *87*, 90-103.

Farris, S., Lewandowski, G., Cox, C.D., and Steward, O. (2014). Selective localization of arc mRNA in dendrites involves activity- and translation-dependent mRNA degradation. J Neurosci *34*, 4481-4493.

Ferre-D'Amare, A.R., Zhou, K., and Doudna, J.A. (1998). Crystal structure of a hepatitis delta virus ribozyme. Nature *395*, 567-574.

Fioriti, L., Myers, C., Huang, Y.Y., Li, X., Stephan, J.S., Trifilieff, P., Colnaghi, L., Kosmidis, S., Drisaldi, B., Pavlopoulos, E.*, et al.* (2015). The Persistence of Hippocampal-Based Memory Requires Protein Synthesis Mediated by the Prion-like Protein CPEB3. Neuron *86*, 1433-1448.

Flavell, S.W., Kim, T.K., Gray, J.M., Harmin, D.A., Hemberg, M., Hong, E.J., Markenscoff-Papadimitriou, E., Bear, D.M., and Greenberg, M.E. (2008). Genome-wide analysis of MEF2 transcriptional program reveals synaptic target

genes and neuronal activity-dependent polyadenylation site selection. Neuron *60*, 1022-1038.

Fontes, M.M., Guvenek, A., Kawaguchi, R., Zheng, D., Huang, A., Ho, V.M., Chen, P.B., Liu, X., O'Dell, T.J., Coppola, G.*, et al.* (2017). Activity-Dependent Regulation of Alternative Cleavage and Polyadenylation During Hippocampal Long-Term Potentiation. Sci Rep *7*, 17377.

Ford, L., Ling, E., Kandel, E.R., and Fioriti, L. (2019). CPEB3 inhibits translation of mRNA targets by localizing them to P bodies. Proceedings of the National Academy of Sciences.

Frazier, K.S. (2015). Antisense oligonucleotide therapies: the promise and the challenges from a toxicologic pathologist's perspective. Toxicol Pathol *43*, 78-89.

Frederiksen, J.K., and Piccirilli, J.A. (2009). Identification of catalytic metal ion ligands in ribozymes. Methods *49*, 148-166.

Gerlier, D., and Thomasset, N. (1986). Use of MTT colorimetric assay to measure cell activation. J Immunol Methods *94*, 57-63.

Gladding, C.M., Fitzjohn, S.M., and Molnar, E. (2009). Metabotropic glutamate receptor-mediated long-term depression: molecular mechanisms. Pharmacol Rev *61*, 395-412.

Haider, S.R., Juan, G., Traganos, F., and Darzynkiewicz, Z. (1997). Immunoseparation and immunodetection of nucleic acids labeled with halogenated nucleotides. Exp Cell Res *234*, 498-506.

Hake, L.E., and Richter, J.D. (1994). CPEB is a specificity factor that mediates cytoplasmic polyadenylation during Xenopus oocyte maturation. Cell *79*, 617-627.

He, L.J., Liu, N., Cheng, T.L., Chen, X.J., Li, Y.D., Shu, Y.S., Qiu, Z.L., and Zhang, X.H. (2014). Conditional deletion of Mecp2 in parvalbumin-expressing GABAergic cells results in the absence of critical period plasticity. Nat Commun *5*, 5036.

Hernandez, A.J., Zovoilis, A., Cifuentes-Rojas, C., Han, L., Bujisic, B., and Lee, J.T. (2020). B2 and ALU retrotransposons are self-cleaving ribozymes whose activity is enhanced by EZH2. Proc Natl Acad Sci U S A *117*, 415-425.

Hong, D., Kurzrock, R., Kim, Y., Woessner, R., Younes, A., Nemunaitis, J., Fowler, N., Zhou, T., Schmidt, J., Jo, M.*, et al.* (2015). AZD9150, a next-generation antisense oligonucleotide inhibitor of STAT3 with early evidence of clinical activity in lymphoma and lung cancer. Sci Transl Med *7*, 314ra185.

Hua, Y., Sahashi, K., Hung, G., Rigo, F., Passini, M.A., Bennett, C.F., and Krainer, A.R. (2010). Antisense correction of SMN2 splicing in the CNS rescues necrosis in a type III SMA mouse model. Genes Dev *24*, 1634-1644.

Huang, Y.S., Kan, M.C., Lin, C.L., and Richter, J.D. (2006). CPEB3 and CPEB4 in neurons: analysis of RNA-binding specificity and translational control of AMPA receptor GluR2 mRNA. EMBO J *25*, 4865-4876.

Igaz, L.M., Vianna, M.R., Medina, J.H., and Izquierdo, I. (2002). Two time periods of hippocampal mRNA synthesis are required for memory consolidation of fear-motivated learning. J Neurosci *22*, 6781-6789.

Ivshina, M., Lasko, P., and Richter, J.D. (2014). Cytoplasmic polyadenylation element binding proteins in development, health, and disease. Annu Rev Cell Dev Biol *30*, 393-415.

Jao, C.Y., and Salic, A. (2008). Exploring RNA transcription and turnover in vivo by using click chemistry. Proc Natl Acad Sci U S A *105*, 15779-15784.

Jeong, S., Sefcikova, J., Tinsley, R.A., Rueda, D., and Walter, N.G. (2003). Trans-acting hepatitis delta virus ribozyme: Catalytic core and global structure are dependent on the 5' substrate sequence. Biochemistry-Us *42*, 7727-7740.

Jimenez, R.M., Polanco, J.A., and Luptak, A. (2015). Chemistry and Biology of Self-Cleaving Ribozymes. Trends Biochem Sci *40*, 648-661.

Juliano, R.L. (2016). The delivery of therapeutic oligonucleotides. Nucleic Acids Res *44*, 6518-6548.

Kandel, E.R. (2001). The molecular biology of memory storage: a dialogue between genes and synapses. Science *294*, 1030-1038.

Kandel, E.R. (2012). The molecular biology of memory: cAMP, PKA, CRE, CREB-1, CREB-2, and CPEB. Mol Brain *5*, 14.

Kenzelmann, M., Maertens, S., Hergenhahn, M., Kueffer, S., Hotz-Wagenblatt, A., Li, L., Wang, S., Ittrich, C., Lemberger, T., Arribas, R.*, et al.* (2007). Microarray analysis of newly synthesized RNA in cells and animals. Proc Natl Acad Sci U S A *104*, 6164-6169.

Khan, M.R., Li, L., Perez-Sanchez, C., Saraf, A., Florens, L., Slaughter, B.D., Unruh, J.R., and Si, K. (2015). Amyloidogenic Oligomerization Transforms Drosophila Orb2 from a Translation Repressor to an Activator. Cell *163*, 1468-1483.

Khorkova, O., and Wahlestedt, C. (2017). Oligonucleotide therapies for disorders of the nervous system. Nat Biotechnol *35*, 249-263.

Kruttner, S., Stepien, B., Noordermeer, J.N., Mommaas, M.A., Mechtler, K., Dickson, B.J., and Keleman, K. (2012). Drosophila CPEB Orb2A mediates memory independent of Its RNA-binding domain. Neuron *76*, 383-395.

Kurreck, J. (2003). Antisense technologies. Improvement through novel chemical modifications. Eur J Biochem *270*, 1628-1644.

Lau, A.G., Irier, H.A., Gu, J., Tian, D., Ku, L., Liu, G., Xia, M., Fritsch, B., Zheng, J.Q., Dingledine, R.*, et al.* (2010). Distinct 3'UTRs differentially regulate activity-dependent translation of brain-derived neurotrophic factor (BDNF). Proc Natl Acad Sci U S A *107*, 15945-15950.

Levin, A.A. (2019). Treating Disease at the RNA Level with Oligonucleotides. N Engl J Med *380*, 57-70.

Lisman, J. (1989). A mechanism for the Hebb and the anti-Hebb processes underlying learning and memory. Proc Natl Acad Sci U S A *86*, 9574-9578.

Luscher, C., and Huber, K.M. (2010). Group 1 mGluR-dependent synaptic long-term depression: mechanisms and implications for circuitry and disease. Neuron *65*, 445-459.

Lynch, M.A. (2004). Long-term potentiation and memory. Physiol Rev *84*, 87-136.

Malenka, R.C., and Bear, M.F. (2004). LTP and LTD: an embarrassment of riches. Neuron *44*, 5-21.

Malinow, R., and Malenka, R.C. (2002). AMPA receptor trafficking and synaptic plasticity. Annu Rev Neurosci *25*, 103-126.

Mansoor, M., and Melendez, A.J. (2008). Advances in antisense oligonucleotide development for target identification, validation, and as novel therapeutics. Gene Regul Syst Bio *2*, 275-295.

Martin, K.C., and Zukin, R.S. (2006). RNA trafficking and local protein synthesis in dendrites: an overview. J Neurosci *26*, 7131-7134.

Mayr, C. (2017). Regulation by 3'-Untranslated Regions. Annu Rev Genet *51*, 171-194.

Mendez, R., Murthy, K.G.K., Ryan, K., Manley, J.L., and Richter, J.D. (2000). Phosphorylation of CPEB by Eg2 mediates the recruitment of CPSF into an active cytoplasmic polyadenylation complex. Molecular Cell *6*, 1253-1259.

Mendez, R., and Richter, J.D. (2001). Translational control by CPEB: a means to the end. Nat Rev Mol Cell Biol *2*, 521-529.

Miniaci, M.C., Kim, J.H., Puthanveettil, S.V., Si, K., Zhu, H., Kandel, E.R., and Bailey, C.H. (2008). Sustained CPEB-dependent local protein synthesis is required to stabilize synaptic growth for persistence of long-term facilitation in Aplysia. Neuron *59*, 1024-1036.

Miura, P., Sanfilippo, P., Shenker, S., and Lai, E.C. (2014). Alternative polyadenylation in the nervous system: to what lengths will 3' UTR extensions take us? Bioessays *36*, 766-777.

Morgan, M., Iaconcig, A., and Muro, A.F. (2010). CPEB2, CPEB3 and CPEB4 are coordinately regulated by miRNAs recognizing conserved binding sites in paralog positions of their 3 '-UTRs. Nucleic Acids Research *38*, 7698-7710.

Moult, P.R., Gladding, C.M., Sanderson, T.M., Fitzjohn, S.M., Bashir, Z.I., Molnar, E., and Collingridge, G.L. (2006). Tyrosine phosphatases regulate AMPA receptor

trafficking during metabotropic glutamate receptor-mediated long-term depression. J Neurosci *26*, 2544-2554.

Mulkey, R.M., Herron, C.E., and Malenka, R.C. (1993). An essential role for protein phosphatases in hippocampal long-term depression. Science *261*, 1051-1055.

Murray, J.B., Terwey, D.P., Maloney, L., Karpeisky, A., Usman, N., Beigelman, L., and Scott, W.G. (1998). The structural basis of hammerhead ribozyme self-cleavage. Cell *92*, 665-673.

Nakahata, Y., and Yasuda, R. (2018). Plasticity of Spine Structure: Local Signaling, Translation and Cytoskeletal Reorganization. Front Synaptic Neurosci *10*, 29.

Nakano, S., and Bevilacqua, P.C. (2001). Proton inventory of the genomic HDV ribozyme in Mg(2+)-containing solutions. J Am Chem Soc *123*, 11333-11334.

Nakano, S., Proctor, D.J., and Bevilacqua, P.C. (2001). Mechanistic characterization of the HDV genomic ribozyme: assessing the catalytic and structural contributions of divalent metal ions within a multichannel reaction mechanism. Biochemistry-Us *40*, 12022-12038.

Neves, G., Cooke, S.F., and Bliss, T.V. (2008). Synaptic plasticity, memory and the hippocampus: a neural network approach to causality. Nat Rev Neurosci *9*, 65-75.

Nguyen, P.V., Abel, T., and Kandel, E.R. (1994). Requirement of a Critical Period of Transcription for Induction of a Late-Phase of Ltp. Science *265*, 1104-1107.

Nicholls, D.G., and Sihra, T.S. (1986). Synaptosomes possess an exocytotic pool of glutamate. Nature *321*, 772-773.

Nishikawa, F., Roy, M., Fauzi, H., and Nishikawa, S. (1999). Detailed analysis of stem I and its 5 ' and 3 ' neighbor regions in the trans-acting HDV ribozyme. Nucleic Acids Research *27*, 403-410.

Olea, M.T., and Nagata, T. (1992). A radioautographic study on RNA synthesis in aging mouse spleen after 3H-uridine labeling in vitro. Cell Mol Biol *38*, 399-405.

Pavlopoulos, E., Trifilieff, P., Chevaleyre, V., Fioriti, L., Zairis, S., Pagano, A., Malleret, G., and Kandel, E.R. (2011). Neuralized1 activates CPEB3: a function for nonproteolytic ubiquitin in synaptic plasticity and memory storage. Cell *147*, 1369-1383.

Peng, S.C., Lai, Y.T., Huang, H.Y., Huang, H.D., and Huang, Y.S. (2010). A novel role of CPEB3 in regulating EGFR gene transcription via association with Stat5b in neurons. Nucleic Acids Res *38*, 7446-7457.

Pignataro, L., Miller, A.N., Ma, L., Midha, S., Protiva, P., Herrera, D.G., and Harrison, N.L. (2007). Alcohol regulates gene expression in neurons via activation of heat shock factor 1. J Neurosci *27*, 12957-12966.

Porensky, P.N., Mitrpant, C., McGovern, V.L., Bevan, A.K., Foust, K.D., Kaspar, B.K., Wilton, S.D., and Burghes, A.H. (2012). A single administration of morpholino antisense oligomer rescues spinal muscular atrophy in mouse. Hum Mol Genet *21*, 1625-1638.

Rahman, S.M., Seki, S., Obika, S., Yoshikawa, H., Miyashita, K., and Imanishi, T. (2008). Design, synthesis, and properties of 2',4'-BNA(NC): a bridged nucleic acid analogue. J Am Chem Soc *130*, 4886-4896.

Rayman, J.B., and Kandel, E.R. (2017). Functional Prions in the Brain. Cold Spring Harb Perspect Biol *9*.

Riccitelli, N., and Luptak, A. (2013). HDV family of self-cleaving ribozymes. Prog Mol Biol Transl Sci *120*, 123-171.

Richter, J.D. (2007). CPEB: a life in translation. Trends Biochem Sci *32*, 279-285.

Ruminski, D.J., Webb, C.H., Riccitelli, N.J., and Luptak, A. (2011). Processing and translation initiation of non-long terminal repeat retrotransposons by hepatitis delta virus (HDV)-like self-cleaving ribozymes. J Biol Chem *286*, 41286-41295.

Russo, J., Heck, A.M., Wilusz, J., and Wilusz, C.J. (2017). Metabolic Labeling and Recovery of Nascent RNA to Accurately Quantify mRNA Stability. Methods *120*, 39-48.

Salehi-Ashtiani, K., Luptak, A., Litovchick, A., and Szostak, J.W. (2006). A genomewide search for ribozymes reveals an HDV-like sequence in the human CPEB3 gene. Science *313*, 1788-1792.

Savtchouk, I., Sun, L., Bender, C.L., Yang, Q., Szabo, G., Gasparini, S., and Liu, S.J. (2016). Topological Regulation of Synaptic AMPA Receptor Expression by the RNA-Binding Protein CPEB3. Cell Rep *17*, 86-103.

Scudiero, D.A., Shoemaker, R.H., Paull, K.D., Monks, A., Tierney, S., Nofziger, T.H., Currens, M.J., Seniff, D., and Boyd, M.R. (1988). Evaluation of a soluble tetrazolium/formazan assay for cell growth and drug sensitivity in culture using human and other tumor cell lines. Cancer Res *48*, 4827-4833.

Serganov, A., and Patel, D.J. (2007). Ribozymes, riboswitches and beyond: regulation of gene expression without proteins. Nat Rev Genet *8*, 776-790.

Seth, P.P., Siwkowski, A., Allerson, C.R., Vasquez, G., Lee, S., Prakash, T.P., Wancewicz, E.V., Witchell, D., and Swayze, E.E. (2009). Short antisense oligonucleotides with novel 2'-4' conformationaly restricted nucleoside analogues show improved potency without increased toxicity in animals. J Med Chem *52*, 10-13.

Sharmeen, L., Kuo, M.Y., Dinter-Gottlieb, G., and Taylor, J. (1988). Antigenomic RNA of human hepatitis delta virus can undergo self-cleavage. J Virol *62*, 2674-2679.

Shen, X.L., and Corey, D.R. (2018). Chemistry, mechanism and clinical status of antisense oligonucleotides and duplex RNAs. Nucleic Acids Research *46*, 1584-1600.

Shepherd, J.D., and Huganir, R.L. (2007). The cell biology of synaptic plasticity: AMPA receptor trafficking. Annu Rev Cell Dev Biol *23*, 613-643.

Shih, I.H., and Been, M.D. (1999). Ribozyme cleavage of a 2,5-phosphodiester linkage: mechanism and a restricted divalent metal-ion requirement. RNA *5*, 1140-1148.

Shiraishi, T., and Nielsen, P.E. (2011). Peptide nucleic acid (PNA) cell penetrating peptide (CPP) conjugates as carriers for cellular delivery of antisense oligomers. Artif DNA PNA XNA *2*, 90-99.

Si, K., Choi, Y.B., White-Grindley, E., Majumdar, A., and Kandel, E.R. (2010). Aplysia CPEB can form prion-like multimers in sensory neurons that contribute to long-term facilitation. Cell *140*, 421-435.

Si, K., Giustetto, M., Etkin, A., Hsu, R., Janisiewicz, A.M., Miniaci, M.C., Kim, J.H., Zhu, H., and Kandel, E.R. (2003a). A neuronal isoform of CPEB regulates local protein

synthesis and stabilizes synapse-specific long-term facilitation in aplysia. Cell *115*, 893-904.

Si, K., Lindquist, S., and Kandel, E.R. (2003b). A neuronal isoform of the aplysia CPEB has prion-like properties. Cell *115*, 879-891.

Singh, N.N., Howell, M.D., Androphy, E.J., and Singh, R.N. (2017). How the discovery of ISS-N1 led to the first medical therapy for spinal muscular atrophy. Gene Ther *24*, 520-526.

Skilandat, M., Rowinska-Zyrek, M., and Sigel, R.K. (2016). Secondary structure confirmation and localization of Mg2+ ions in the mammalian CPEB3 ribozyme. RNA *22*, 750-763.

Smith, C.I.E., and Zain, R. (2019). Therapeutic Oligonucleotides: State of the Art. Annu Rev Pharmacol Toxicol *59*, 605-630.

Soler-Bistue, A., Zorreguieta, A., and Tolmasky, M.E. (2019). Bridged Nucleic Acids Reloaded. Molecules *24*.

Sridharan, K., and Gogtay, N.J. (2016). Therapeutic nucleic acids: current clinical status. Br J Clin Pharmacol *82*, 659-672.

Stephan, J.S., Fioriti, L., Lamba, N., Colnaghi, L., Karl, K., Derkatch, I.L., and Kandel, E.R. (2015). The CPEB3 Protein Is a Functional Prion that Interacts with the Actin Cytoskeleton. Cell Rep *11*, 1772-1785.

Summerton, J., and Weller, D. (1997). Morpholino antisense oligomers: design, preparation, and properties. Antisense Nucleic Acid Drug Dev *7*, 187-195.

Summerton, J.E. (2003). Morpholinos and PNAs compared. Lett Pept Sci *10*, 215-236.

Sutton, M.A., and Schuman, E.M. (2006). Dendritic protein synthesis, synaptic plasticity, and memory. Cell *127*, 49-58.

Tani, H., and Akimitsu, N. (2012). Genome-wide technology for determining RNA stability in mammalian cells: historical perspective and recent advantages based on modified nucleotide labeling. RNA Biol *9*, 1233-1238.

Theis, M., Si, K., and Kandel, E.R. (2003). Two previously undescribed members of the mouse CPEB family of genes and their inducible expression in the principal cell layers of the hippocampus. Proc Natl Acad Sci U S A *100*, 9602-9607.

Ucker, D.S., and Yamamoto, K.R. (1984). Early events in the stimulation of mammary tumor virus RNA synthesis by glucocorticoids. Novel assays of transcription rates. J Biol Chem *259*, 7416-7420.

Vogler, C., Spalek, K., Aerni, A., Demougin, P., Muller, A., Huynh, K.D., Papassotiropoulos, A., and de Quervain, D.J. (2009). CPEB3 is associated with human episodic memory. Front Behav Neurosci *3*, 4.

Wahlestedt, C., Salmi, P., Good, L., Kela, J., Johnsson, T., Hokfelt, T., Broberger, C., Porreca, F., Lai, J., Ren, K.*, et al.* (2000). Potent and nontoxic antisense oligonucleotides containing locked nucleic acids. Proc Natl Acad Sci U S A *97*, 5633-5638.

Waltereit, R., and Weller, M. (2003). Signaling from cAMP/PKA to MAPK and synaptic plasticity. Mol Neurobiol *27*, 99-106.

Wang, X.P., and Cooper, N.G. (2009). Characterization of the transcripts and protein isoforms for cytoplasmic polyadenylation element binding protein-3 (CPEB3) in the mouse retina. BMC Mol Biol *10*, 109.

Wang, Y.X. (2011). Superparamagnetic iron oxide based MRI contrast agents: Current status of clinical application. Quant Imaging Med Surg *1*, 35-40.

Webb, C.H., and Luptak, A. (2011). HDV-like self-cleaving ribozymes. RNA Biol *8*, 719-727.

Webb, C.H., Riccitelli, N.J., Ruminski, D.J., and Luptak, A. (2009). Widespread occurrence of self-cleaving ribozymes. Science *326*, 953.

Weinberg, Z., Kim, P.B., Chen, T.H., Li, S., Harris, K.A., Lunse, C.E., and Breaker, R.R. (2015). New classes of self-cleaving ribozymes revealed by comparative genomics analysis. Nat Chem Biol *11*, 606-610.

Wen, Z., Nguyen, H.N., Guo, Z., Lalli, M.A., Wang, X., Su, Y., Kim, N.S., Yoon, K.J., Shin, J., Zhang, C.*, et al.* (2014). Synaptic dysregulation in a human iPS cell model of mental disorders. Nature *515*, 414-418.

Woodford, T.A., Schlegel, R., and Pardee, A.B. (1988). Selective isolation of newly synthesized mammalian mRNA after in vivo labeling with 4-thiouridine or 6-thioguanosine. Anal Biochem *171*, 166-172.

Wu, H.J., Lima, W.F., Zhang, H., Fan, A., Sun, H., and Crooke, S.T. (2004). Determination of the role of the human RNase H1 in the pharmacology of DNA-like antisense drugs. Journal of Biological Chemistry *279*, 17181-17189.

Wu, L., Wells, D., Tay, J., Mendis, D., Abbott, M.A., Barnitt, A., Quinlan, E., Heynen, A., Fallon, J.R., and Richter, J.D. (1998). CPEB-mediated cytoplasmic polyadenylation and the regulation of experience-dependent translation of alpha-CaMKII mRNA at synapses. Neuron *21*, 1129-1139.

Yin, W., and Rogge, M. (2019). Targeting RNA: A Transformative Therapeutic Strategy. Clin Transl Sci *12*, 98-112.

Yuste, R., and Bonhoeffer, T. (2001). Morphological changes in dendritic spines associated with long-term synaptic plasticity. Annu Rev Neurosci *24*, 1071-1089.

Zajaczkowski, E.L., Zhao, Q.Y., Zhang, Z.H., Li, X., Wei, W., Marshall, P.R., Leighton, L.J., Nainar, S., Feng, C., Spitale, R.C.*, et al.* (2018). Bioorthogonal Metabolic Labeling of Nascent RNA in Neurons Improves the Sensitivity of Transcriptome-Wide Profiling. ACS Chem Neurosci *9*, 1858-1865.

Zhou, Q., Xiao, M., and Nicoll, R.A. (2001). Contribution of cytoskeleton to the internalization of AMPA receptors. Proc Natl Acad Sci U S A *98*, 1261-1266.

Chapter 4: Role of the CPEB3 Ribozyme in Memory Consolidation

4.1 Introduction

Synaptic strengthening is a prominent feature of memory formation and reconsolidation. Oligomerization of *Drosophila* CPEB (also known as Orb2) has been shown to occur during stable long-term memory formation, and aggregation of the functional prion-like CPEB3 regulates synaptic protein synthesis, which is crucial for the persistence of memory (Fioriti et al., 2015; Majumdar et al., 2012; Pavlopoulos et al., 2011; Stephan et al., 2015). Similar to *Aplysia* CPEB, Orb2 has two conformational states: monomeric and aggregated states. Previous studies have shown that in the absence of the prion-like domain of Orb2, *D. melanogaster* fails to form long-term male-courtship memory (Keleman et al., 2007). In mouse, CPEB3 coverts from a recessive monomeric state to a prion-like aggregated state in response to synaptic activation (Si and Kandel, 2016). Different knockout studies have been conducted to determine the effects of CPEB3 on LTM. The conditional forebrain-restricted CPEB3 KO mice exhibited impaired synaptic plasticity, spatial memory consolidation, and maintenance (Fioriti et al., 2015; Stephan et al., 2015). In contrast, global CPEB3 KO mice displayed enhanced hippocampus-dependent memory in the Morris water maze, but exhibited elevated short-term fear response during acquisition and extinction of contextual fear memory (Chao et al., 2013). Although these results provide evidence for a role of the *CPEB3* gene in memory, it is unclear how these distinct KO phenotypes contribute to

the persistence of long-term memory. Furthermore, the function of the CPEB3 ribozyme remains to be established. Given that a SNP in the human CPEB3 ribozyme has been shown to increase the ribozyme self-scission rate (Salehi-Ashtiani et al., 2006) and to impact human episodic memory (Vogler et al., 2009), the ribozyme self-scission likely mediates pre-mRNA processing and consequently translational control. Intronic ribozymes have previously been shown to modulate the levels of spliced mRNAs in *cis* (Fong et al., 2009; Lacadie et al., 2006). Moreover, the case of the CPEB3 ribozyme provides a unique opportunity for control of the CPEB3 mRNA production through modulation of the ribozyme activity. To study the CPEB3 ribozyme's role in memory consolidation, we inhibited the CPEB3 ribozyme *in vivo* using ASOs. Unlike the cases of mouse KO models of *CPEB3*, the ASO approach to ribozyme down-regulation represents an RNA-level pharmacological intervention, which affords far greater spatial and temporal control, and hence finer manipulation of *CPEB3* expression.

4.2 Results and Discussion

CPEB3 ribozyme ASO leads to an increase of CPEB3 mRNA in the CA1 hippocampus

To investigate whether the CPEB3 ribozyme exhibits similar effects in regulating synaptic plasticity *in vivo*, 8-10 weeks old C57BL/6 mice were stereotaxically infused with either ASO, scrambled ASO, or vehicle into the CA1 region of the dorsal hippocampus, the major region involved in memory consolidation and persistence (**Fig. 4.1A**). Two days after ASO injection, dorsal hippocampus tissues were dissected for gene expression analysis. First, CPEB3 ribozyme expression was measured to evaluate whether ASO can inhibit its activity *in vivo*. Infusion of ASO targeting the CPEB3 ribozyme significantly reduces ribozyme activity in the dorsal hippocampus (**Fig. S4.1A**; one-way ANOVA with Sidak's *post hoc* tests, $F_{(2,14)} = 4.033$, $P = 0.0414$). Next, we tested whether CPEB3 mRNA is altered by CPEB3 ribozyme inhibition. We found that administration of ASO leads to an increase of CPEB3 mRNA in the CA1 hippocampus (**Fig. 4.1B**; exons 2–3: one-way ANOVA with Sidak's *post hoc* tests, $F_{(2,15)} = 9.322$, $P = 0.0024$; exons 3–6: one-way ANOVA with Sidak's *post hoc* tests, $F_{(2,15)} = 10.17$, $P = 0.0016$; exons 6–9: one-way ANOVA with Sidak's *post hoc* tests, $F_{(2,15)} = 9.187$, $P = 0.0025$), suggesting that the ASO prevents ribozyme self-scission during CPEB3 pre-mRNA transcription, thereby increasing CPEB3 mRNA expression. As a control, a different intronic region of CPEB3 was measured to test the specificity of the ASO, and no significant difference between ASO, scrambled ASO, and vehicle in the 4^{th} intron was observed, confirming that the ASO is highly selective for the ribozyme (**Fig. S4.1B**; one-way ANOVA with Sidak's *post hoc* tests, $F_{(2,15)} = 0.4189$, $P = 0.6652$).

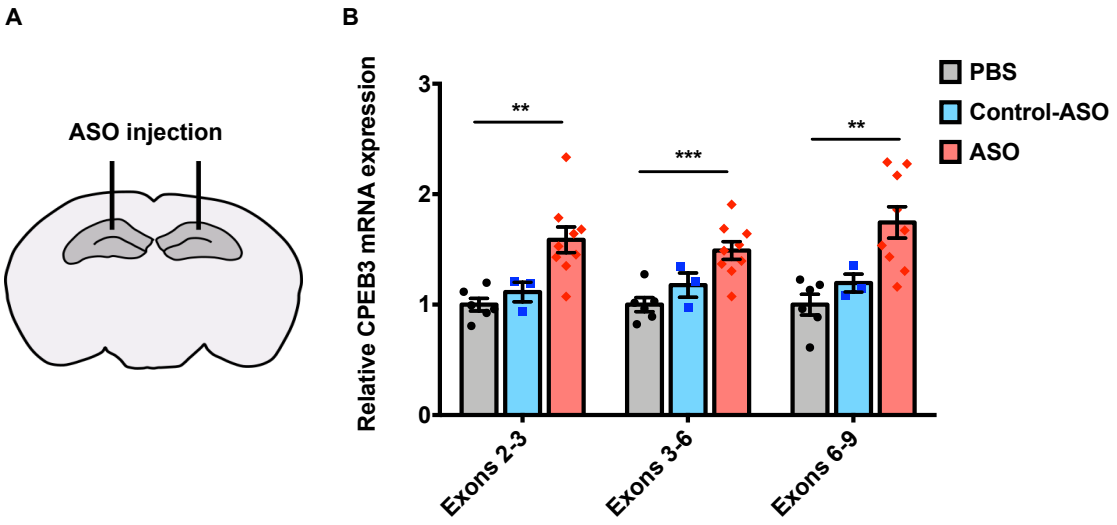

Fig. 4.1. CPEB3 ribozyme ASO leads to an increase of CPEB3 mRNA in the CA1 hippocampus. (A) Schematic representation of stereotaxic procedure. ASO, scrambled ASO, or vehicle was bilaterally infused to the mouse CA1 hippocampus. (B) qRT-PCR analysis of CPEB3 mRNA (exons 2–3, 3–6, and 6–9). CPEB3 mRNA expression is upregulated in the CPEB3 ribozyme ASO treatment group compared to controls (one-way ANOVA with Sidak's *post hoc* tests. $^{**}P < 0.01$, $^{***}P < 0.001$). Data are presented as mean ± SEM.

Inhibition of CPEB3 ribozyme in the CA1 hippocampus regulates the activity of CPEB3 on its polyadenylation targets GluA1, GluA2, and PSD-95 mRNA

Previous studies have suggested CPEB3 regulates GluA1 and GluA2 polyadenylation, in which CPEB3 CKO mice fail to elongate poly(A) tail of GluA1 and GluA2 mRNA after Morris water maze training. Additionally, overexpression of CPEB3 changes the length of GluA1 and GluA2 mRNA poly(A) tail, and overexpression of Neurl1 or expression of CPEB3 fused to ubiquitin results in an elongation of poly(A) tail of GluA1 and GluA2 mRNA and the subsequent translation (Fioriti et al., 2015; Pavlopoulos et al., 2011). We first measured CPEB3 protein expression in the dorsal hippocampus in the basal state after ASO administration, and we did not observe any significant difference between ASO and control (**Fig. S4.2 A and B**; unpaired *t* test, $t = 1.486$, $df = 3.288$, $P = 0.2261$). We next explored whether the CPEB3 ribozyme regulates PRPs gene expression in the mouse hippocampus. No significant differences between ASO and control in GluA1, GluA2, PSD-95, and NR2B transcripts were observed (**Fig. 4.2A**; GluA1: unpaired *t* test, $t = 1.655$, $df = 5.858$, $P = 0.1503$. GluA2: unpaired *t* test, $t = 0.5476$, $df = 10.96$, $P = 0.5949$. PSD-95: unpaired *t* test, $t = 0.9838$, $df = 8.760$, $P = 0.3516$. NR2B: unpaired *t* test, $t = 1.250$, $df = 11.11$, $P = 0.2369$). This suggests that the regulation of CPEB3 ribozyme does not affect PRPs transcription. Likewise, we examined whether CPEB3 ribozyme regulates translation of PRPs. Immunoblotting analysis revealed that CPEB3 ribozyme targeting ASO does not affect PRPs expression compared to the control in naïve mice (**Fig. S4.2 A** and **C**; GluA1: unpaired *t* test, $t = 1.020$, $df = 2.667$, $P = 0.3910$. GluA2: unpaired *t* test, $t = 0.1815$, $df = 3.837$, $P = 0.8651$. PSD-95: unpaired *t* test, $t = 2.056$, $df = 2.586$, $P = 0.1465$. NR2B:

unpaired *t* test, $t = 1.868$, $df = 4.000$, $P = 0.1351$), suggesting that CPEB3 ribozyme activity does not alter neither transcriptional or translational regulation of PRPs in naïve mice.

The mechanism by which cytoplasmic polyadenylation regulates mRNA translation in the synapto-dendritic compartment has been proposed to identify the role of CPEBs in synaptic plasticity (Drisaldi et al., 2015; Du and Richter, 2005; Huang et al., 2006; Wells et al., 2001; Wu et al., 1998). To further delineate whether the regulation of CPEB3 ribozyme is involved in polyadenylation processes, 3′ rapid amplification of cDNA ends (3′ RACE) was performed to examine the 3′ end sequence. Using the oligo-dT adapter primer to enrich poly(A) sequences and using gene-specific primers to measure poly(A) and mRNA exon junctions, we found that CPEB3 ribozyme ASO administration leads to an increase in GluA1, GluA2, and PSD-95 mRNA polyadenylation in the mouse dorsal hippocampus (**Fig. 4.2B**; GluA1: unpaired *t* test, $t = 2.535$, $df = 10.44$, $P = 0.0287$. GluA2: unpaired *t* test, $t = 2.327$, $df = 11.02$, $P = 0.0400$. PSD-95: unpaired *t* test, $t = 4.254$, $df = 9.808$, $P = 0.0018$). In contrast, there is no significant difference between control and ASO groups in NR2B mRNA polyadenylation (**Fig. 4.2B**; NR2B: unpaired *t* test, $t = 0.9846$, $df = 8.020$, $P = 0.3536$). These data support a model that the inhibition of the CPEB3 ribozyme might modulate its protein expression and subsequently regulate polyadenylation of AMPARs and PSD-95. Indeed, as an RNA binding protein, CPEB3 has been shown to bind to 3′ UTR of GluA1, GluA2, and PSD-95 mRNA and regulate polyadenylation and translation (Chao et al., 2013; Fioriti et al., 2015; Huang et al., 2006; Pavlopoulos et al., 2011). Similarly to

previous reports, we found that modulation of CPEB3 protein levels through CPEB3 ribozyme inhibition can alter GluA1, GluA2, and PSD-95 polyadenylation in the basal state, suggesting that the CPEB3 ribozyme might serve a role in post-transcriptional regulation and 3′ mRNA processing.

The 3′ UTR of mRNA has been found to mediate post-transcriptional gene regulation, where it possesses *cis*-acting regulatory elements that can be recognized by RNA-binding proteins (RBPs) and miRNAs (Matoulkova et al., 2012).. Recent reports suggest that the 3′ UTR and poly(A) tail play an important role in regulating RNA stability, nuclear export, and translation efficiency (Jackson and Standart, 1990; Kuersten and Goodwin, 2003; Mayr, 2017; Sachs and Wahle, 1993). Further, Tushev and colleagues discovered high levels of 3′ UTR diversity in hippocampal neurons, in which neuronal transcripts exhibit multiple 3′ UTR isoforms that contribute to synaptic plasticity (Tushev et al., 2018). To investigate whether the CPEB3 ribozyme is involved in post-transcriptional gene regulation in synaptic plasticity, particularly changes in lengths of 3′ UTR, we sought to measure specific PAS using qRT-PCR and compared the difference in PAS between control and ASO groups. We found that administration of CPEB3 ribozyme ASO resulted in an increase in GluA2 polyadenylation (**Fig. 4.2C**: unpaired *t* test, $t = 2.692$, $df = 7.159$, $P = 0.0304$). Corroborating with previous studies in which CPEB3 was shown to interact with GluA2 3′ UTR *in vitro* and *in vivo* (Huang et al., 2006), our results provide further evidence to support the previous findings that CPEB3 can regulate GluA2 mRNA and its polyadenylation in the dorsal hippocampus. In addition, we also measured PAS in other plasticity-related genes, and we did not

observe any difference in PAS in GluA1, PSD-95, and NR2B (**Fig. 4.2C:** GluA1: unpaired *t* test, $t = 0.4218$, $df = 10.22$, $P = 0.6819$. PSD-95: unpaired *t* test, $t = 1.694$, $df = 10.07$, $P = 0.1208$. NR2B: unpaired *t* test, $t = 1.393$, $df = 6.467$, $P = 0.2096$).

Combined, our data support the role of the CPEB3 ribozyme in post-transcriptional regulation in the mouse CA1 hippocampus, which might contribute to mediate synaptic plasticity.

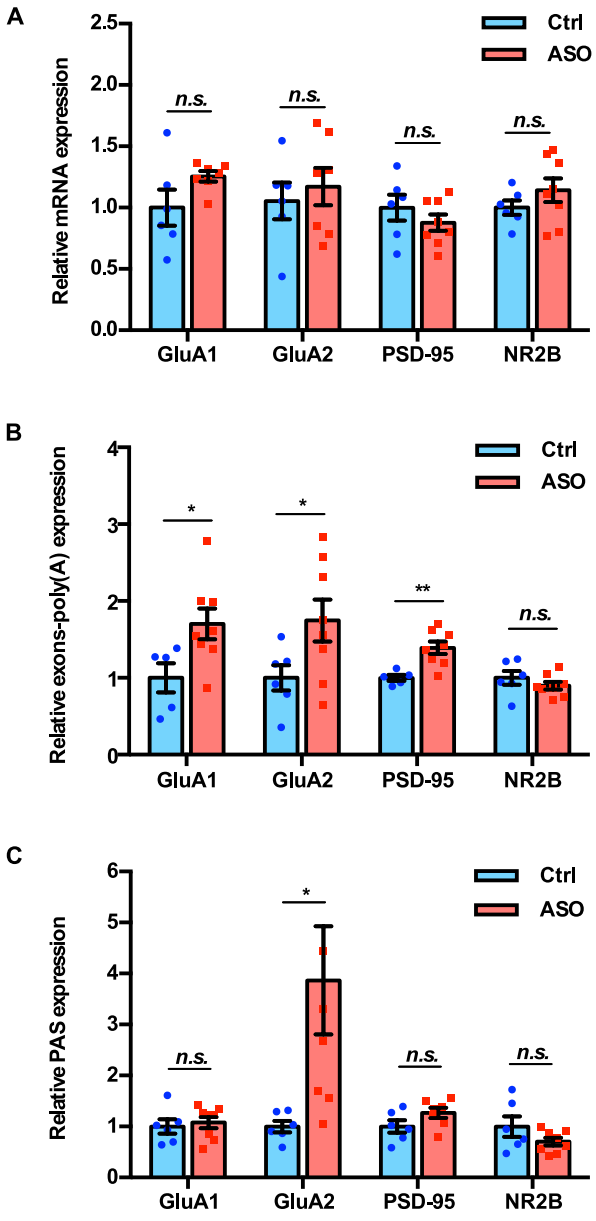

Fig. 4.2. CPEB3 ribozyme regulates polyadenylation of plasticity-related genes. (A) Inhibition of CPEB3 ribozyme does not affect transcription of plasticity-related genes. No significant difference in mRNA expression between ASO and control was observed (unpaired *t* test, *n.s.* not significant). (B) Effect of CPEB3 ribozyme ASO on polyadenylation in the CA1 hippocampus. 3′ RACE analysis showed a significant increase in polyadenylation of GluA1, GluA2, and PSD-95 in ASO-infused mice

(unpaired *t* test, **P* < 0.05, ***P* < 0.01, *n.s.* not significant). (C) Effect of CPEB3 ribozyme ASO on specific PAS in the CA1 hippocampus. Specific polyadenylation sites of plasticity-related gene were identified based on the UCSC genome browser. Nested qPCR was performed using primers in close proximity to the known poly(A) site of each gene. CPEB3 ribozyme ASO-infused mice showed a significant increase in GluA2 PAS (unpaired *t* test, **P* < 0.05, *n.s.* not significant). Data are presented as mean ± SEM.

Inhibition of CPEB3 ribozyme in the dorsal hippocampus enhances long-term memory

To assess whether inhibition of the CPEB3 ribozyme improves memory formation and consolidation, we examined the CPEB3 ribozyme with respect to long-term memory using object location memory (OLM) task (**Fig. 4.3A**). The OLM task has been widely used to study hippocampal-dependent spatial memory function, which is based on mice's innate preference for novelty and capability to discriminate spatial relationships between novel and familiar locations (Vogel-Ciernia et al., 2013; Vogel-Ciernia and Wood, 2014). During the testing session, mice could retrieve the memory that encoded for the objects they were exposed to in the training session. Mice were infused with CPEB3 ribozyme ASO, scrambled ASO, or vehicle bilaterally to the CA1 dorsal hippocampus 48 hours prior to OLM training. Notably, the CPEB3 ribozyme ASO group showed a significant increase in DI compared to control groups between training and testing (**Fig. 4.3B**: two-way ANOVA: ASO x session $F_{(2,40)}$ = 6.600, P = 0.0033), suggesting that ASO-infused mice have a robust preference for exploring the object in the novel location. We observed no significant difference in training DI, indicating that mice exhibit no preference for either object (**Fig. 4.3B**: one-way ANOVA with Sidak's *post hoc* tests, $F_{(2,20)}$ = 0.2269, P = 0.7991). Likewise, during training and testing sessions, ASO-infused mice and control mice displayed similar total exploration time, suggesting that mice have similar explorative behavior (**Fig. 4.3C**; Training: one-way ANOVA with Sidak's *post hoc* tests, $F_{(2,20)}$ = 0.3528, P = 0.7070. Testing: one-way ANOVA with Sidak's *post hoc* tests, $F_{(2,20)}$ = 1.188, P = 0.3255). These results provide strong evidence that CPEB3 is critical for long-term memory, and the effect of the CPEB3 ribozyme might facilitate the conversion of a training period to LTM.

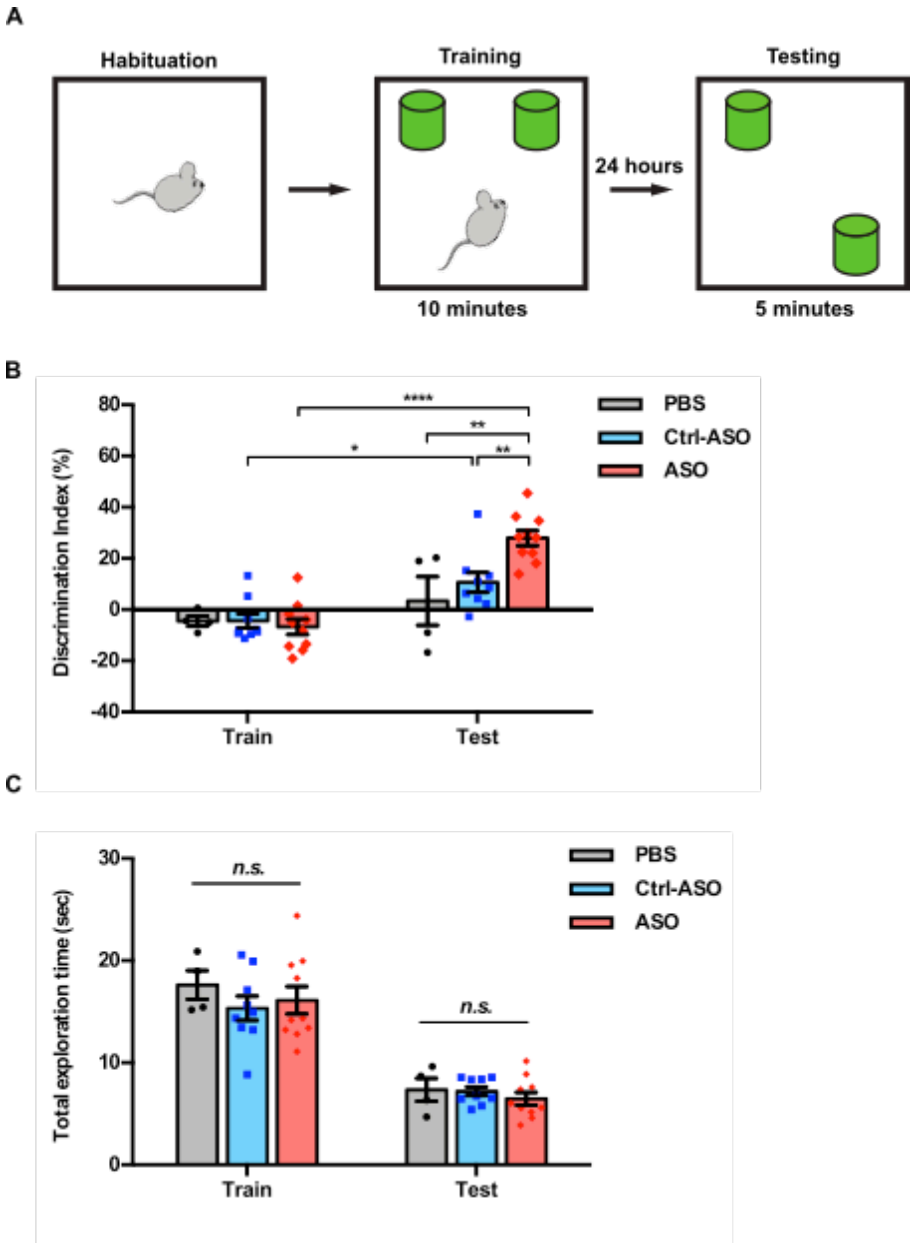

Fig. 4.3. Inhibition of CPEB3 ribozyme enhances long-term hippocampal memory. (A) Experimental procedure for OLM. (B) CPEB3 ribozyme ASO-infused mice showed a significantly higher discrimination index than scrambled ASO or vehicle in OLM testing (two-way ANOVA with Sidak's *post hoc* tests, **P* < 0.05, *****P* < 0.0001). (C) CPEB3 ribozyme ASO and control mice displayed similar total exploration time in both training

and testing sessions (one-way ANOVA with Sidak's *post hoc* tests, *n.s.* not significant). Data are presented as mean ± SEM.

CPEB3 ribozyme ASO leads to an upregulation in CPEB3 and PRPs protein expression during memory consolidation

Learning-induced changes in gene expression and protein synthesis are essential for memory formation and consolidation (Kandel, 2001, 2012). To determine whether upregulation of CPEB3 mRNA by ASO leads to a change in CPEB3 protein expression, we analyzed the dorsal hippocampal homogenates and synaptosomal fractions to evaluate the CPEB3 ribozyme regulation after learning. After OLM testing, mice were sacrificed, and the dorsal hippocampal homogenates and synaptosomal fractions were analyzed by immunoblotting. Administration of CPEB3 ribozyme ASO leads to a significant increase in CPEB3 protein expression in the CA1 hippocampal homogenates and crude synaptosomes after OLM (**Fig. 4.4 A and B**; hippocampal homogenates: unpaired *t* test, $t = 2.345$, $df = 17.00$, $P = 0.0314$. **Fig. 4.4 A and D**; synaptosomes: unpaired *t* test, $t = 2.403$, $df = 11.11$, $P = 0.0349$). This result confirms that ASO-mediated knockdown of the CPEB3 ribozyme facilitates CPEB3 mRNA processing, and training induces an increase in CPEB3 translation. To determine whether increased CPEB3 further regulates PRPs translation, GluA1, GluA2, PSD-95, and NR2B protein levels were also measured. No significant difference in PRPs protein levels between ASO and control in hippocampal homogenates was observed (**Fig. 4.4 A and C**; GluA1: unpaired *t* test, $t = 0.3751$, $df = 15.96$, $P = 0.7125$. GluA2: unpaired *t* test, $t = 0.9432$, $df = 15.16$, $P = 0.3604$. PSD-95: unpaired *t* test, $t = 0.2849$, $df = 17.63$, $P = 0.7790$. NR2B: unpaired *t* test, $t = 0.9415$, $df = 17.32$, $P = 0.3594$). Strikingly, GluA1, PSD-95, and NR2B protein levels were elevated in ASO-infused mice relative to scrambled ASO control in synaptosomal fractions (**Fig. 4.4 A and E**: GluA1: unpaired *t*

test, t = 2.433, df = 15.83, P = 0.0272. PSD-95: unpaired t test, t = 2.115, df = 17.25, P = 0.0493. NR2B: unpaired t test, t = 3.174, df = 12.42, P = 0.0077). However, we found that the GluA2 protein level remained unaffected between control and ASO groups (**Fig. 4.4 A and E**; unpaired t test, t = 1.497, df = 14.40, P = 0.1559). This could be explained by the fact that AMPARs trafficking is a dynamic process, and AMPARs are mobilized to the post-synaptic surface membrane in response to neuronal activity (Diering and Huganir, 2018). Fractionation of synaptic proteins at the postsynaptic membrane could be employed to elucidate the relationship between the CPEB3 ribozyme and GluA2 in the future. Together, our findings indicate that blocking CPEB3 ribozyme activity leads to an increase in CPEB3 protein production after OLM, and upregulation of CPEB3 by OLM further mediates GluA1, PSD-95, and NR2B translation. This observation is consistent with the fact that training induces CPEB3 protein expression, and ablation of CPEB3 abolishes the activity-dependent translation of GluA1 and GluA2 in the mouse hippocampus (Fioriti et al., 2015). Specifically, it has been suggested that CPEB3 coverts to prion-like aggregates in stimulated synapses that mediate hippocampal synaptic plasticity and facilitate memory storage (Si and Kandel, 2016). Long-term memory formation and consolidation is dependent on transcriptional and translational regulation. As training can produce long-term memory, it is likely that CPEB3 ribozyme inhibition leads to an increase in CPEB3 protein expression and further facilitates experience-induced translational processes.

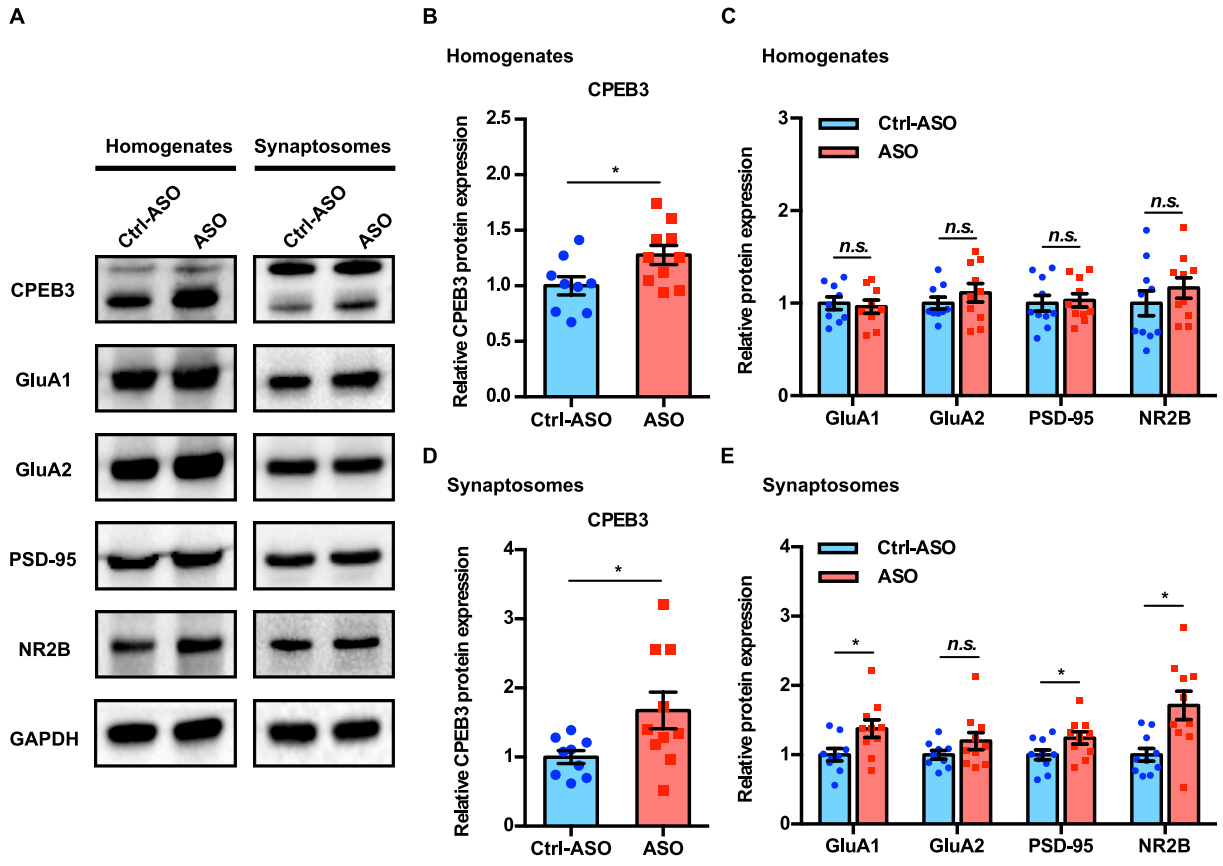

Fig. 4.4. CPEB3 ribozyme ASO leads to upregulation of CPEB3 and PRPs protein expression after OLM. (A) Representative image of immunoblotting showing CPEB3, GluA1, GluA2, PSD-95, and NR2B. GAPDH is used as a loading control. (B) Quantification of CPEB3 protein expression in hippocampal homogenates. CPEB3 ribozyme ASO-infused mice showed a significant increase in CPEB3 expression after OLM (unpaired *t* test, $*P < 0.05$). (C) Quantification of PRPs protein expression in hippocampal homogenates. There was no significant difference in PRPs expression between ASO and scrambled ASO groups (unpaired *t* test, *n.s.* not significant). (D) Quantification of CPEB3 protein expression in synaptosomes. ASO-infused mice showed a significant increase in CPEB3 protein level after OLM (unpaired *t* test, $*P <$

0.05). (E) Quantification of PRPs expression in synaptosomes. PRPs levels from the synaptosome fractions are increased in ASO-infused mice after OLM (unpaired *t* test, **P* < 0.05, *n.s.* not significant). Data are presented as mean ± SEM.

4.3 Conclusions

Transcriptional regulation, *de novo* protein synthesis, and molecular and cellular cascades have been implicated in long-lasting forms of neuronal plasticity and memory processes. In the present study, we investigated whether the CPEB3 ribozyme plays a role in modulating synaptic consolidation *in vivo*. We demonstrated that the administration of ASO targeting the CPEB3 ribozyme in the dorsal hippocampus leads to an increase in CPEB3 mRNA. We also found that CPEB3 ribozyme plays a role in regulating polyadenylation of GluA1, GluA2, and PSD-95. Our data delineate an important step forward in understanding the molecular mechanisms of the CPEB3 ribozyme in post-transcriptional pre-mRNA processing and its subsequent translation in the mouse CA1 hippocampus. Furthermore, behavioral analysis revealed that inhibition of CPEB3 ribozyme improves long-term memory for OLM. Modulation of the CPEB3 ribozyme by ASO and OLM training induce activity-dependent upregulation of CPEB3 and PRPs. These molecular changes might represent a possible mechanism by which the CPEB3 ribozyme regulates synaptic structures and functions required for synaptic plasticity and memory consolidation.

4.4 Material and Methods

Stereotaxic surgeries

C57/BL6J mice (8-10 weeks old, Jackson Laboratory), housed under standard conditions with light-control (12-h light / 12-h dark cycles), and were anaesthetized with an isoflurane (1-3%)/oxygen vapor mixture. Mice were infused bilaterally with ASO, scramble ASO diluted in sterile PBS, or vehicle to the CA1 region of the dorsal hippocampus. The following coordinates were used, relative to bregma: medial-lateral (ML), ±1.5 mm; anterior-posterior (AP), −2.0 mm; dorsal-ventral (DV), −1.5 mm. ASOs or vehicle (1 nmol/µL) were infused bilaterally at a rate of 0.1µL/min using a Neuros Hamilton syringe (Hamilton company) with a syringe pump (Harvard Apparatus). The injectors were left in place for 2 minutes to allow diffusion then were slowly removed at a rate of 0.1 mm per 15s. The incision site was sutured and mice were allowed to recover on a warming pad then returned to cages. For all surgeries, mice were randomly assigned to the different conditions to avoid grouping same treatment conditions in time.

Quantitative RT-PCR analysis

Total RNA was isolated from the mouse hippocampus using TRIZOL reagent (Invitrogen) according to the manufacturer's protocol. RNA concentration was measured using a NanoDrop ND-1000 spectrophotometer (Thermo Fisher Scientific). Total RNA was reverse transcribed using random decamers and M-MLV reverse transcriptase (Promega)/Superscript II RNase H reverse transcriptase (Invitrogen). Quantitative RT-

PCR was performed on a BioRad CFX Connect system using iTaq Universal SYBR® Green Supermix (BioRad). Designed primers were acquired from Integrated DNA Technologies, Inc. and provided in Table 4. Desired amplicons were verified by melting curve analysis and followed by gel electrophoresis. The starting quantity of DNA from each sample was determined by interpolation of the threshold cycle (Ct) from a standard curve of each primer set. Relative gene expression levels were normalized to the endogenous gene *GAPDH*.

Immunoblotting

Mouse hippocampal tissues were collected in RIPA lysis buffer with protease inhibitor and phosphatase inhibitor (Santa Cruz Biotechnology). Crude synaptosomal fractions were prepared as previously described (Wirths, 2017). Protein concentrations were measured using bicinchonic acid (BCA) protein assay (Pierce Biotechnology). Protein samples were loaded on 10% sodium dodecyl sulfate polyacrylamide (SDS-PAGE) gels and separated by electrophoresis. Gels were electro-transferred onto polyvinylidene fluoride (PVDF) membranes using a semi-dry transfer system (BioRad). Membranes were either blocked with 5% nonfat milk or 5% bovine serum albumin (BSA) in Tris-buffered saline/Tween 20 (0.1% [vol/vol]) (TBST) for 1 hour at room temperature. Membranes were incubated with primary antibodies (Table 5) overnight at 4 ºC. After primary antibody incubation, membranes were washed three times with TBST and then incubated with secondary antibodies (Table 6) for 1 hour at room temperature. Bands were detected using an enhanced chemiluminescence (ECL) kit (Thermo Fisher

Scientific), visualized using BioRad Chemidoc MP imaging system, and analyzed by Image Lab software (BioRad). GAPDH was used as a loading control.

3′ RACE

Total RNA was extracted from the mouse CA1 hippocampus. 3′ rapid amplification of cDNA ends (3′ RACE) was performed to study the alternative polyadenylation. cDNA was synthesized using oligo(dT) primers with 3′ RACE adapter primer sequence at the 5′ ends. This cDNA library results in a universal sequence at 3′ end. A gene-specific primer (GSP) and an anchor primer that targets the poly(A) tail region were used for the first PCR using the following protocol: 95 °C for 3 minutes, followed by 30 cycles of 95 °C for 30 seconds, 55 °C for 30 seconds, and 72 °C for 3 minutes, with a final extension of 72 °C for 5 minutes. To improve specificity, a nested PCR was then carried out using nested primers. Upon amplification condition optimization, a quantitative PCR was performed on the first diluted PCR product, and a standard curve of the primer set was generated to determine the effect of relative expression of 3′-mRNA and alternative polyadenylation. All primers used in this study are listed in table 7.

Object location memory tasks (OLM)

The OLM was performed to assess hippocampus-dependent memory, as previously described (Lopez et al., 2016; Vogel-Ciernia et al., 2013; Vogel-Ciernia and Wood, 2014). Briefly, naïve C57/BL6J mice (8–12 weeks old; n = 10-12/group; ASOs, scrambled ASO) were be trained and tested. Prior to training, mice were handled 1–2 minutes for 5 days and then habituated to the experimental apparatus 5 minutes for 6

consecutive days in the absence of objects. During training, mice were placed into the apparatus with two identical objects and allowed to explore two objects for 10 minutes. Twenty-four hours after training, mice were exposed to the same arena, and long-term memory was tested for 5 minutes, where two identical objects were present and one of which was placed in a novel location. For all experiments, objects and locations were counterbalanced across all groups to reduce biases. Videos of training and testing sessions were analyzed for discrimination index (DI) and total exploration time of objects, and were scored by observers blind to the treatment. The exploration of the objects were scored when the orientation of the mouse's snout toward the object within a distance of 1 cm or when the nose was touching the object. The relative exploration time was calculated as discrimination index ($DI = (t_{novel} - t_{familiar}) / (t_{novel} + t_{familiar}) \times 100\%$). Mice that demonstrate a location or object preference during the training trial ($DI > \pm 20$) were removed from the analysis.

Statistical analysis

Data are presented as means ± SEM. Statistical differences were determined using unpaired Student's *t* test when comparing between 2 independent groups, and one-way ANOVA with Sidak's *post hoc* tests when comparing across 3 or more independent groups. OLM data were analyzed with two-way ANOVA followed by Sidak's *post hoc* tests. $P < 0.05$ was considered significant.

4.5 Supplementary Figures

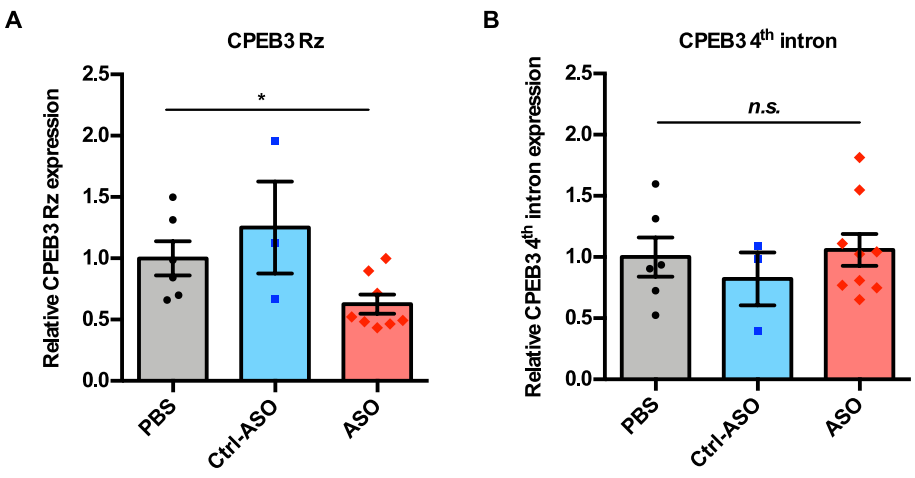

Fig. S4.1. Inhibition of the CPEB3 ribozyme by ASO. (A) Validation of knockdown CPEB3 ribozyme *in vivo*. Administration of CPEB3 ribozyme ASO to the mouse CA1 hippocampus leads to a decrease in CPEB3 ribozyme expression (one-way ANOVA with Sidak's *post hoc* tests, $*P < 0.05$). (B) The lead ASO has high specificity *in vivo*. qRT-PCR analysis of the 4th intron of the *CPEB3* gene demonstrates that there was no significant difference between controls and ASO groups (one-way ANOVA with Sidak's *post hoc* tests, *n.s.* not significant). Data are presented as mean ± SEM.

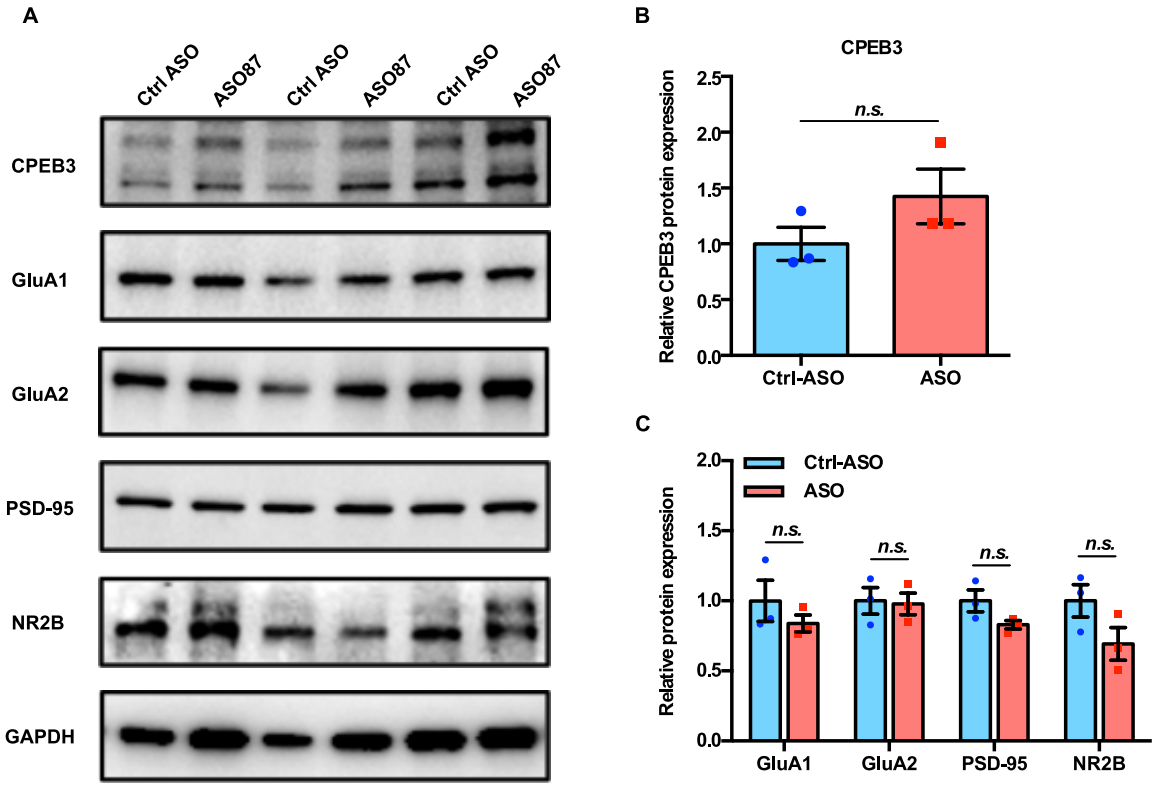

Fig S4.2. Effect of CPEB3 ribozyme on protein expression in the dorsal hippocampus. (A) Representative image of immunoblotting analysis. GAPDH is used as a loading control. (B) Quantification of CPEB3 protein expression. There was no significant difference in CPEB3 protein expression between scrambled ASO and ASO groups (unpaired *t* test, *n.s.* not significant). (C) Quantification of PRPs protein expression. There was no significant difference in PRPs protein levels between scrambled ASO and ASO groups (unpaired *t* test, *n.s.* not significant). Data are presented as mean ± SEM.

4.6 References

Chao, H.W., Tsai, L.Y., Lu, Y.L., Lin, P.Y., Huang, W.H., Chou, H.J., Lu, W.H., Lin, H.C., Lee, P.T., and Huang, Y.S. (2013). Deletion of CPEB3 enhances hippocampus-dependent memory via increasing expressions of PSD95 and NMDA receptors. J Neurosci *33*, 17008-17022.

Diering, G.H., and Huganir, R.L. (2018). The AMPA Receptor Code of Synaptic Plasticity. Neuron *100*, 314-329.

Drisaldi, B., Colnaghi, L., Fioriti, L., Rao, N., Myers, C., Snyder, A.M., Metzger, D.J., Tarasoff, J., Konstantinov, E., Fraser, P.E.*, et al.* (2015). SUMOylation Is an Inhibitory Constraint that Regulates the Prion-like Aggregation and Activity of CPEB3. Cell Rep *11*, 1694-1702.

Du, L., and Richter, J.D. (2005). Activity-dependent polyadenylation in neurons. RNA *11*, 1340-1347.

Fioriti, L., Myers, C., Huang, Y.Y., Li, X., Stephan, J.S., Trifilieff, P., Colnaghi, L., Kosmidis, S., Drisaldi, B., Pavlopoulos, E.*, et al.* (2015). The Persistence of Hippocampal-Based Memory Requires Protein Synthesis Mediated by the Prion-like Protein CPEB3. Neuron *86*, 1433-1448.

Fong, N., Ohman, M., and Bentley, D.L. (2009). Fast ribozyme cleavage releases transcripts from RNA polymerase II and aborts co-transcriptional pre-mRNA processing. Nat Struct Mol Biol *16*, 916-922.

Huang, Y.S., Kan, M.C., Lin, C.L., and Richter, J.D. (2006). CPEB3 and CPEB4 in neurons: analysis of RNA-binding specificity and translational control of AMPA receptor GluR2 mRNA. EMBO J *25*, 4865-4876.

Jackson, R.J., and Standart, N. (1990). Do the poly(A) tail and 3' untranslated region control mRNA translation? Cell *62*, 15-24.

Kandel, E.R. (2001). The molecular biology of memory storage: a dialogue between genes and synapses. Science *294*, 1030-1038.

Kandel, E.R. (2012). The molecular biology of memory: cAMP, PKA, CRE, CREB-1, CREB-2, and CPEB. Mol Brain *5*, 14.

Keleman, K., Kruttner, S., Alenius, M., and Dickson, B.J. (2007). Function of the Drosophila CPEB protein Orb2 in long-term courtship memory. Nat Neurosci *10*, 1587-1593.

Kuersten, S., and Goodwin, E.B. (2003). The power of the 3' UTR: translational control and development. Nat Rev Genet *4*, 626-637.

Lacadie, S.A., Tardiff, D.F., Kadener, S., and Rosbash, M. (2006). In vivo commitment to yeast cotranscriptiona splicing is sensitive to transcription elongation mutants. Gene Dev *20*, 2055-2066.

Lopez, A.J., Kramar, E., Matheos, D.P., White, A.O., Kwapis, J., Vogel-Ciernia, A., Sakata, K., Espinoza, M., and Wood, M.A. (2016). Promoter-Specific Effects of DREADD Modulation on Hippocampal Synaptic Plasticity and Memory Formation. J Neurosci *36*, 3588-3599.

Majumdar, A., Cesario, W.C., White-Grindley, E., Jiang, H., Ren, F., Khan, M.R., Li, L., Choi, E.M., Kannan, K., Guo, F.*, et al.* (2012). Critical role of amyloid-like oligomers of Drosophila Orb2 in the persistence of memory. Cell *148*, 515-529.

Matoulkova, E., Michalova, E., Vojtesek, B., and Hrstka, R. (2012). The role of the 3' untranslated region in post-transcriptional regulation of protein expression in mammalian cells. RNA Biol *9*, 563-576.

Mayr, C. (2017). Regulation by 3'-Untranslated Regions. Annu Rev Genet *51*, 171-194.

Pavlopoulos, E., Trifilieff, P., Chevaleyre, V., Fioriti, L., Zairis, S., Pagano, A., Malleret, G., and Kandel, E.R. (2011). Neuralized1 activates CPEB3: a function for nonproteolytic ubiquitin in synaptic plasticity and memory storage. Cell *147*, 1369-1383.

Sachs, A., and Wahle, E. (1993). Poly(A) tail metabolism and function in eucaryotes. J Biol Chem *268*, 22955-22958.

Salehi-Ashtiani, K., Luptak, A., Litovchick, A., and Szostak, J.W. (2006). A genomewide search for ribozymes reveals an HDV-like sequence in the human CPEB3 gene. Science *313*, 1788-1792.

Si, K., and Kandel, E.R. (2016). The Role of Functional Prion-Like Proteins in the Persistence of Memory. Cold Spring Harb Perspect Biol *8*, a021774.

Stephan, J.S., Fioriti, L., Lamba, N., Colnaghi, L., Karl, K., Derkatch, I.L., and Kandel, E.R. (2015). The CPEB3 Protein Is a Functional Prion that Interacts with the Actin Cytoskeleton. Cell Rep *11*, 1772-1785.

Tushev, G., Glock, C., Heumuller, M., Biever, A., Jovanovic, M., and Schuman, E.M. (2018). Alternative 3 ' UTRs Modify the Localization, Regulatory Potential, Stability, and Plasticity of mRNAs in Neuronal Compartments. Neuron *98*, 495-+.

Vogel-Ciernia, A., Matheos, D.P., Barrett, R.M., Kramar, E.A., Azzawi, S., Chen, Y., Magnan, C.N., Zeller, M., Sylvain, A., Haettig, J.*, et al.* (2013). The neuron-

specific chromatin regulatory subunit BAF53b is necessary for synaptic plasticity and memory. Nat Neurosci *16*, 552-561.

Vogel-Ciernia, A., and Wood, M.A. (2014). Examining object location and object recognition memory in mice. Curr Protoc Neurosci *69*, 8 31 31-17.

Vogler, C., Spalek, K., Aerni, A., Demougin, P., Muller, A., Huynh, K.D., Papassotiropoulos, A., and de Quervain, D.J. (2009). CPEB3 is associated with human episodic memory. Front Behav Neurosci *3*, 4.

Wells, D.G., Dong, X., Quinlan, E.M., Huang, Y.S., Bear, M.F., Richter, J.D., and Fallon, J.R. (2001). A role for the cytoplasmic polyadenylation element in NMDA receptor-regulated mRNA translation in neurons. J Neurosci *21*, 9541-9548.

Wirths, O. (2017). Preparation of Crude Synaptosomal Fractions from Mouse Brains and Spinal Cords. Bio-Protocol *7*.

Wu, L., Wells, D., Tay, J., Mendis, D., Abbott, M.A., Barnitt, A., Quinlan, E., Heynen, A., Fallon, J.R., and Richter, J.D. (1998). CPEB-mediated cytoplasmic polyadenylation and the regulation of experience-dependent translation of alpha-CaMKII mRNA at synapses. Neuron *21*, 1129-1139.